ESTIMATION OF CONCENTRATE GRADE IN PLATINUM FLOTATION BASED ON FROTH IMAGE ANALYSIS

By

Corné Marais

Thesis presented in partial fulfilment

of the requirements for the degree

MASTER OF SCIENCE IN ENGINEERING

(EXTRACTIVE METALLURGICAL ENGINEERING)

in the Department of Process Engineering

at the University of Stellenbosch

Supervised by

Prof. C Aldrich

STELLENBOSCH

December 2010

DECLARATION

I, the undersigned, hereby declare that the work contained in this thesis is my own original work and that I have not previously in its entirety or in part submitted it at any university for a degree. I certify that the work has been undertaken solely by the candidate, except where due acknowledgement is provided.

…………………………….. ………………

Signature   Date

ABSTRACT

Flotation is an important processing step in the mineral processing industry wherein valuable minerals are extracted. Flotation is a difficult process to control due to its complexity, meaning that the reversal of series of changes will not necessarily bring the process back to its original state. Expert knowledge is incorporated in flotation control through operator experience and intervention, which is subject to many challenges, creating the need for improvement in control. The performance of a flotation cell is often determined by evaluating froth appearance. The application of image analysis to capture, evaluate and monitor froth appearance poses multiple benefits such as consistent and reliable froth appearance evaluation.

The objective for this study was to conduct a laboratory study for the collection of froth images with the purpose of evaluating the feasibility of using image information to predict platinum froth grade.

Laboratory test work was performed according to a fractional factorial experimental design. Six variables were considered: air flowrate, pulp level and collector, activator, frother and depressant dosages. The laboratory study results were quantified by assay analysis. Analysis of variance only revealed the significant effect of pulp height and collector addition on flotation performance. Data pre-processing revealed information regarding feature correlations and variance contributions. Data analysis from captured images achieved reliable froth grade predictions using random forest classification and artificial neural network (ANN) regression techniques. Random forest classification accuracies of 86.8% and 75.5% were achieved for the following respective datasets: image data of each individual experiment (average of all experiments) and all image data. The applied ANN models achieved R^2 values 0.943 and 0.828 for the same 2 datasets. An industrial case study was done wherein a series of step changes in air flowrate was made on a specific flotation cell. The limited industrial case study results supported laboratory study results. Multiple linear regression performed very well, reaching R^2 values up to 0.964. Neural networks achieved slightly better with R^2 values of up to 0.997.

Based on the findings, the following main conclusions were drawn from this study:

- Reliable predictions using classification and regression models on image data were proved possible in concept by the laboratory study, and supported by results from an industrial case study on a narrow system.

The following main recommendations were made for further investigation:

- Research over a larger range of operating conditions is needed to find a more comprehensive solution.
- Investigations should be conducted to determine hardware requirements and specifications in terms of minimum resolution, lighting requirements, sampling frequency and data storage. Software requirements, specifications and maintenance challenges should also be investigated for implementation purposes once a more comprehensive solution has been found.
- Strategies in terms of camera placement and model building will need to follow, giving special attention to a strategy to handle ore composition change.

Keywords: flotation, image analysis, machine vision, platinum

OPSOMMING

Flotasie is 'n belangrike proses in die mineraal proseseringsbedryf vermoeid met die ontginning van waardevolle minerale. Die proses is moelik om te beheer vanweë sy kompleksiteit, wat verwys na die onvermoë om die proses terug te bring na sy oorspronklike toestand deur 'n reeks veranderinge om te keer. In die algemeen word spesialis kennis deel van prosesbeheer deur die toepassing van operateurs se ervaring en ingryping, wat opsigself verskeie uitdagings bied wat die behoefte aan verbeterde beheertoestelle en strategieë daarstel. Die werkverrigting van flotasieselle word gereeld beoordeel op grond van die voorkoms van die skuim. Die gebruik van beeldverwerking om dié inligting vas te vang vir monitering en evaluering doeleindes hou verskeie voordele in, bv. konsikwente en betroubare evaluasie van die skuimvoorkoms.

Die doelwitte vir hierdie studie was om 'n laboratorium studie te loods vir die opname van skuimbeelde, met die doel om die bruikbaarheid van beeldinligting vir die voorspelling van die flotasieprodukkwaliteit, te ondersoek.

Die laboratorium gevallestudie is uitgevoer aan die hand van 'n fraksionele faktoriale eksperimentele ontwerp. Ses veranderlikes was ondersoek naamlik, lugvloeitempo, pulphoogte en versamelaar aktiveerder en depressant toevoeging. Die studie se resultate is gekwantifiseer deur die analise van die skuim inhoud. 'n Analise van variansie het slegs die invloed van pulphoogte en versamelaartoevoeging op die flotasievertoning uitgelig. Data voorverwerking het inligting uitgelig rondom die veranderlikes se verhouding met mekaar. Data analise metodes, naamlik lukrake klassifiseringswoude en neurale netwerk regressie, is toegepas op die versamelde beelddata en het belowende resultate gelewer. Lukrake klassifiseringswoude het klasse gedentifiseer met akkuraathede van 86.8% en 75.5% vir die volgende onderskeie datastelle: individuele eksperimente se beeld data (gemiddeld oor alle eksperimentele lopies), alle beelddata as een stel. Die neurale netwerke het R^2 waardes van 0.943 rn 0.828 gelewer vir dieselfde 2 datastelle. Die beperkte nywerheidsgevallestudie het verandering in lugvloeitempo toegelaat vir 'n enkele flotasie sel. Die resultate het die bevindinge van die laboratorium gevallestudie gesteun. Veelvoudige lineere regressie het R^2 waardes van tot en met 0.964 gelewer. Neurale netwerke het daarop verbeter met waardes tot en met 0.997.

Die volgende hoof gevolgtrekkinge was duidelik vanuit die resultate:

–   Betroubare voorspellings was moontlik met die toepassing van klassifikasie en regressie modelle op die laboratorium studie data. Die resultate is ondersteun deur soortgelyke resultate van die beperkte nywerheidsgevallestudie.

Die volgende hoof aanbevelings was gemaak vir verdere navorsing:

–   Navorsing oor 'n wyer reeks proseskondisies is nodig om 'n meer omvattende oplossing te vind.
–   'n Ondersoek moet geloods word om die hardeware vereistes en spesifikasies in terme van die minimum beeld resolusie, beligting vereistes, monsterneming tempo en die berging van data te bepaal. Sagteware vereistes, spesifikasies en instandhouding uitdagings moet ook ondersoek word vir implementasie doeleindes sodra 'n meer omvattende oplossing gevind is.
–   Strategieë in verband met die plasing van kamers en die ontwikkeling van modelle is nodig, waarin spesiale aandag gegee moet word om die probleem van veranderende ertssamestelling op te los.

Sleutelwoorde: flotasie, beeld verwerking, masjienvisie, platinum

ACKNOWLEDGEMENTS

Firstly I would like to give honour to my heavenly Father for His grace and provision throughout this study.

Thank you to my friends and family for their support and encouragement. A special thank you to my parents and my grandmother whom I dedicate this thesis to. To my boyfriend, Neil Yzelle, I would not have been able to do this without your support. And to my closest friends, Keenan and Irané Bence and Lidia Auret, I thank you for your contributions and loving support.

To my supervisor, Prof Chris Aldrich, thank you for your mentorship and guidance and the opportunity to learn so much the past few years.

I would also like to thank the following people for their much appreciated contribution during this project:

Anglo Platinum: Neville Plint, De Villiers Groenewald

Anglo American: Doug Philips, Bernard Oostendorp

Stone Three Venture Technology (Pty) Ltd: Attie Labuschagne

University of Cape Town: Sam Morar, Jenny Wiese, Martin Harris, Jenny Sweet

Stellenbosch University: JP Barnard, John Burchell, Gorden Jemwa, Diane Hartley, Alvin Petersen, Elton Thyse, Hanlie Botha

Imperial College London: Jan Cilliers, Barry Shean

TABLE OF CONTENTS

NOMENCLATURE

Commonly used Acronyms

PGM   Platinum Group Metals

BIC   Bushveld Igneous Complex

UG2   Upper Group 2 Reef

KPI   Key Performance Indicator

RGB   Red, Green and Blue spectral features

HSI   Hue, Saturation and Intensity spectral features

HSV   Hue, Saturation and Values spectral features

CIE   International Commission on Illumination

GLDM   Gray Level Dependence Matrix

AGDP   Anglo Graduate Development Programme

ANN   Artificial Neural Network

MLP   Multi-layer Perceptron

RBF   Radial Basis Function

PSA   Particle Size Analyser/Analysis

Main symbols

R Recovery

τ Residence time

γ Probability

X Input matrix

x Input vector

Y Output matrix (set of output vectors)

y Output vector

v Velocity

h Height

Q Volumetric flowrate

c weir width

G Grade

Ψ	Flux
S	Surface area
ζ	Volume fraction of the froth that is air
T	Score matrix
P	Loading matrix
t	Score vector
p	Loading vector
E	Residual matrix
θ	Image features
β	Loadings
d	Intersample spacing
a	Intersample direction in terms of an angle
$Ę$	Energy
$ę$	Entropy
$Ļ$	Inertia
$Ļ$	Local homogeneity
$Ç$	Correlation
μ	Mean
σ	Standard deviation
W^H	Network weight matrix between input and hidden nodes
w^H	Network weight
W^O	Network weight matrix between hidden and output nodes
w^O	Network weight
φ	Neural network activation function
$RMSE$	Root-mean-square error
SSE	Sum of squared error
m	Mass
$\emptyset$	Independent identically distributed random vector (random forest classifier)

Subscripts

o	Overall
f	Froth
p	Pulp

P	Concentrate product
F	Feed
c	Collision
a	Attachment
d	Detachment
t	True flotation
e	Entrainment
w	Water
α	Air
b	Bubble

Other

Indices are indicated with i, j, k, l, m, n, p

Corresponding index sizes are indicated with I, J, K, L, M, N, P

CHAPTER 1
INTRODUCTION

1. THE ROLE OF FLOTATION IN MINERAL PROCESSING

The minerals processing industry is concerned with the extraction and refinement of valuable minerals from ore. Comminution processes reduce the size of the ore with the primary goal of liberating the valuable minerals. Primary and secondary crushing is followed by milling to produce the desired particle size distribution as mill product. In the next phase, extraction, the flotation process extracts the valuable mineral from the milled ore typically employing regents. The extracted product is then further refined at high temperatures and with chemical treatments to purify the valuable mineral. Extraction by flotation is the focus of this study.
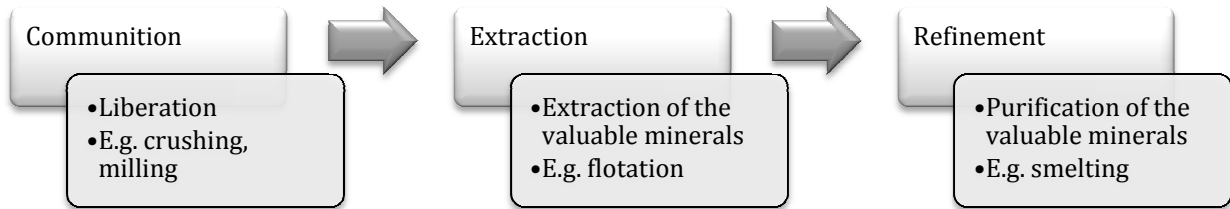
Communition	Extraction	Refinement
• Liberation • E.g. crushing, milling	• Extraction of the valuable minerals • E.g. flotation	• Purification of the valuable minerals • E.g. smelting

Figure 1.1: Minerals processes.

In flotation, an understanding of processes occurring in the froth phase has long been held key to understanding the overall behaviour of froth flotation systems (Glembotskii 1972; Cutting et al. 1986; McKee 1991; Mathe et al. 1998). The structure of froths developed on the pulp surfaces of industrial scale froth flotation cells has a significant effect on both the grade and recovery of valuable minerals in the concentrate. These effects are well known at the process operation level, so that in practice, experienced plant operators are able to visually classify froth types into different categories, each of which is associated with a typical operating strategy (Moolman et al. 1996a; Holtham et al. 2002). Although experienced process operators are able to infer the state of the flotation system from the appearance of the froth, they may not be able to diagnose conditions associated with more subtle structures in the froth, or be able to control the system with consistent reliability. This need, coupled with rapid improvement in instrumentation and computer infrastructure, has led to the development of machine vision systems for froth image analysis early in the previous decade. Since the initial work done by Symonds et al. (1992) and Moolman et al. (1994), these systems have seen rapid growth and commercialization. Unfortunately, not all mineral types processed have benefitted equally from these developments.

Figure 1.2 shows a pie chart that gives an indication, based on published work, of the application of froth imaging systems for the different mineral types in the mineral processing industry. The majority of applications ($\sim$ 48.2%) have been reported in the base metals (BM) industry, which mostly includes copper, lead and zinc, with a few papers related to nickel, magnesium and tin. Application in the coal industries ($\sim$ 30.4%) ranks second, followed by application in the

precious metals industry (~ 12.5%) e.g. the platinum group metals (PGM) represented here. The balance of the applications reported in the literature (~ 8.9%) is associated with oxides, such as P_2O_5, SiO_2 and CaO. Although these applications were successful, not all of these were implemented successfully into the plant control system.
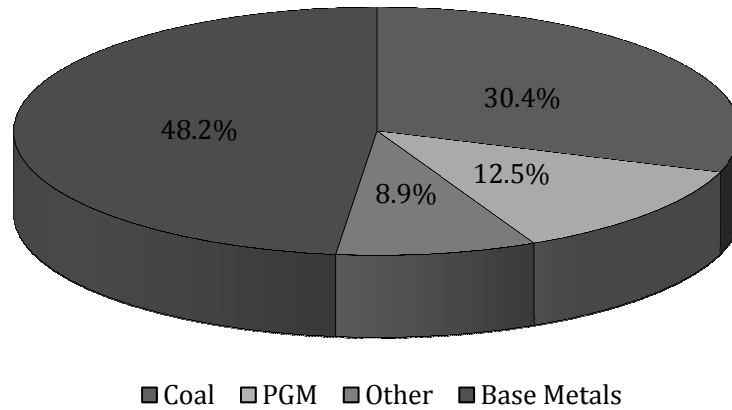

Figure 1.2: Application of machine vision systems in the metallurgical industries, as reported in literature (adapted from Aldrich et al. (2010)).

Flotation control is complex, meaning that the reversal of a series of changes will not necessarily cause the system to return to its original state (Carter 2010). Furthermore, froths with similar appearances may be caused by different sets of metallurgical parameters (Moolman et al. 1995b). The flotation of ore in which trace amount of minerals are present (e.g. platinum flotation) is also considered to be more difficult to control than the flotation of ore that is rich in valuable mineral (e.g. copper and zinc). In light of these challenges the successful and efficient control of machine vision systems has not yet fixed itself in the precious metals industry. This thesis will look closer at platinum flotation and the feasibility of using froth image information to predict platinum flotation froth grade for the purpose of monitoring flotation systems with the use of machine vision.

2. OBJECTIVE

The objective for this study is to

> *Evaluate the feasibility of using froth image information to predict platinum flotation froth grade.*

This will be accomplished with

– a critical literature survey on the use of machine vision for flotation monitoring and control
– the collection of flotation froth images from a laboratory study and an industrial case study
– the extraction of image features from collected flotation froth images
– an investigation of the relationship between image features and froth grade

– the application of linear and non-linear models to predict flotation froth grade from image features

3. SCOPE

Although this project attempts to address some issues regarding monitoring and control solutions for flotation plants, this project does not provide a solution ready for implementation. The study explores the possibilities of predicting the concentrate grade from image analysis and aims to prove the concept. The techniques used are not necessarily the best for the specific application, as the objective was not to find the best solution, but rather to find an indication that a solution might be possible given that further research is done. This research project evaluates the prediction of froth grade as a key performance indicator, although many other indicators such as mass pull and recovery may be considered, they are not included in this thesis.

4. LAYOUT

This thesis will look at metallurgy and the role of significant operating variables on the flotation of valuable minerals. The insight gained from the literature study will aid in understanding and interpreting results from laboratory and industrial experiments. The setup in the industry will be introduced and the control strategies that are typically applied will be discussed briefly. After this the use of image analysis on flotation froths will be explored. The materials and methods used will be presented, followed by results and discussions. Finally, conclusions will be drawn with recommendations for future research and action.

CHAPTER 2
LITERATURE REVIEW

1. THE BASIC CONCEPTS OF FLOTATION

Comminution processes are followed by extraction techniques for the retrieval of valuable minerals. In this study the extraction of PGMs through the process of flotation was examined. The microscopic and macroscopic processes within the flotation process will be addressed in this section.

Mill product, in the form of fine ore particles, is transferred to a flotation cell. Reagents are added to manipulate the mineral surface and pulp fluid properties. Air is introduced to the cell from the bottom as illustrated in Figure 2.1. As bubbles travel through the pulp, hydrophobic rendered mineral particles (PGMs) attach to the bubble surface due to bubble-particle interaction. Once bubbles have risen to the top, they enter the froth phase. Layers of froth build up as more bubbles pushes from beneath. The froth overflows a weir at a certain height and flows to a concentrate sump.

Figure 2.1 A single mechanical flotation cell.
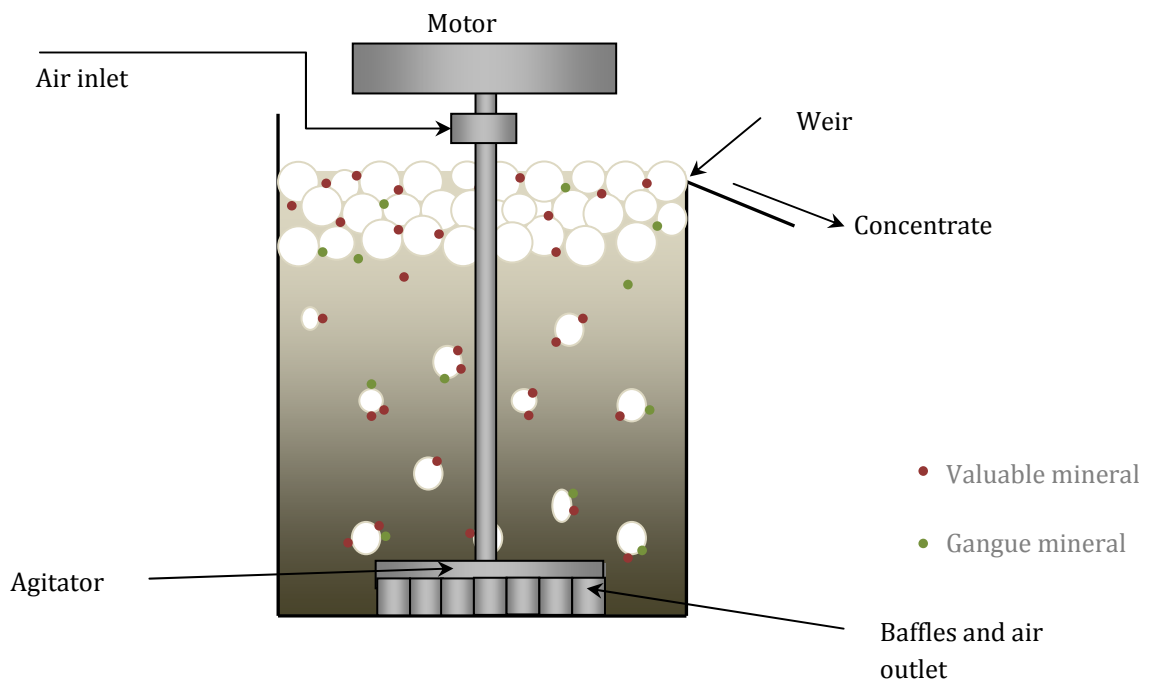
The relationship between input and output variables to the flotation process (as illustrated in Figure 2.2) is now considered. The ore type, reagents and process conditions are all input variables that affect the flotation process. The flotation process is often described in terms of two phases namely the froth and pulp phases (Vera et al. 2002; Mathe et al. 1998, 2000). The

role of each input variable will be discussed with specific emphasis on PGM flotation. Thereafter the effects of the input variables on the flotation process will be discussed in terms of the two phases followed by a discussion on the effects of the flotation process on the visual and target output variables.
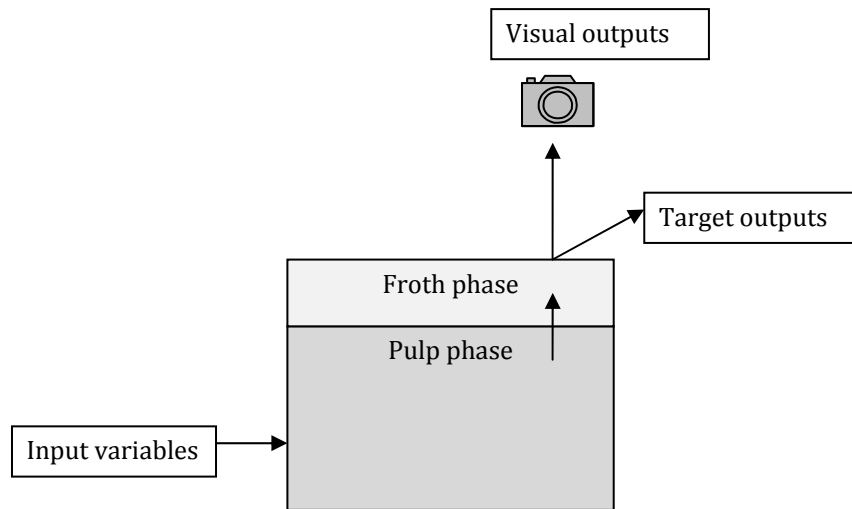

Figure 2.2: Illustration depicting the relation between input variables and output variables for a single flotation cell.

1.1 Input variables

Ore type, reagents and process conditions affect the pulp and froth phases. It is therefore important to understand the role that input variables play. The roles of the significant input variables will be briefly discussed.

1.1.1 Ore type

In South-Africa, platinum group metals are found in the Bushveld Igneous Complex (BIC). The Merensky Reef and the Upper Group 2 (UG2) Reef are mined from the BIC. These two reefs both comprise layers of chromite (~70 wt%) and metal-rich seams. These metal-rich seems consist predominantly of platinum, palladium, rhodium and ruthenium which form the platinum group metals (~4 ppm). Other gangue minerals are pyroxene (~20 wt%), feldspar (~5 wt%), talc (~3 wt%) and base metal sulphides (<1 wt%). (Ekmekçi 2003)

1.1.2 Reagents

Reagents alter the structure and composition of the adsorption layers on the bubble surface, and the nature of the mineral coating on these surfaces. There are two primary reagents used in flotation, namely collector and frother. Modifier reagents are often utilised to manipulate the chemical environment for optimal performance.

i.   Collector

Most ore types, including BIC ores, are naturally hydrophilic. Collectors are reagents that adsorb onto the mineral surface by means of an electrochemical mechanism, as illustrated in Figure 2.3, rendering the mineral particle hydrophobic. Hydrophobic mineral particles

attach to air bubbles, and are transported to the froth phase. Flotation without the addition of a collector is impossible as minerals are naturally hydrophilic. Collector is used in small amounts to ensure a monomolecular layer on the particle surface (starvation state). An excess of collector addition to the pulp can however decrease selectivity and therefore also decrease the product quality. It could also result in the development of a multi-layer of collector molecules on the particles, which decreases the hydrophobicity. This will adversely affect the recovery of the valuable mineral to the product. Xanthates are typical PGM collectors. (Wills 1997; Gupta et al. 2006)
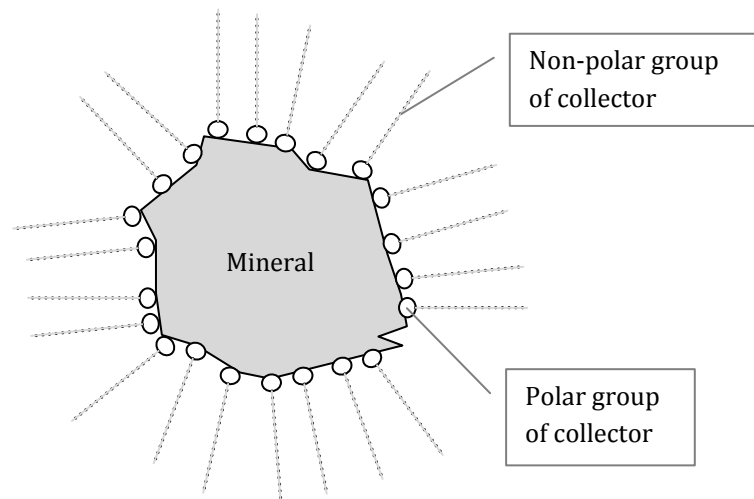

Figure 2.3: Illustration depicting the attachment of collector molecules to the mineral surface.

ii. Frother

Frothers have a molecular architecture that is similar to collectors. The attachment of the frother molecules to air bubbles is illustrated in Figure 2.4. Frothers are responsible for reducing the surface tension by interacting with the water content of the slurry. This reagent improves dispersion of air bubbles in the pulp phase and provides a stable air-water interface in the froth phase to avoid particle drop-back to the pulp. Stabilisation of the froth occurs when the frother adsorbs on the air-water interface due to its surface activity. The addition of excess frother to the pulp can lead to an overly stable froth causing difficulties for downstream processes such as transport through pumping and dewatering through thickening. (Wills 1997; Gupta et al. 2006; Finch et al. 2008)
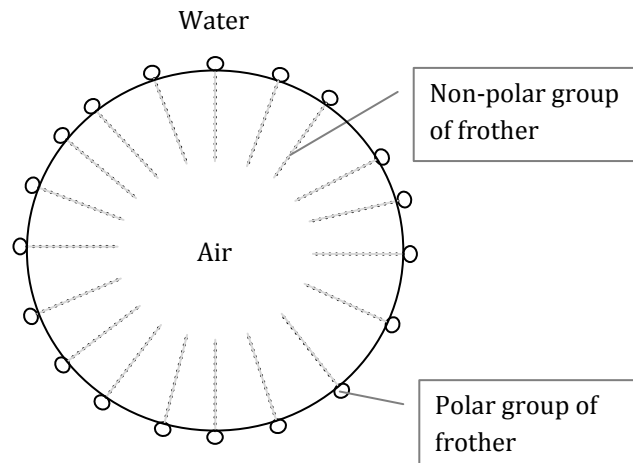
Figure 2.4: Illustration showing the stabilising action of frother molecules.

iii.   *Modifiers*

Modifiers are reagents used to manipulate the environment of the pulp for improved flotation performance e.g. activators, depressants and pH modifiers. Each of the modifiers is discussed briefly.

a   Activator

The activator reagent alters the chemical nature of the mineral surface, to allow collector absorption. The activator therefore regulates the mineral surface areas covered by collector. Great losses in PGMs occur when pyrrhotite is poorly floated. Copper sulphate ($CuSO_4$) is added for the activation of the pyrrhotite ($Fe^{2+}_{0.95}S$) surface. Copper sulphate, like many other activators, is a soluble salt that ionise in solution to form copper sulphide according to the following reaction:

$$FeS + Cu^{2+} \leftrightarrow CuS + Fe^{2+}$$
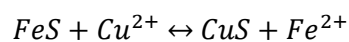
The copper sulphide reacts with xanthate to form insoluble copper xanthate to render the pyrrhotite surface hydrophobic. (Wills 1997; Bradshaw et al. 2006)

b   Depressant

Depressants are used to regulate selectivity by retarding the attachment of the collector to the mineral surface. In some cases depression occurs naturally when slime coats the mineral surface. Polymeric depressants, e.g. guar gums, work in a similar fashion and are used for PGM flotation. (Wills 1997; Gupta et al. 2006)

c   pH modifiers

The addition of reagents affects the pH of the pulp. According to Wills (1997a), for any concentration of xanthate collector, there is a pH value below which any given mineral will float and above which it will not float. The critical pH value depends on the nature of the mineral, collector type and concentration, and temperature. It is therefore important to have a delicate balance between reagent concentrations and the pH of the pulp. Flotation is typically carried out in an alkaline environment where most collectors are

stable and corrosion to equipment is minimal. The pH is regulated by the addition of lime or sulphuric acid. (Wills 1997)

1.1.3 Impeller speed

Mechanical agitation is the main driving force of the bulk fluid movement while the flow pattern is governed by the cell characteristics e.g. geometry of the cell and impeller. The impeller imparts kinetic energy that allows efficient gas dispersion and particle suspension while also facilitating bubble-particle interaction. (Deglon 2005; Gupta et al. 2006)

1.1.4 Air flowrate

The air that enters the flotation cell carries the hydrophobic rendered particles into the froth phase due to the upward buoyancy force acting on each bubble. The rate of air flow is known to influence the froth stability and consequently also influences the flotation cell performance. More insight will be given in the discussion of the variable effects. (Hadler et al. 2009; Laplante et al. 1983a, 1983b; Laplante 1984)

1.1.5 Aperture size

The size of air bubbles in the pulp influences the particle-bubble interaction in the pulp phase. Bubble size is determined by the aperture size of the air inlet among others discussed elsewhere (section 1.2.1 – i). (Moolman et al. 1996b; Gupta et al. 2006)

1.1.6 Particle size distribution

The particle size distribution is chosen to ensure sufficient liberation of the valuable mineral and still be of a floatable size. For a given ore type, there exists a maximum particle size above which the particle cannot be floated due to the large gravitational force associated with heavy particles. (Trahar 1981; Moolman et al. 1996b; Gupta et al. 2006)

1.1.7 Pulp level

The pulp level is used to control the height of the froth in a flotation cell. The froth height is an important parameter considered when steering the cell performance to its target performance. Section 1.2.2 will give more insight into this matter. (McKee 1991; Muller et al. 2010)

1.1.8 Temperature

The temperature of the slurry is not controlled due to energy considerations. Slurries from the mill generally have more energy than slurries later in the process when it will have cooled down naturally. Although temperature is not varied purposefully, it does have some effect on the flotation. Temperature may influence the rate of flotation depending on the ore type treated. More generally, temperature affects the froth phase viscosity. (O'Connor 1990; Moolman et al. 1996b)

1.2 The flotation process

This section will briefly describe the effects of significant input variables on the flotation process in terms of a two phase description of the flotation process (Figure 2.5), a concept that is widely

acknowledged (Mathe et al. 1998; Vera et al. 2002; Yianatos et al. 2008). The purpose of each phase is defined, followed by a discussion of the influence of relevant input variables on the performance of each phase.
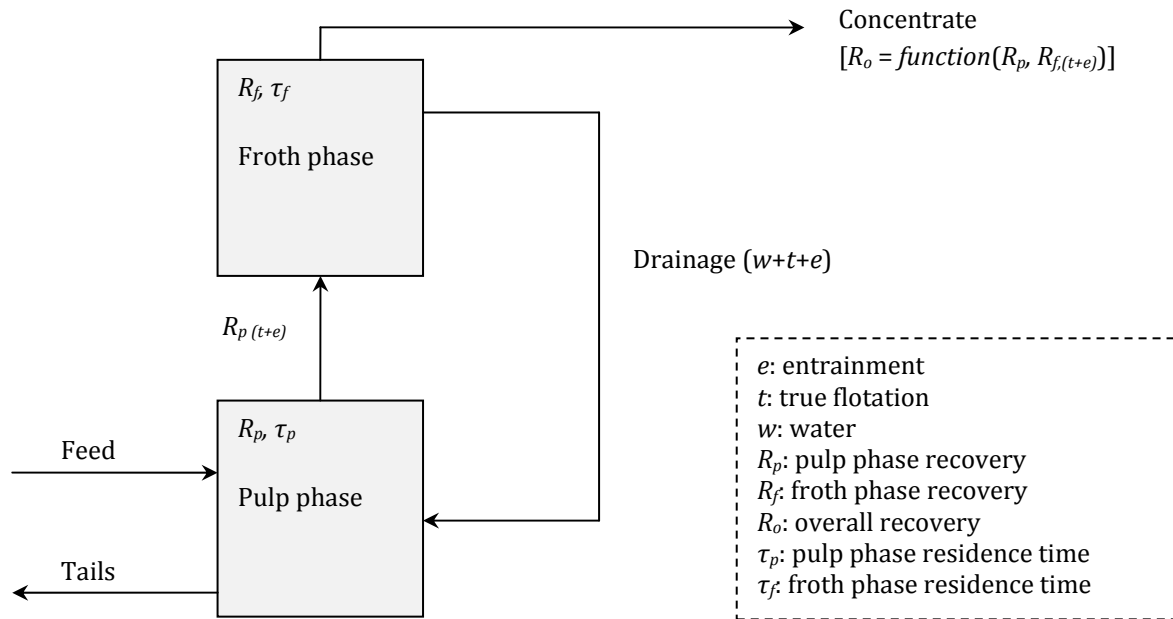

Figure 2.5: Two-phase flotation process (Mathe et al. 1998; Vera et al. 2002).

1.2.1 *Pulp phase*

The pulp phase in the flotation cell is the region where bubble-particle interactions occur to facilitate the collection of minerals onto the air bubble surface to produce bubble-particle aggregates. Bubble-particle interactions occurring in the pulp phase are governed by a number of forces: hydrodynamic resistance, inertial forces, gravitational forces, surface forces and capillary forces. They can be quantified by considering the bubble-particle interactions of collision, attachment and detachment independently. The overall probability of collection (γ_o) can therefore be described as the probabilities of these parts: γ_c - probability of collision; γ_a - probability of attachment after collision; γ_d - probability that detachment will occur. (Nguyen et al. 2009; Shahbazi et al. 2009)

$$\gamma_o = \gamma_c \gamma_a (1 - \gamma_d) \tag{1}$$

The overall probability of collection is directly related to the material recovered to the froth phase (R_f) which is the performance indicator of the pulp phase.

i. *Collision*

Collision is governed by bubble and particle mechanics as well as the physio-chemical aspects of water flowing around bubbles in the presence of the reagents. The probability of collision can be related to the number of particles and the number of bubbles in the flotation cell. Increasing amounts of either creates more interaction opportunities. The collision probability is also promoted as turbulence increases. The aperture size of the air inlet, the air flowrate, the addition of frother as dispersion agent, the impeller speed and the solids

concentration inside the flotation cell are all input variables affecting the collision probability. Their directions of effect on the collision probability are illustrated in Figure 2.6. (Nguyen et al. 2009; Shahbazi et al. 2009)
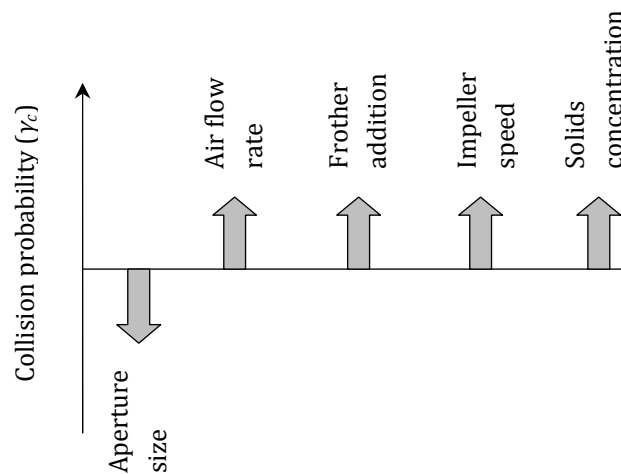

Figure 2.6: Diagram indicating the directions of the input variable effects on the probability of collision inside the pulp phase of the flotation cell for increasing magnitudes of each variable.

ii.   *Attachment*

The probability of attachment is determined by the surface area on the mineral that is available for collector adsorption, as well as the surface area on the bubble that is available for attachment. Attachment is a function of intermolecular and colloidal forces. This implies that the probability of attachment depends on the collector, activator and particle properties of the mineral surface on a molecular level. The amount of bubbles and their size influences the collective bubble surface area available for attachment of the mineral onto the air bubble. (Nguyen et al. 2006, 2009)

iii.   *Detachment*

The detachment probability is influenced by capillary force, particle weight and the turbulent eddies caused by a bubble's rise through the pulp. Increased turbulence in a flotation cell does not only increase the probability of collision, but unfortunately also increase the probability of detachment, although to a lesser extent. The opposing forces of gravity and buoyancy on the attached minerals also affect the detachment probability. If the gravitational force is excessively high, the particle will detach from the bubble. (Nguyen et al. 2009; Dai et al. 1999)

1.2.2   Froth phase

The froth phase in a flotation cell is the region where the bubble-particle aggregate from the pulp phase collects and undergoes further sub-processes to improve the pulp phase product quality. The following transfer processes occurs in the froth phase: selective transfer of material from the pulp phase to the froth by particle bubble attachment (true flotation); non-selective transfer of material from the pulp phase to the froth by entrainment; drop back of material from

froth to the pulp phase (selective and non-selective); and mechanical or hydraulic transfer of material from the froth phase into the concentrate. The performance of the froth phase is defined by the total amount of valuable material reporting to the concentrate with respect to the pulp phase product, i.e. the froth phase recovery (R_f). These transfer process are summarised subsequently. (Mathe et al. 1998)

i. *True flotation*

Bubble-particle aggregates rising from the pulp phase travel through the pulp-froth interface. These bubble-particle aggregates gradually move up in the froth layer as the top layer is removed from the flotation cell and more bubble-particle aggregates enter from below. True flotation refers only to particles that have attached selectively to bubbles due to their hydrophobicity. True flotation is therefore mainly dependent on the performance of the pulp phase.

ii. *Entrainment*

Entrainment is a non-selective process whereby fluid from the pulp phase carrying unattached particles enters the froth phase. Unattached particles are carried upwards through the interface due to an upwards water flux caused by the upward movement of the bubble-particle aggregates. The magnitude of the upwards water flux is mainly dependent on the rate of air flow. The amount of entrained material reporting to the concentrate is primarily determined by the characteristics of the froth phase rather than the conditions in the pulp phase. The mass of entrained particles have been found to decrease exponentially with increase in froth height as these unattached particles drain from bubbles. (Neethling et al. 2002a; Mathe et al. 1998)

iii. *Drainage*

Drainage is the sub-process in flotation whereby fluid and particles travel down the froth boundaries due to gravitational forces as illustrated in Figure 2.7. The aqueous bubble shell is the layer around the bubble that contains mostly hydrophobic particles, forming the bubble-particle aggregate. The next layer is the inter-bubble lamella, which consist of liquid and unattached particles. Unattached particles in the lamellae can fall out of the froth phase back into the pulp phase or they can reattach to the bubble-particle aggregates below. The probability of unattached particles falling out of the froth is governed by the lamella properties, downward gravitational forces as well as upward water flux. Drainage is an important part of the upgrading of the ore through flotation as it enhances the selectivity of the process. (Neethling et al. 2008, 2002; Cilliers et al. 1998)
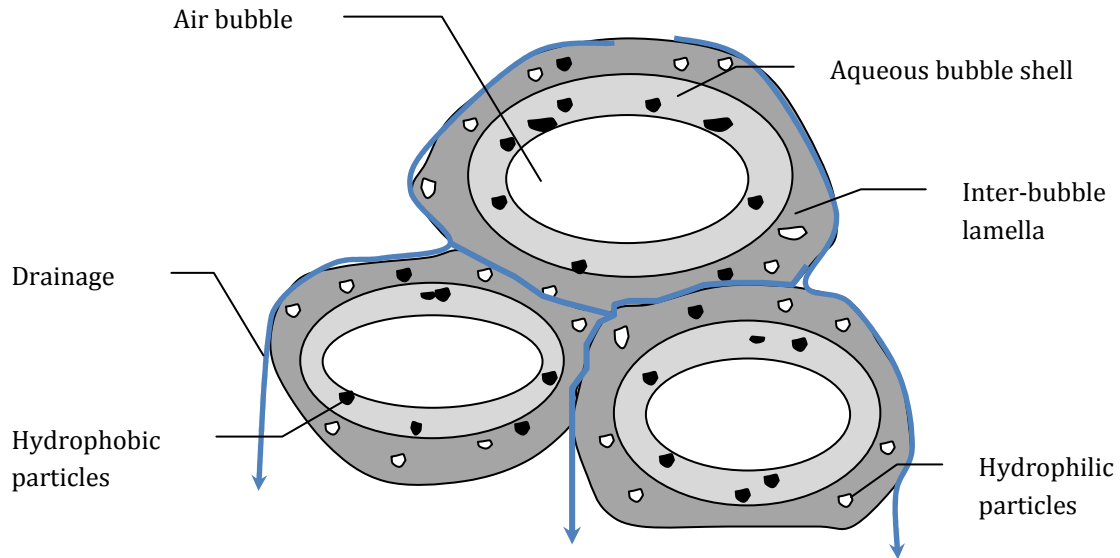
Figure 2.7: Illustration of the inner workings in the froth phase as suggested by Cilliers et al. 1998.

iv.   Froth transfer

Froth transfer refers to the movement of the froth in the horizontal direction towards the weir where it overflows to the concentrate stream. The rate of froth transfer is related to the froth residence time which can be manipulated by adjusting the pulp level and the air flowrate (Supomo et al. 2008; Muller et al. 2010). Some flotation cells are equipped with a mechanical paddle to scrape the froth into the concentrate overflow (Gupta et al. 2006; Wills 1997).

1.3   Output variables

Output variables refer variables that can be measured to give an indication of the flotation performance. Flotation performance is measured both by visual inspection and product quality and quantity measures.

1.3.1   Visual outputs

Certain effects of the flotation process variables can be detected by evaluating the appearance of the froth. The froth appearance is based on the uppermost froth layer and is therefore mostly affected by the froth phase characteristics and performance.

i.   Bubble size

The upper froth layer bubble size is a product of both the pulp and froth phase conditions and performances. The pulp phase conditions influencing the bubble-particle aggregate size at the pulp-froth interface are the aperture size at the air inlet and bubble dispersion. The froth phase conditions influencing the upper froth layer bubble size are the froth residence time and the rate of drainage as determined by the lamellae properties. (Moolman et al. 1996b)

ii.   Bubble shape

The shape of the bubbles in the upper froth layer is mostly determined by the froth layer depth. Bubble-particle aggregates with aqueous bubble shells and lamellae that are thick and watery have a much rounder appearance due to fluid filling the spaces between them. As layers become thinner due to water drainage, aggregates push against one another and compete for space. As aggregates crowd around one another, their shapes take on a polyhedral form. Ongoing drainage may also cause the film between two adjacent bubbles to rupture and form a single, larger bubble. Similar to bubble size the key froth phase contributors to the upper froth layer bubble shape are froth residence time and the rate of draining due to the lamellae properties. (Moolman et al. 1995b, 1996b)

iii.   Velocity

The velocity of the upper froth layer refers to the speed of horizontal movement of the froth towards the weir. The velocity relates to the froth residence time and is primarily manipulated by the pulp level and air flowrate settings.

iv.   Stability

Froth stability is defined as the amount of bubble bursts per unit area in the upper layer of the froth. These instabilities can be ascribed to either of the following events: (1) bubbles are not stable due to a weak structure and consequently burst; or (2) bubbles are too stable and cannot support the heavy mineral load leading to collapse. Fortunately, it is easy to distinguish between these two events as the bubble size, shape and colour will reveal the source of the instability. It is widely acknowledged that the froth stability is largely dependent on the air flowrate to the cell due to its effect on the froth phase characteristics, more particularly the rate of drainage. (Moolman et al. 1996b; Hadler et al. 2009)

v.   Colour

The intensity value of the froth expressed as a greyscale value reveals information regarding the mineral loading on the bubbles. Red, green and blue colour components are dependent on the ore type and its composition and may also reveal information regarding the froth composition. (Hargrave et al. 1996, 1997; Kaartinen et al. 2006a)

1.3.2   Target outputs

The most commonly used key performance indicators (KPIs) of the flotation process are that of recovery, grade and mass pull.

i.   Recovery

The overall recovery represents the total mass of valuable material that report to the concentrate as a percentage of the total mass of valuable material that was fed.

$$\% \, R_o = \frac{m_P}{m_F} \times 100 \qquad\qquad (2)$$

The total recovery is the combined effect of the pulp and froth phase recoveries. The residence time of the froth should be sufficient to allow the bulk of the entrained particles to drop back into the pulp so that the concentrate quality is not compromised excessively.

ii. Grade

The concentrate grade represents the upgraded product quality and is the total mass of valuable material that reports to the concentrate as a percentage of the total mass of solids reporting to the concentrate.

$$\% \, G = \frac{m_{P,PGM}}{m_P} \times 100 \qquad\qquad (3)$$

Factors influencing flotation selectivity, such as collection and drainage, are important for producing concentrate of a desirable grade.

iii. Mass pull

Mass pull is simply the mass of the concentrate overflowing the weir. Mass pull can be regarded as a KPI as plants require a certain throughput of product. The pulp phase recovery and froth residence time are key parameters influencing the mass pull. The mass pull is mostly manipulated by adjusting the air flowrate and pulp height. (Supomo et al. 2008; Muller et al. 2010)

2. FLOTATION IN PRACTICE

2.1 Industrial setup

Flotation in industry is a continuous process wherein a number of flotation cells are linked in series to form a bank of cells as illustrated in Figure 2.8. The overflowing concentrate of each cell and final tailings of a bank are sent to the appropriate downstream processes based on expected grade. The tailings stream is used to regulate the pulp levels inside the bank.
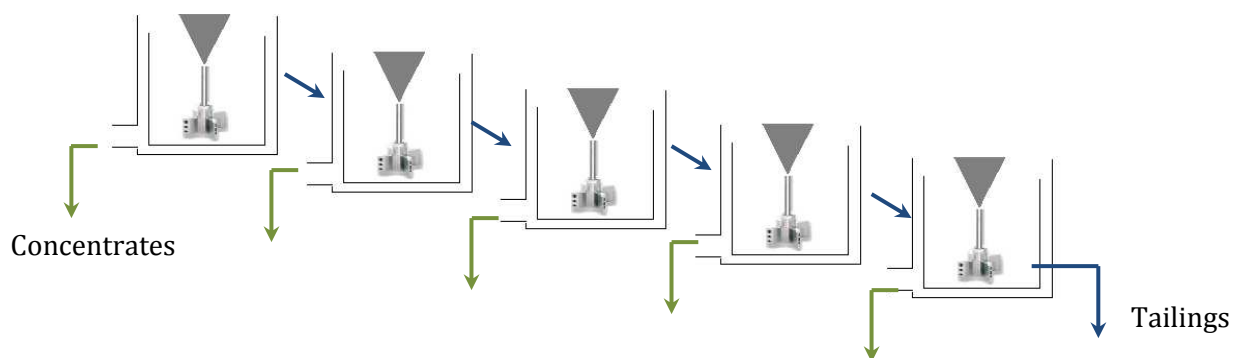

Concentrates

Tailings

Figure 2.8: Diagram of cells in the flotation bank.

A flotation circuit consist of a number of flotation banks, each with a different function. In a basic flotation circuit there are two sections: the rougher section and the scavenger section (Figure 2.9). There are typically two sets of banks in each of the rougher and scavenger sections: the primary banks and the cleaner banks. Each bank of cells has a different objective. The primary banks typically aim to recover as much valuable material as possible, from which the cleaner banks will upgrade the recovered material to obtain the desired grade. Due to the complex configuration of the concentrate and tails process streams of the flotation section as well as the varying feed compositions and characteristics, the overall flotation process requires a control solution able to cater for each one of these factors given certain target set points.
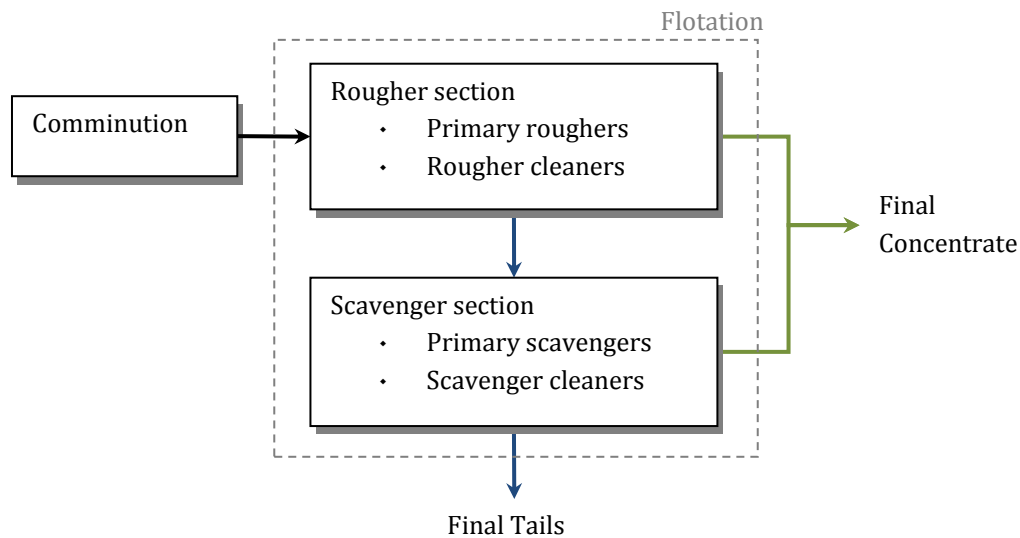

Figure 2.9: Diagram of the basic layout of a flotation circuit.

2.2   Advanced control strategies

Expert knowledge is incorporated in flotation control through operator experience and intervention. The current industrial strategy relies on the operator presence on the plant as well as their ability to observe while keeping the objectives for each bank in mind. This strategy is also dependent on the troubleshooting abilities of the operators and their interpretation of the froth appearance which is limited to their experience and training. Inconsistency is also introduced upon shift change as each operator's judgment is different. Another recent strategy that has been applied successfully involves the mass pull as KPI. Each cell has a target mass pull based on the target performance indicators for the specific cell. The air flowrate and pulp level is manipulated to adjust the mass pull to the desired setpoint using generic rules. The mass pull is a calculated from flow meters and densitometers where available, otherwise it is inferred from the air flowrate and pulp level. Since the introduction of machine vision systems in the 1980's a lot of research and development effort has gone into the use of machine vision systems as an alternative for or addition to existing flotation control strategies. (Muller et al. 2010; Supomo et al. 2008)

Process control strategies based on the online availability of froth features can be grouped into four categories. The first is based on the identification of froth structures, indicative of specific process conditions with which specific control actions can be associated. The second can be

termed inferential control, where the froth features are used to infer operational variables in the process, such as the reagent concentration in the froth, or the recoveries and grades in flotation cells. The third strategy is based on the use of process maps or control charts, which can be used to detect deviations in the process and possibly identify the nature of these conditions and control actions required to rectify these conditions. Finally, in a more recent development, froth image variables (e.g. colour, bubble size, bubble shape, velocity, stability, etc.) have been included in what can be termed classical control strategies. These will be investigated in more detail in section 3.1. (Aldrich et al. 2010)

Unfortunately only a few commercial systems have been developed and used in the industry. The following table (Table 2.1) gives an overview of the major commercial froth imaging systems, viz. VisioFroth (Metso), SmartFroth (University of Cape Town, UCT), JKFrothCam (Julius Kruttschnitt Mineral Research Centre - JKMRC), AceFlot (Chile), FrothMaster (Outokumpu). Several of these systems have had their origin in cooperation between academia and industry. For example, SmartFroth was developed by the University of Cape Town and Stone Three in South Africa, JKFrothCam between the University of Queensland and JKMRC in Australia, Frothmaster was originally developed at the University of Stellenbosch in South Africa, and AceFlot had its origins at the Catholic University of Chile. (Aldrich et al. 2010)

Table 2.1: Commercial flotation froth imaging systems.

System	AceFlot	Frothmaster	JKFrothCam	SmartFroth	VisioFroth
Company/ Institution	Chile	Outokumpu, Finland	JKMRC, Australia	UCT, South Africa	Metso
Year of Launch	1994	1996	1999	2000	2001
Major Installations	Chile	Finland, Cadia Valley, Australia	Australia	Anglo Platinum (South Africa)	Escondida (Chile), Freeport (Indonesia), Australia

All these systems are capable of estimating bubble size distributions, typically by means of segmentation algorithms, froth colour, froth speed and stability, as well as a wide array of other froth statistics, and as such there appears little that differentiates the software on the basis of analytical capabilities. In commercial installations, these systems are often integrated with plant-wide process control software.

2.2.1 Advantages of machine vision systems

One of the major advantages of machine vision systems is the consistency with which the appearance of the froth can be analysed. Having consistent quantifiable analysis could be very useful in supporting operators in their decision making. In a recent report by Du Plessis et al. (2010) in the investigation of sampling frequencies of concentrate grade, a sampling period of

shorter than 1.9 minutes is required to avoid aliasing. This sampling frequency is not currently possible. Machine vision would allow an even higher sampling frequency. Both higher and lower frequency data can be recorded in an historian database from which it will also available for research and development purposes, offline fault diagnoses and operator training. Machine vision systems also allow a constant availability of data. Permitting that the hardware is working, all cells can be monitored uninterrupted while remaining non intrusive to the process. The immediate availability of data with almost no time delay in results means that data is available in real time and can be implemented in a control loop. Closed loop control could be implemented by implementing machine vision as a monitoring tool. Such control is not feasible when operators manually manipulate cells. (Forbes 2007a; Van Schalkwyk 2002; Wright 1999)

2.2.2 Problems and limitations of machine vision systems

There are some physical constraints related to the setup of a machine vision system on the plant. The camera should be situated at an appropriate location that takes a recording representative of the whole cell which is not always possible. Furthermore, the camera should be able to withstand extreme plant and weather conditions as it will be exposed to a harsh plant environment. Initialising a system will require that calibration and model building is done per cell. The data necessary for model building should include most of the operational states to ensure that the variability of the process is captured. Making changes to setpoints for this purpose should be done very carefully as continuous and satisfactory plant performance is prerequisite. Therefore it is suggested that model building is done on historical data over a long period of time. This will unfortunately take longer and the actions of the operators will have to be taken into account e.g. manually changing valve positions, cleaning cells, etc.

Once implemented the maintenance e.g. cleaning the lens of the camera is important. The model implemented should be also validated on a regular basis to ensure that it is still applicable. One of the biggest problems in this regard is the influence of variability in ore type. This is one of the most difficult disturbances to detect and correct for on the plant.

3. FROTH IMAGE ANALYSIS

3.1 Machine vision control research and development

Research and development into the application of machine vision in froth flotation systems has increased rapidly since its introduction in the late 1980's. During this time various ways to connect the froth image features to target outputs for flotation cells have been investigated in order to control cells more effectively. These control strategies are discussed in detail in this section together with its commercial applications.

3.1.1 Identification of froth structures representative of known operational states

One of the first applications of machine vision systems was to identify froth structures, in accordance with plant practice, where operators identify froth structures as an indication of the condition of a flotation cell. Features describing the froth appearance are typically used as predictor variables to identify predefined froth classes, which are in turn determined by

heuristic experience from plant staff. Since this is a classification problem, any of a large number of classifiers can be used, such as linear discriminant analysis, learning vector quantisation neural networks, nearest neighbour methods, multilayer perceptrons, etc. Apart from assisting process operators, this approach also lends itself to supervised control by means of expert or knowledge-based systems (e.g. Cipriano et al. 1997, 1998). Aldrich et al. (1997b) have shown that such classifiers can also be automated for inclusion in fuzzy control systems by use of inductive trees and genetic algorithms. Cipriano et al. (1998) have reported the use of a machine vision system (AceFlot) to extract an array of features from froths in copper flotation rougher cells, which are then used by a knowledge-based system with IF-THEN rules to identify the operational state of the flotation cell and the corresponding control action required. Bonifazi et al. (1999) have used a combination of features reflecting froth colour and bubble morphology to define froth classes based on mineral content. Zhu et al. (2008) reported the use of leaning vector quantization neural networks and rough sets to identify the state of a haematite flotation plant based on textural features extracted from digital images of the froth.

3.1.2 *Inferential estimation of operational variables*

A key froth control issue is the question of which variables are the most important and should be measured, and how they affect the flotation performance. Some important variables are not easy to measure or their results are not readily available. To overcome this problem, variables that are measurable, of which image features are an example, can in some cases be used to infer this important but unavailable variable. Various froth models have been developed and explored to identify the key variables. The two most prominent model types for are 1) fundamental CFD-type models based on the froth physics, and 2) semi-empirical models, such as proposed by Zheng et al. (2004). Semi-empirical models often use simplified equations derived from fundamental models. Cilliers (2009) has recently reviewed physics-based froth simulation and some of the simplified equations from that approach.

An understanding of the fundamental phenomena occurring in the froth phase is essential for forming generic relationships between froth features and the flotation performance. More recently, the air recovery, the fraction of air entering the cell that overflows into the concentrate rather than bursting on the surface, has become more widely recognised as being important. This is a form of froth stability measurement.

In the fundamentally-based froth models of Neethling and co-workers, the air recovery is a necessary boundary condition to calculate the froth flow lines. Further, a number of simplified flotation relationships have been derived from the full differential equations; overflowing liquid rate (Neethling et al. 2003a), froth recovery (Neethling et al. 2008) and entrainment (Neethling et al. 2009). All these relationships include the air recovery explicitly. The overflowing liquid rate model (Neethling et al. 2003b) is based on foam drainage theory and, for unstable froths such as in roughers and scavengers, depends strongly on the air recovery. This model was demonstrated to accurately predict the water recovery in two-phase foam systems, and, with some calibration, also three-phase froth systems (Zheng et al. 2006).

The semi-empirical froth-based flotation model by Woodburn et al. (1994) combines a conceptual froth structure with the kinetics of flotation. They base the flotation kinetics on the flux of bubble surface area overflowing from the cell:

$$\Psi_b = R_\alpha Q_\alpha S_b \approx (\zeta \; v_f \; h_f \; c) \; S_b \tag{4}$$

In this model the flux of bubble surface area (Ψ_b) is calculated from the volumetric air flowrate into the cell (Q_α), the specific bubble area (S_b) and the air recovery, R_α. This is approximately the same as relating Ψ_b to the specific bubble area, froth velocity (v_f), froth height (h_f), weir width (c) and the volume fraction of the froth that is air (ζ), usually taken as unity. Although they do not directly measure the air recovery, they estimated it from still images. Ventura-Medina et al. (2002), attempted to relate Ψ_b to the mass flows of valuable material, gangue and water – based on the froth structure (Neethling et al. 1998, 2000; Murphy et al. 1998). Experimental data did not, however, correlate well with the model and this was attributed to varying froth stability. Realising this, Barbian et al. (2003), suggested that R_α could be used as a quantitative indication of the froth stability. The value of α can be calculated by eqn. (5), where froth image analysis is used to determine the velocity of the froth at the surface (Barbian et al. 2005, 2006, 2007). The height of the froth overflowing the weir can be measured conveniently using a laser distance device, or also by image analysis.

$$R_\alpha \approx \zeta \; v_f \; h_f \; c/Q_\alpha \tag{5}$$

It was noted that variation of air rate, froth depth and frother concentration all directly affected the flotation performance due to the direct effect of these parameters on the froth stability. It was also observed that greater air recovery values resulted in improved flotation performance. Recently Hadler et al. (2009) showed that varying the air rate to individual cells in a bank to maximise the air recovery produces the highest recovery. Froth image analysis is a simple method of determining the air flow to obtain this peak in air recovery, by measuring the froth velocity and, potentially, the depth overflowing the weir. This has important implications for control as a single quantitative variable can be measured and maximised.

Cruz et al. (1998) have investigated the application of video-based sensors to analyse the ash content of coal in flotation cells, while Wang et al. (2001) have likewise reported satisfactory results with regression models used to relate the ash content of floated coal to image features. In a separate long term study, Kaartinen et al. (2006b) focused on the control of the zinc flotation process at the Pyhäsalmi Mine in Finland. Using a multi-camera system proved to be very helpful in the analysis of the process. A strong correlation between image variables and concentrate grades were evident. Some of the image variables reacted 15 min earlier on disturbances than the online X-ray analyzer and could in principle be added to the control strategy for significantly improved process performance. Runge et al. (2007) have shown that the concentrate tonnage flow on a copper flotation plant is highly correlated with the froth velocity, while the grades in the cells were related to the velocity, as well as the froth stability.

3.1.3   Use of process control charts

Apart from the identification of specific froth classes as an indication of process conditions, the operator can also be assisted by use of process control charts, where the froth features, and by implication the state of the flotation process, can be tracked online. For example, Moolman et al. (1994) and Van Deventer (1996) used self-organizing (Kohonen) neural networks to map grey level dependence matrix features from froth images to two-dimensional process charts. Jemwa et al. (2006) have discussed the monitoring of froth flotation plants from image features by use

of biplots and kernel methods, as case studies in mineral processing. Although these charts are powerful plant automation tools, interpretation of fault conditions are not straightforward, since these need to be related to the image features. However, Liu et al. (2005) has recently reported an interesting application, where they have demonstrated control of the plant by guiding the process towards a froth exemplar associated with optimal plant performance.

3.1.4   Classical control

The literature on the use of image variables in flotation control is very sparse. In the Esprit LTR Project no 24931 (ChaCo Project) attempting to design flotation control systems exploiting froth image data, it is reported that the flotation processes were so complicated that ordinary model based control design methods could not be applied. The dynamics of the process was sufficiently slow so that froth stability did not appear to be a major problem in control. Instead, the more important issue was to identify a control configuration, which would guarantee satisfactory operation and enable process optimisation. For the majority of the output variables it was difficult to find the best possible reference values in different operating conditions. Therefore the reference values had been replaced by upper and lower alarm limits and the purpose of the control was to maintain the output between these limits. The final optimisation was based on learning during normal operation. These control algorithms consisted of logical IF-THEN statements and had been realized by the PROSCON automation system.

Van Olst et al. (2000) used Outokumpu's FrothMaster system to measure the speed of froth over the lip of a cell and used this information to control the mass recovery of two flotation cells in series which were pulling inconsistently with respect to each other, owing to differences in hydrostatic heads between the cells. According to these authors, they could control the speed of the froth to within 5% of its set point by manipulating the froth level, frother addition rate and the aeration rate. Supomo et al. (2008), having a similar strategy reported an increase in recovery of 3.4% at PT Freeport's copper-gold rougher circuit in Papua, Indonesia. The adaptive control strategy is customised around Metso Minerals' VisioFroth system, which is used to measure the surface froth velocity in individual rougher cells. The froth velocity is directly related to the mass pull and the control system is then used to adjust the froth depth, to optimise the froth velocity and the mass pull.

Kaartinen et al. (2006b) reported the use of the red colour of the froth, bubble size, bubble collapse rate, as well as reagent addition rates to control a zinc rougher flotation circuit. Brown et al. (2001) have reported the use of froth speed, level, frother addition rate and aeration rate in a simple scheme to control a flotation circuit. More recently, Liu et al. (2008) have proposed the use of a causal model to predict future froth appearance based on manipulated and process variables. Their results suggest the possibility of using advanced model based approaches to control flotation circuits based on the appearance of the froth.

Zu et al. (2008) have investigated the use of textural froth features from a hematite flotation process to control reagent addition to the plant. A learning vector quantisation neural network, as well as rough sets were used to estimate the state of the process and hence the required adjustment to the reagent dosage.

More recently, Núñez et al. (2008, 2009) have discussed the development of dynamic models for control of flotation plants. These state space (autoregressive moving average) models were based on the analysis of sequences of froth images and could be used to predict the froth dynamics, including froth speed, satisfactorily. These predictions could be used as virtual measurements for expert control.

3.1.5   Overview of selected success stories

A few selected successes are summarised in Table 2.2, proving that froth image analysis has the potential to significantly impact plant production and control. Image analysis was mostly applied to identify predefined operational states and was often implemented as expert systems. Although some research has shown that grade can be predicted with image features, the successes were mostly in the base metal industry. The opportunity for evaluate the feasibility of using image features alone to predict key performance indicators are therefore evident from the literature especially in the precious metal industry.

Table 2.2: Overview of selected success stories.

Authors	Flotation system	Froth features	Model type	Comments
Aldrich et al. 1997b	Copper	Texture features	Classification trees Back propagation neural network classification	91.4% classification accuracy of froth type (runny, ideal, sticky) 95% classification accuracy of froth type (runny, ideal, sticky)
Cipriano et al. 1998	Copper	Colour, stability, velocity and bubbe size and shape	Fuzzy logic controllers using froth features	Development of commercial system AceFlot
Bonifazi et al. 2000	Complex sulphide ore	Bubble shape and colour	Multiple regression	Zn grade forecast from colour, bubble 3D fractal dimension and reagent dosage with $R^2 = 0.95$ Pb grade forecast from colour, bubble 3D fractal dimension and reagent dosage with $R^2 = 0.89$ MgO grade forecast from colour and 3D fractal dimension with $R^2 = 0.92$
Kaartinen et al. 2006b	Zinc	Colour, stability and bubble size	Fuzzy logic controllers using froth features	Overall plant recovery improvement of 1.3%
Supomo et al. 2008		Velocity	Logic controllers using froth features	2.4% increase in rougher recovery
Hargrave et al. 1997	Tin	Colour - red and grey level	Multiple regression	Sn grade prediction from red level with $R^2 = 0.94$
Morar et al. 2005	Copper	Colour, stability and velocity	Multiple regression	Cu grade prediction with $R^2 = 0.64$
Bartolacci et al. 2006	Zinc	Multivariate Image Analysis	Partial least squares	Zn grade prediction error = 1.55; Pb grade prediction error = 0.073; Fe grade prediction error = 0.74
		Grey level cooccurence matrix	Partial least squares	Zn grade prediction error = 1.58; Pb grade prediction error = 0.065; Fe grade prediction error = 0.81 Development of commercial system iFroth
Holtham et al. 2002		Texture spectrum analysis	Classification	Development of commercial system JKFrothCam

Authors	Flotation system	Froth features	Model type	Comments
Forbes et al. 2007b	Copper	Dynamic bubble size distribution	Unsupervised furthest-neighbour clustering for learning classes; Linear regression for relating velocity to Cu grade	99.95-100 % confidence of classification differences
Forbes et al. 2004a	Copper and platinum	Dynamic bubble size distribution	Classification	Cu and Pt correct bubble size distribution classifications up to 95%

3.2 Image feature extraction

For analytical purposes, a froth image can be viewed as a three-way array of data, as illustrated in Figure 2.10. In this figure, the digitized froth image is characterized by a matrix of pixel intensities, as well as three spectral features (red, green and blue or RGB). The size of the array depends on the resolution of the image, which can range from a few thousand to a few million pixels. It is from a series of such images that the state of the flotation system can be analyzed.
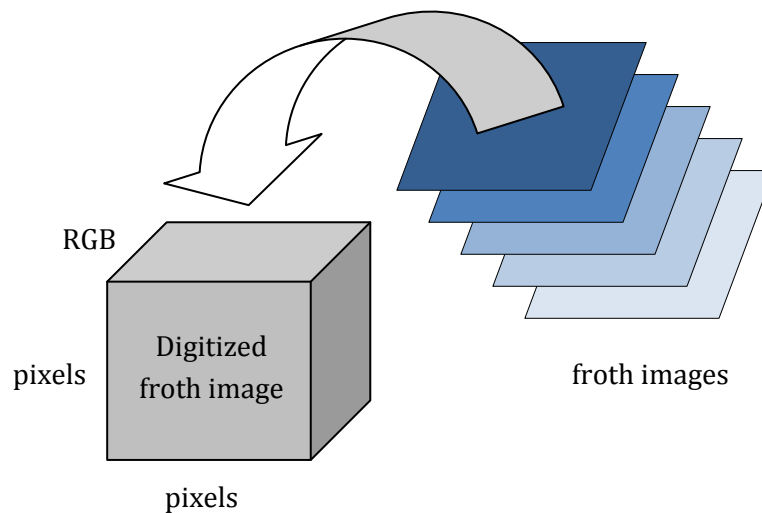

Figure 2.10: A digital froth image as a three-way array of data.

In Figure 2.11, the types of features that can be extracted from these images are summarized. These include the extraction of physically meaningful features, such as bubble size and shape, statistical features facilitating pattern recognition and dynamic features representing the movement and stability of the froth. Unlike the first two groups, the third group of features is derived from sequences of images.
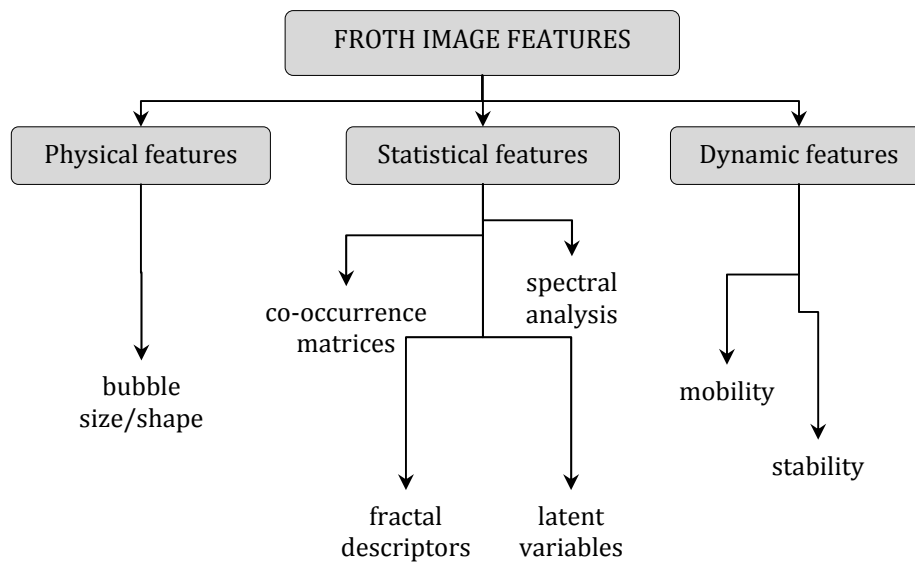
Figure 2.11: Approaches to feature extraction from flotation froth images.

The analytical procedures for extracting these features are described in more detail below and an overview of these methods is given in Table 2.3.

Table 2.3: Overview of feature extraction from froth images.

Type	Froth variables or features	Methods	References
Physical	Bubble size & shape	Edge	Banford et al. 1998; Wang et al. 1999, 2003; Forbes et al. 2004a, 2006; Lin et al. 2007a, 2007b
		Watershed	Sadr-Kazemi et al. 1997; Ventura-Medina et al. 2000; Forbes et al. 2004b; Yang et al. 2008
	Colour	RGB	Gebhardt et al. 1993; Oestreich et al. 1995; Hargrave et al. 1996, 1997, 1998; Bonifazi et al. 2005a, 2005b; Vathavooran et al. 2006; Morar et al. 2005
Statistical	FFT coefficients	FFT analysis	Moolman et al. 1994
	Wavelets coefficients	Wavelet analysis	Bartolacci et al. 2006; Liu et al. 2008, 2007
	Textural variables	Localized pixel intensities	Holtham et al. 2002; Hargrave et al. 1998
	Co-occurrence matrix variables	Co-matrix methods	Moolman et al. 1994, 1995a, 1995b; Aldrich et al. 1995, 1997; Bezuidenhout et al. 1997
	Fractal descriptor	Fractals	Hargrave et al. 1998, 1997; Bonifazi et al. 2000
	Latent variables	PCA	Liu et al. 2005, 2007, 2008; Bartolacci et al. 2006
		Neural networks	Moolman et al. 1995c; Niemi et al. 1997; Hyötyniemi et al. 2000; Jeanmeure et al. 1998; Zimmerman et al. 1996; Estrada-Ruiz et al. 2009
Dynamic	Mobility	Bubble tracking	Botha 1999
		Block matching	Moolman et al. 1994; Holtham et al. 2002; Barbian et al. 2007; Supomo et al. 2008; Forbes et al. 2007a
		Pixel tracing	Nguyen et al. 1997
	Stability	Average pixel	Moolman 1995a; Moolman et al. 1995b
		Bubble dynamics	Barbian et al. 2003, 2005, 2006

3.2.1 *Physical features*

For all practical purposes, the physically meaningful features of the froth are the bubble size distribution and bubble shapes of the froth. These features can be computed directly from digitized images of the froths by use of methods in which the image is segmented in order to explicitly identify individual bubble films on the froth surface. Variants of edge detection algorithms, in which segmentation of the image is based on the detection of sharp transitions in the brightness (pixel intensities) of the image is commonly used for this purpose, as well as other approaches, such as those based on the watershed algorithm (Yang et al. 2008).

i.   *Edge detection algorithms*

In a recent study, Wang et al. (2003) have found that the gradients of the pixel intensities between bubbles in froth images are too small to be detected reliably by classical edge detection functions. Moreover, the gradients of the pixel intensities on the white spots on the top of the bubbles are large, which leads to further confounding of classic methods, such as discussed by Cany (1986), Fu et al. (1981) and Pal et al. (1993). As a consequence, Wang et al. (1999, 2003) have proposed the use of valley edge detection and valley edge tracing to segment froth images. With valley edge detection, the focus is on the detection of valley edges between the bubbles, disregarding the edges of the texture on a bubble. Images are pre-processed to filter out noise and then image pixels are evaluated as possible edge candidates, by checking to see if they are the lowest points in valleys in certain directions. This is followed by a cleanup procedure based on valley edge tracing to ensure that there are no gaps between valley edges. The authors have concluded that this approach is significantly more reliable and orders of magnitude faster than previous methods to segment froth images. Another improvement in image segmentation was proposed by Citir et al. (2004) based on iterative application of a two-stage procedure to identify local minima in pixel intensities, followed by border thinning, after which bubble diameters are calculated. This approach was more accurate for the larger the bubble sizes, i.e. like other algorithms it works better with higher resolution images, not taking the increased computational time into account.

ii.   *Watershed algorithms*

Watershed algorithms are morphological approaches based on a simulation of water rising from a set of markers, as indicated in Figure 2.12. In this figure, three minima are shown (*a*, *c* and *e*), where *a* and *e* are identified as starting points (black markers). Points *b* and *d* are maxima. Moreover, *d* is identified as a watershed point, since it does not flood from the two markers. The approach therefore identifies regional maxima by locating trends in pixel intensities along different scan lines.
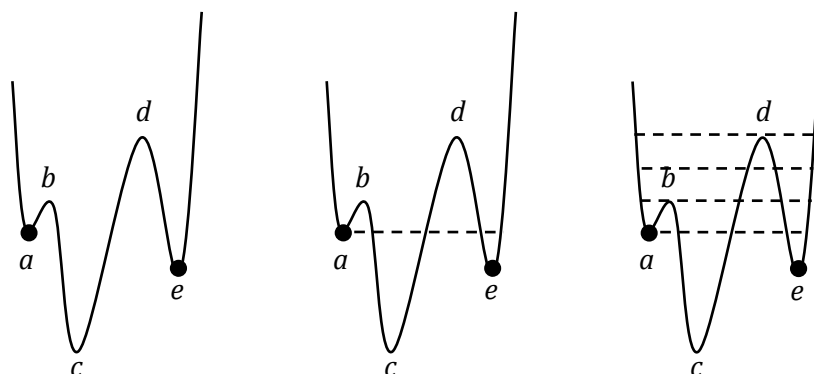
Figure 2.12: Froth image segmentation with the watershed algorithm.

Although the approach is robust in the sense that it is not as dependent on uniform lighting as other methods, the positions of the markers evidently play a critical role in the performance of the technique. Pre-processing, in which the marker image is determined, is therefore of crucial importance. Since each bubble displays a localized reflection, often as a result of the spotlights that are used on industrial camera setups or other sources of lighting, they can be used as bubble markers. In this context, Sadr-Kazemi et al. (1997) have proposed a robust method based on histogram equalization, correction and reconstruction of images to construct markers. This facilitated both the extraction of bubble size and shape distributions.

iii.   Froth colour

The use of colour information for grade predictions is complicated by the interference of ambient and seasonal lighting variations. A number of colour coordinate systems are available such as red, green and blue (RGB), hue, saturation and intensity (HSI) or hue, saturation, and values (HSV). The use of the CIE lab coordinate system is motivated by Morar et al. (2005) due to the component of luminance that is decoupled from the colour information, thereby lessening the effect of ambient light changes. The robustness in using CIE Lab colour features for grade prediction was investigated by Morar and his colleagues Reddick et al. (2009) with copper flotation. They have concluded that colour information alone is not an adequate enough indicator of concentrate grade but could be useful for controlling other variables such as reagent addition. Earlier work by Hargrave et al. (1997) on a tin concentrator successfully predicted the grade of the froth with red colour using simple regression curve fitting. Although PGM flotation froth in general does not show much variation in colour, the pixel intensities should indicate information regarding the mineral loadings on the bubbles and is worth investigating.

iv.   Other physical features

Apart from the bubble morphology and colour of the froth, other physical features may also provide useful information on the flotation process. This includes the use of a load algorithm to measure the mineral coverage of the bubbles. This approach is based on observations made at the zinc flotation circuit of the Pyhäsalmi mine in Finland, where it was noticed that bubbles with a high mineral load in the flotation circuit did not have total reflectance points

or bright spots on their tops. Instead, these bubbles exhibited black windows on their tops, the proportion of which could give an indication of poor loading of the bubbles.

v.   Challenges in the extraction of physical features

One of the challenges associated with the extraction of physical features is in its ability to correctly segment images. Images are often incorrectly segmented due to a wide bubble distribution. Finer bubbles are often segmented as large bubbles, since the occurrence of relatively bright localized reflections in fine froth is scarce. (Neethling et al. 2003a, 2009; Aldrich et al. 2010)

Neethling et al. (2003a) raise two further issues with the extracted froth surface film size distributions. The first concerns the averaging of the measured distribution into a single value partially addressed by authors such as Ventura-Medina et al. (2000). The second involves the estimation of the characteristics of the total volume of froth overflowing the weir from appearance of the surface film. The layers immediately below the surface film which form the predominant proportion of the overflowing volume cannot be corrected for readily.

The use of quantitative bubble size measurements from image analysis either directly for control or as the basis for model-based control has therefore not yet satisfactorily been resolved. Statistical approaches have, possibly as a result of this, been developed.

3.2.2   Statistical features

Statistical features apply statistics to the image data such as the pixel values, neighbour relations, patterns and bubble size distribution. Each of the identified statistical features and their variations are discussed.

i.   Fast Fourier transforms

More involved analyses include those based on Fourier spectra and wavelets. By means of Fast Fourier Transforms (FFT), digitized images can be transformed from the spatial or grey scale domain to the spectral domain. For example, Moolman et al. (1995d) correlated the sum of the coefficients in the power spectrum with the average bubble sizes of froth images obtained from a copper flotation plant.

ii.   Wavelet transforms

Wavelet transforms can be interpreted as correlations between the data (pixel intensities) and the time shifted and rescaled mother. Continuous wavelet transform is readily applied to image in a two-dimensional discrete form. Wavelet transforms are considered to be superior to other algorithms for texture analysis, such as those based on FFT and grey level co-occurrence matrices. They are more computationally efficient and robust to varying lighting conditions than segmentation algorithms. (Bharati et al. 2004)

iii.   Fractal descriptors

Fractal descriptors are based on the notion of self similarity in the bubble size distributions of the froth images. If the bubbles on the froth surface can be identified at different scales,

then their area distribution follows a power law distribution. Hargrave et al. (1998) have investigated the use of Sierpinski fractals to characterise coal froths that had exhibited bimodal fractal behavior, which could be related to the ratio of larger to smaller bubbles within the froth. Bonifazi et al. (2000) experimented with copper and lead froths, and observed that the froth structure could be characterized by two different fractal dimensions. There was no evident correlation between these fractal descriptors of the froth and metal grades, but they could be used with other predictors to predict metal grades in the froth.

iv.   Co-occurrence matrices and their variants

A co-occurrence matrix is defined over an image to be the distribution of co-occurring values at a given offset. Co-occurrence matrices have been used extensively to characterize image textures and several variants have been found useful in the context of froth image analysis. These include spatial and neighbouring grey level dependence matrix methods Moolman et al. (1995b, 1995d). The most significant disadvantage of the co-occurrence matrix is their computational inefficiency, since it depends on the number of grey levels in the entire image. Since texture is usually measured in a small region, a large number of entries are zero and although they need to be processed, they do not contribute to the texture description of the region. The problem is compounded when the images are composed of a large number of gray levels. Moreover, repeated processing may be needed should the image dynamic range vary. (Aldrich et al. 2010)

v.   Texture spectrum analysis

With texture spectrum analysis, features are extracted by scanning the image with a 9 pixel-matrix, as shown in Figure 2.13. The 8 neighbouring pixels can either assume a value less than, equal to or greater than the value of the central pixel, giving rise to 3^8 which equals 6561 combinations. The indices of these combinations (texture unit numbers) constitute the texture spectrum of the image. The use of texture spectrum analysis combined with pixel tracing to evaluate the froth surface has been investigated by Holtham et al. (2002) and implemented in JKFrothCam software.
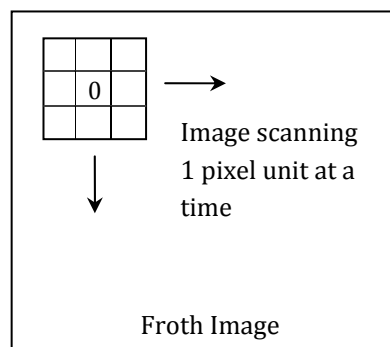

Figure 2.13: Texture spectrum approach to feature extraction from froth images.

vi.   Latent variables

(a) **Principal component analysis:** Multivariate image analysis is a versatile approach to analyse spatial and spectral correlation in images, whether separately or simultaneously. In general, the approach deals with stacks of congruent images or three-

way data arrays, where two dimensions represent geometrical coordinates and one dimension represents a spectral coordinate. If the image X' has dimensions (I x J x K), then it can be decomposed into an IJ x K matrix, X, that can be decomposed by use of principal component analysis into the sum of outer product vectors t_j (scores) and p_j (loadings) plus a residual matrix E:

$$X = TPT + E = t_1p_1T + t_2p_2T + \cdots + t_kp_kT + E \tag{6}$$

where k is less than or equal to the smaller dimension of X. In this case, the spatial information is lost. For example, a 256 x 256 image in red green and blue (RGB), would give a 256 x 256 x 3 array, that will be unfolded in to a 65536 x 3 matrix and may decomposed into a 65536 x 1 score matrix (T), a 3 x 1 loading matrix (P) and a 65536 x 3 residual matrix (E). Liu et al. (2005) discuss the application of multi-resolution multivariate image analysis.

(b) Hebbian learning: The generalized Hebbian algorithm extracts features from images, so that the original images can be reconstructed as a weighted sum of the components, according to eq. (7).

$$f(X) = \sum_{i=1}^{I} \beta_i(X)\theta_i \tag{7}$$

The vector *f(X)* represents the image or some function of the image, coded in a one-dimensional structure. θ_i represent the *I* image features, while $\beta_i(k)$ are the loadings of feature θ_i. The number of features (*I*) is typically much smaller than the *k* elements in the image. Examples of the application of this approach in froth image analysis can be found in Niemi et al. (1997) and Hyötyniemi et al. (2000).

(c) Multilayer perceptrons: In the form of auto-associative neural networks or auto-encoders, multilayer perceptrons provide a natural means to extract features from froth images, as demonstrated by Moolman et al. (1995c). In essence, the image is sampled or processed, by converting the two- or higher-dimensional array into a single vector, which is then passed to the neural network. The network attempts to reconstruct the vector (and hence the image), by passing the data through a bottleneck layer, that essentially extracts latent variables or features from the image. In a different approach, Estrada-Ruiz et al. (2009) and Pérez-Garibay et al. (2010) have used a multilayer perceptron to relate the bubble lumination intensities to the size distributions of the bubbles.

(d) Cellular neural networks: Cellular neural networks typically consist of a finite number of locally interconnected nonlinear process units that collectively can show emergent behaviour. The cells are often defined in a 2-dimensional Euclidean geometry, like a grid. A few applications have been reported, in which these networks have been used for their ability to rapidly process froth images (Zimmerman et al. 1996; Jeanmeure et al. 1998).

3.2.3 Dynamic features

Dynamic features refer to descriptors designed to capture the movement or dynamic behaviour of the froth, such as the froth mobility, as well as stability.

i. Mobility

Motion estimation in froths is difficult, owing to the smoothness of the images, as well as the effects of bubbles bursting and merging. Furthermore, although the froth as a whole has an average motion, it is relatively stagnant in the centre of flotation cell, while moving rapidly where it overflows into the launder.

(a) **Bubble tracking:** In bubble motion analysis, the movement of the localized reflections of light on the bubble surfaces is tracked. Bubble-based motion analysis calculates a motion vector for each bubble marker. Although this is useful in motion tracking of individual bubbles over extended periods of time, calculating statistics on this information can be problematic, as the motion information is extracted at irregular intervals. In addition, detailed mobility information is sometimes required for predetermined sub-regions of the froth surface (Botha 1999; Botha et al. 1999).

(b) **Block matching:** With block matching algorithms motion vectors can be calculated at regular intervals in predetermined regions of interest. This is accomplished by partitioning the source image into non-overlapping blocks and then attempting to match each of these blocks to the corresponding block in the target image. Each source block is then cross-correlated with all the possible overlapping target blocks in its search region. The position of the matching block is identified as the position at which maximum cross correlation is achieved. Figure 2.14 gives an indication of typical results obtained with bubble and region based approaches to froth motion analysis.
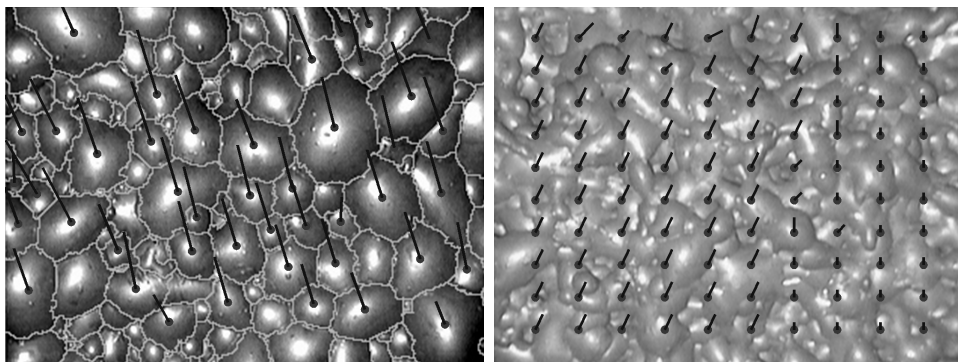

Figure 2.14: Bubble tracking (left) and block matching (right) motion analysis.

Using this method, Barbian et al. (2007) describes an algorithm whereby a normalised height map is produced and the location of the maximum value shows the image displacement needed to maximise the image correlation. The normalised peak is the cross correlation peak measurement, and gives a value of between unity and zero – where a high value would represent a 'mobile' froth and conversely a lower value would indicate a more 'viscous', dry froth. The cross correlation peak was found to be related to concentrate grade.

(c) Cluster matching: The algorithm clusters two successive frames of an image sequence based on position and intensity. Displacement estimates are subsequently obtained by matching the cluster centres between successive frames using cluster features such as position, intensity, shape and average gray-scale difference. Francis (2001) and Kottke et al. (1994) concluded that although cluster based motion estimation algorithms were fast, they performed comparatively poorly on froth images.

(d) Pixel tracing: The algorithm was developed by Nguyen et al. (1995) and is used in JKFrothCam produced by JKTech. In essence, it is a correlation based algorithm, where a block in the centre of an image is compared with corresponding blocks in a subsequent image. The motion vector is determined by the blocks with the highest correlation. It is fast, since it does not search the entire motion search space, but may sacrifice accuracy in the process. The algorithm was used by Nguyen et al. (1997), as well as Holtham et al. (2002).

ii.   Stability

Stability measurements provide an indication of the appearance and disappearance of bubbles from the froth. As with velocity measurements, these methods are also based on the analysis of sequences of froth images. One of the first approaches proposed by Moolman et al. (1995b) was the calculation of the average intensity of an average image of a sequence of images. The more rapid the change in the images, the more blurred the average and the more its intensity would approach an intermediate value. This crude approach was confounded with the velocity of the froth as well, and more sophisticated approaches were subsequently considered by various authors. In these methods, the images are first aligned, so as not to confound calculations with the froth velocity. The images are then pair-wise subtracted from one another, after which the residual values could be further analyzed. More recently, Zanin et al. (2009) have made use of Metso's VisioFroth software to infer the stability of flotation froths from digital images of the froth bubbles in porphyry copper plants. Several authors, such as Barbian et al. (2003, 2005, 2006), have proposed methods whereby the froth stability can be inferred from other measured features of the froth.

CHAPTER 3
MATERIALS AND METHODS

1. LABORATORY STUDY

Laboratory test work is used for a number of reasons such as assisting in plant design, evaluating existing plant performance and evaluating new reagents, configurations and exploratory drill cores. A single batch laboratory cell is used to simulate the operation of a bank of cells; therefore experimental procedures differ based on the design of the plant being simulated. To represent each cell in a bank there is a specified time interval that the froth is sampled from the laboratory cell. Each subsequent interval of samples represents a successive cell in series in the bank. (Wills 1997)

1.1 Ore preparation

The Upper Ground 2 (UG2) ore received from Anglo Platinum's Waterval concentrator was sampled to ensure that each sample is representative of the bulk of the feed to the mill. The ore was received in quantities of 2kg within which all particles were smaller than 3mm. The ore was then sampled with a rotating splitter to obtain the correct amount of ore according to the specific experiment's requirements.

In order to prepare the ore for flotation test work, the ore needed to be ground to the desired particle size. According to Wills (1997) batch laboratory rod mills produces a particle size distribution that closely resembles that of the closed circuit ball mill which was used in the industry. Therefore, for each experiment, the representative ore sample was transferred to the batch rod mill with a volume of 9L. Fifteen rods were used, weighing 14kg in total.

A grinding curve was obtained to characterise the performance of the mill specific to the batch milling conditions and ore type. A series of runs were performed for which the ore was milled for different durations. A sample of each run was analysed for its particle size distribution with a particle size analyser (PSA) using laser diffraction. For each run the percentage passing a threshold value was identified, each supplying a single point of the grinding curve. The grinding curve (a straight line) was then used to predict the milling duration necessary to meet the grinding requirements.

1.2 Batch flotation

A series of batch flotation test were done at the University of Stellenbosch on a 4.5 L Barker laboratory flotation cell equipped with a fixed rotor and aerator unit (Figure 3.1).
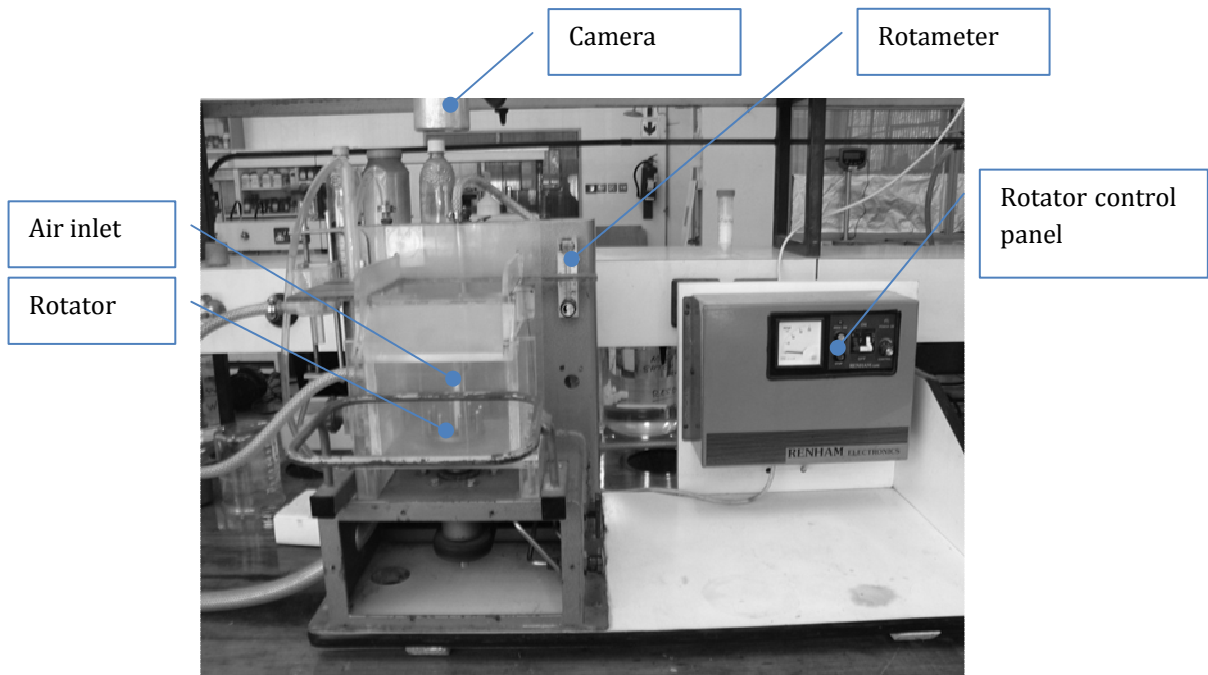
Figure 3.1: Photograph of the batch flotation cell used for these experiments.

The fractional factorial experimental design was of the form 2^{6-3} i.e. an $1/8^{th}$ fraction of runs generated by binary combination of six factors measured at two levels as summarised in Table 3.1.

Table 3.1: Fractional factorial, design including results.

Run	x_1	x_2	x_3	x_4	x_5	x_6
1	-	-	+	-	+	-
2	-	+	+	+	-	-
3	-	+	-	-	-	+
4	-	-	-	+	+	+
5	+	-	-	-	-	-
6	+	+	-	+	+	-
7	+	+	+	-	+	+
8	+	-	+	+	-	+

The experiments were conducted in completely random order to avoid biased results. Six variables were considered: air flowrate (x_1), pulp level (x_2), collector (x_3), activator (x_4), frother (x_5) and depressant (x_6). The collector used was Sodium isobutyl xanthate (SIBX), the activator used was dithiocarbamate referred to by its trade name - Senkol 65, the depressant was a polysaccharide named Gempolym KU9, and the frother was polyether polyol referred to by its trade name - XP200. A series of scoping tests were done to find the two levels for the design, the restriction being the mass pull. The mass pull minimum had to allow a froth height such that it can be scraped off as a sample. The mass pull maximum had to not overflow the cell spontaneously. The levels that were used are summarised in Table 3.2.

Table 3.2: Levels of factors used in the experiments.

Variable	High (+)	Low (-)
Air flowrate (L/min)	6	4
Impeller speed (rpm)	1100	900
Pulp height (cm below weir)	2	3
Particle size (-75µm)	60%	80%
$CuSO_4$ (g/t)	66	54
1st conditioning (g/t)		
SIBX (collector)	88	72
Senkol 65 (activator)	22	18
KU9 (depressant)	55	45
XP 200 (frother)	55	45
2nd conditioning(g/t)		
SIBX (collector)	99	81
Senkol 65 (activator)	0	0
KU9 (depressant)	33	27
XP 200 (frother)	11	9

In this study the impeller speed, particle size, aperture size of the air inlet and the initial density was kept constant. The impeller speed and particle size are generally kept constant on an industrial plant; their effects can be investigated by adding another 1/8th fraction to the experimental design. The aperture size of the air inlet was restricted by the physical setup. The initial pulp density for all experiments were the same, however the density changed as the experiments proceeded due to the sample removal.

1.2.1 Experimental procedure

A representative sample of ore was milled in a 9L rod mill to obtain the desired particle size. Copper sulphate ($CuSO_4$), acting as activator, was added to the mill to ensure that the freshly liberated precious metal was contacted immediately. The pulp from the mill was then transferred to the batch flotation cell. The rotator was set to a speed that could maintain a well mixed pulp. An initial conditioning stage was performed where the specified amount of collector and activator was added and allowed to condition for 2 minutes. There after the depressant and frother were added and again 2 minutes were allowed for conditioning. At this point pH and temperature were measured. The air flowrate, impeller speed and pulp height was then adjusted according to specifications and a froth build up time of approximately 30 seconds was allowed. Directly after this samples were taken as presented in Figure 3.2. Froth was scraped off every 20 seconds for a specified duration: Float 1 lasted 2 minutes, float 2 was 6 minutes, float 3 was 12 minutes and the last two floats were 10 minutes each. A second conditioning, similar to the first, commenced after the third float, with different dosage specifications (Table 3.2). The sampling of float 4 commenced immediately thereafter followed by float 5. The 5 floats, a feed sample and the remaining tails were filtered, dried and assay analysed separately.

	t_{float} (min)	Reagent addition			
		Collector	Activator	Depressant	Frother
Take feed sample					
Condition 1a	2	x	x		
Condition 1b	2			x	x
Measurements - pH, T(°C)					
Air on (allow 30s froth build-up time)					
Float 1	2	Scrape every 20 seconds			
Float 2	6	Scrape every 20 seconds			
Float 3	12	Scrape every 20 seconds			
Condition 2a	2	x	x		
Condition 2b	2			x	x
Float 4	10	Scrape every 20 seconds			
Float 5	10	Scrape every 20 seconds			
Measurements - pH, T(°C)					
Tails		When finished			

Figure 3.2: Illustration of sample taking

Video recordings were made of the froth with the use of the Sanyo Xacti, high definition (1280 x 720), waterproof video camera, at a frame rate of 29.976 frames per second (fps). A custom built LED light, consisting of a configuration of six 1W LEDs, provided lighting in such a way as to minimize the interference of ambient light. It was situated approximately 25cm above the cell.

1.2.2 Image acquisition

For each experimental run, which lasted approximately 1½ h, approximately 85000 images of size 1280 x 720 were collected. These images were processed offline by means of the Matlab 6.2 image processing toolbox on a standard PC to give matrices with elements representing the red, green and blue values of each pixel for each frame. These RGB matrices were converted to grey scale for further analysis.

1.3   Feature extraction

The nature of the froth in the laboratory scale cell precluded the use of traditional segmentation techniques such as watershed. From Figure 3.3 it is evident that the bubbles are not heavily loaded and there are a lot of clear windows. The bubbles therefore look darker inside than at the edges of the bubbles as they touch; furthermore the bubbles are also very small and not all of them had clearly identifiable reflection points. Watershed segmentation did not identify the individual small bubbles, but saw an area of this very fine froth as one bubble. It is for this reason that statistical features were extracted. The in-house statistical feature extraction technique referred to as texture feature extraction was used.

Once the images had been converted to a matrix of pixel intensities, textural features were extracted from the image data. Five features were extracted from the grey level co-occurrence matrices of the images, namely contrast, correlation, energy, entropy, and homogeneity, as described in more detail below.

Textural features are statistical measures used to describe the localised patterns on the image. The spatial grey level dependence matrix (SGLDM) is based on the estimation of the second-order joint conditional probability density functions, *g(i,j,d,a)*, *a* = 0°, 45°, 90°, 135°. Each *g(i,j,d,a)* is the probability of going from grey level *i* to grey level *j* , given that the intersample spacing is *d* and the direction is given by angle *a*. If an image has *l* grey levels, then the density functions can be represented as *l* x *l* matrices. Each matrix can be computed from a digital image by counting the number of times each pair of grey levels occurs with separation *d* and in the direction specified by *a*. It is assumed that the textural information is sufficiently specified by the full set of four spatial grey level dependence matrices. Haralick et al. (1973) proposed a set of measures for characterizing these matrices. The features (*f_{nm}*, *n:* settings (1-4), *m:* features (1-5).) used most often, and also used here, are as follows:

i.   *Energy($f_{n,1}$):*

$$E = \sum_i \sum_j [g(i,j,d,a)]^2 \tag{8}$$

This is a measure of the homogeneity of the image. For an image which is not homogeneous the matrix will have a large number of small entries off the diagonal, and hence the energy (*E*) will be small. The diagonal and region close to the diagonal represent transitions between similar grey levels.

ii.   *Entropy ($f_{n,2}$):*

$$e = -\sum_i \sum_j [g(i,j,d,a).log(g(i,j,d,a))] \tag{9}$$

The entropy is a measure of the complexity of the image, i.e. a complex image tends to have a higher entropy value than a simple one.

iii.   *Inertia ($f_{n,3}$):*

$$I = \sum_i \sum_j [(i-j)^2 g(i,j,d,a)] \tag{10}$$

The inertia is a measure of the number of local variations in the image. Therefore an image with a large number of local variations will have a larger value of inertia.

iv.   *Local homogeneity ($f_{n,4}$):*

$$L = \sum_i \sum_j \left[\frac{g(i,j,d,a)}{(1-(i+j))^2} \right] \tag{11}$$

This parameter is a measure of the tendency of similar grey levels to be neighbours.

v.   Correlation ($f_{n,5}$):

$$\varsigma = \sum_i \sum_j \left[\frac{(i - \mu_x)(j - \mu_y).\left(g(i,j,d,a)\right)}{(\sigma_x \sigma_y)} \right] \qquad (12)$$

where μ_x and σ_x are respectively the mean and standard deviation of the row sums of the matrix, and μ_y and σ_y are the mean and standard deviation of the column sums. This is a measure of the grey level linear dependencies in the image. (Haralick et al. 1973)

Each of these features were calculated at five different image settings (see Figure 3.3): grey scale (s_1), histogram equalized (s_2), contrast enhanced (s_3) and binary (s_4) resulting in a total of 20 image features. Each of these settings are briefly discussed.

(a)   (b)   (c)
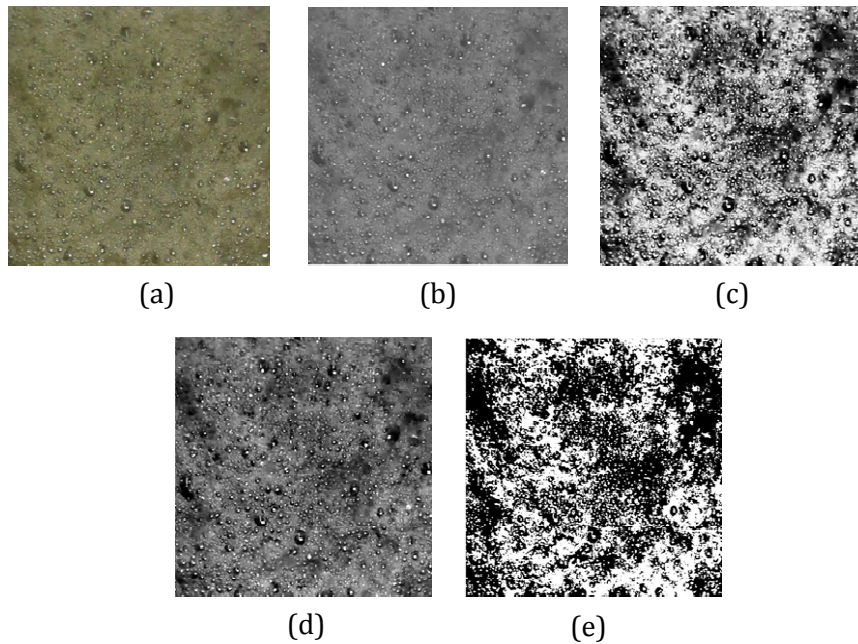
(d)   (e)

Figure 3.3: A froth image at the different settings: (a) RGB image, (b) Gray scale/intensity image, (c) histogram equalised image, (d) contrast enhanced image and (e) binary image.

Histogram equalisation (Figure 3.3c) improved the contrast of images by transforming the intensity values of the pixels so that the histogram of the output image closely matched a specified histogram. Contrast enhancement (Figure 3.3d) refers to the process of adjusting a grey scale image to new values so that 1% of data is saturated at low and high intensities of the input image, thereby increasing the contrast of the output image. Thresholding was applied to obtain a binary image (Figure 3.3e). A global threshold was chosen such as to minimize interclass variance of black and white pixels (Otsu 1979). Values larger than the threshold were replaced by the largest intensity value (white) and lower values were changed to the lowest intensity value (black).

In summary, each image in the video was treated as illustrated in Figure 3.4, resulting in a total of 20 texture features per image.
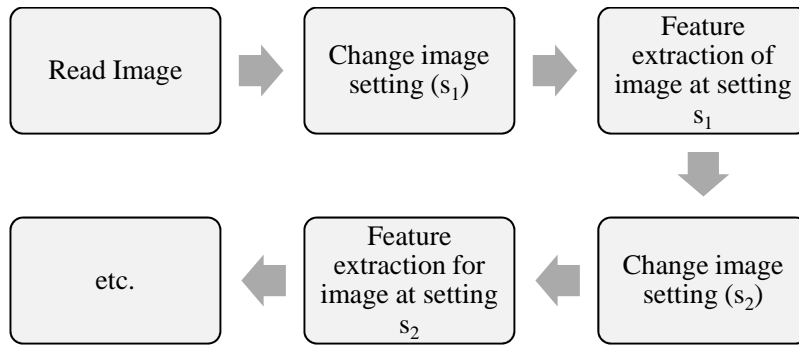

Figure 3.4: Flow diagram of feature extraction for an image.

2. CASE STUDY

A data campaign was done at Anglo Platinum's Mogalakwena North concentrator in Mokopane in July 2009 in collaboration with the Advanced Graduate Development Programme (AGDP) graduates employed by Anglo American.

2.1 Scope

In light of the project objectives, which involve model building, it was necessary to obtain data that include all possible process states. Unfortunately such experimental work on the plant could affect the plant production significantly and was not possible therefore a smaller range of conditions had to be tested. Due to the recent interest in air flowrate optimisation, one of the objectives of the data campaign was to do a series of air flowrate step changes on cells that were important to the metallurgists on the specific plant. The froth of a primary cleaner cell was recorded while air flowrate changes were made. Due to the limited range of operating conditions investigated and the unavailability of certain operating conditions, this case study was aimed at supporting the laboratory case study in some of its findings.

2.2 Procedures specifications

The mass pull controller of the flotation section was deactivated and the plant was allowed to stabilise. A number of stepwise changes were made in the air flowrate of the concentrator flotation cell. Subsequent to each change, time was allowed for the flotation cell to stabilise. This was established with visual inspection and took approximately 30 minutes. Once the cell was stable, a concentrate sample was taken. In total, the study lasted 4 hours.

The same equipment was used for the case study as for the laboratory study. The area where the camera was placed was covered to further the minimization of ambient light interference (see Figure 3.5). The camera was situated approximately 15 cm above the weir.
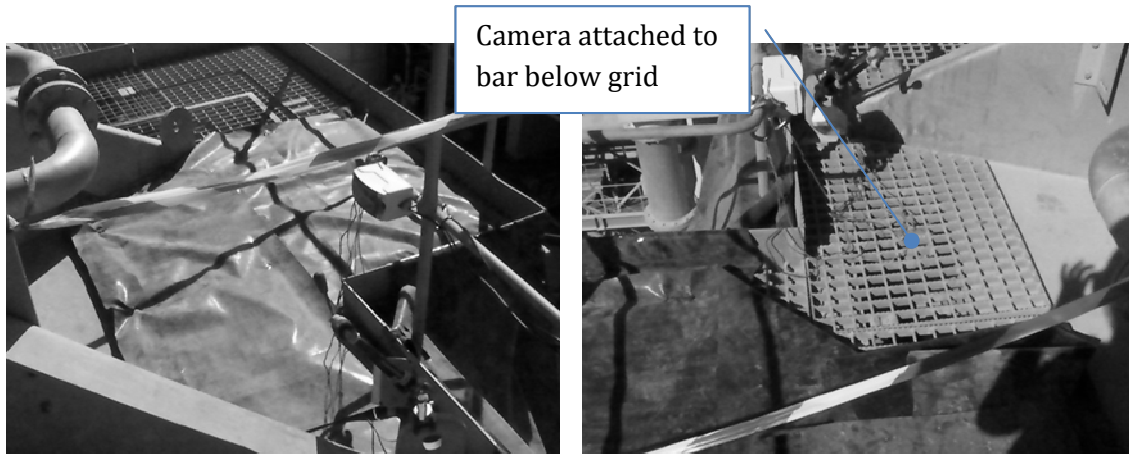
*Figure 3.5: Photographs of the case study setup. Left: Setup with canvas over grid.
Right: Setup with canvas open, view from opposite side.*

2.3   Image acquisition

For the total duration of 4 hours, approximately 424420 images of size 1280 x 720 were collected. These images were processed offline by means of the Matlab 6.2 image processing toolbox on a standard PC to give matrices with elements representing the red, green and blue values of each pixel for each frame. These RGB matrices were converted to grey scale for further analysis. The images were also processed with SmartFroth software to give a vector of features for each image.

2.4   Feature extraction

Textural features were extracted as with the experimental image analysis (section 1.3, this Chapter). Additional to this, physical and dynamic features were extracted using SmartFroth software. (Refer to Table 3.3).

2.5   Problems and limitations

A few difficulties have been experienced on the plant. Each is mentioned below and should be taken into consideration when interpreting data analysis results.

2.5.1   Lighting

In order to keep the lighting constant during filming, black canvas material was used to cover the grid as well as the sides of the cell where light could come through. Due to the sample taking to the side of the cell, that particular area could not be covered completely and the morning light influenced the lighting conditions, at least for the first 20-30 minutes.

2.5.2   Colour

A colour calibration patch was not used as this was difficult to secure on the setup with the limited amount of time and space that was available.

2.5.3 Instrumentation

The air valve on the specific cell showed unexpected erratic behaviour until reaching what seemed to be steady state.

2.5.4 Steady state

Steady state was established by visual inspection of the change in froth in conjunction with the monitoring of the air flowrate measurement in the operating room.

Table 3.3: Physical and dynamic collection of features.

Bubble size	Mean bubble area (normalised)
	Ellipsoidal bubble diameter (area weighted)
	Equivalent bubble diameter (area weighted)
	Specific surface area (area weighted)
	Weighted mean bubble area
	Ratio of small bubbles
	Ratio of medium bubbles
	Ratio of large bubbles
Bubble shape	Circularity
	Sphericity
Colour	Average red value
	Average green value
	Average blue value
	Average grey value
	Average Colour Lab L
	Average Colour Lab a
	Average Colour Lab b
	Average Colour Lch L
	Average Colour Lch C
	Average Colour Lch H
Velocity	Velocity in x direction (bubble tracking)
	Velocity in y direction (bubble tracking)
	Velocity in r direction (bubble tracking)
	Velocity in x direction (block matching)
	Velocity in y direction (block matching)
	Velocity in r direction (block matching)
Stability	Stability (correlation peak)
	Stability (normalised sum of absolute differences)
	Stability (percentage of pixels above threshold)

3. DATA ANALYSIS

A classification and regression technique was applied to the available datasets to establish the feasibility of using image features to determine platinum froth grade. Although many techniques may be suitable, the selection of an optimal data analytical technique does not form part of this study. Random forests were selected as the classification technique due to the ease of use of this technique and its ability to handle large datasets with relative ease (Genuer et al., 2008). Neural networks have been chosen as the regression technique because of the availability of software to find optimal configurations as well as the processing power associated with its parallel architecture. Each of the techniques will be introduced, followed by the details of its application to this study.

3.1   Random forest classification

Random forest classification is a technique using an ensemble of decision trees. The working of a single ensemble member (i.e. a single decision tree) will be described followed by the operation of an ensemble of decision trees and the problem specific application details.

3.1.1   Decision trees

A single decision tree is a series of consecutive IF-THEN rules. The dataset in the very first node of the tree is divided into two nodes based on an IF-THEN rule. A number of these rules are tested and the rule that produces the most homogeneous or pure groups are selected for the specific split. The example in Figure 3.6 shows a single tree classifying a dataset with two variables x_1 and x_2 into two classes: A and B. For the first split: If variable x_1 has a value smaller than k_1, then the data point will fall into the left node, otherwise it will fall into the right node. If a group can no longer be divided into separate groups, then that node is a terminal node and a class can be assigned to that node. The very first node in the tree is called the root node. A node that can be divided is called a parent node and its subgroups are called child nodes. A terminal node is also called a leaf node. (Ripley 2009)
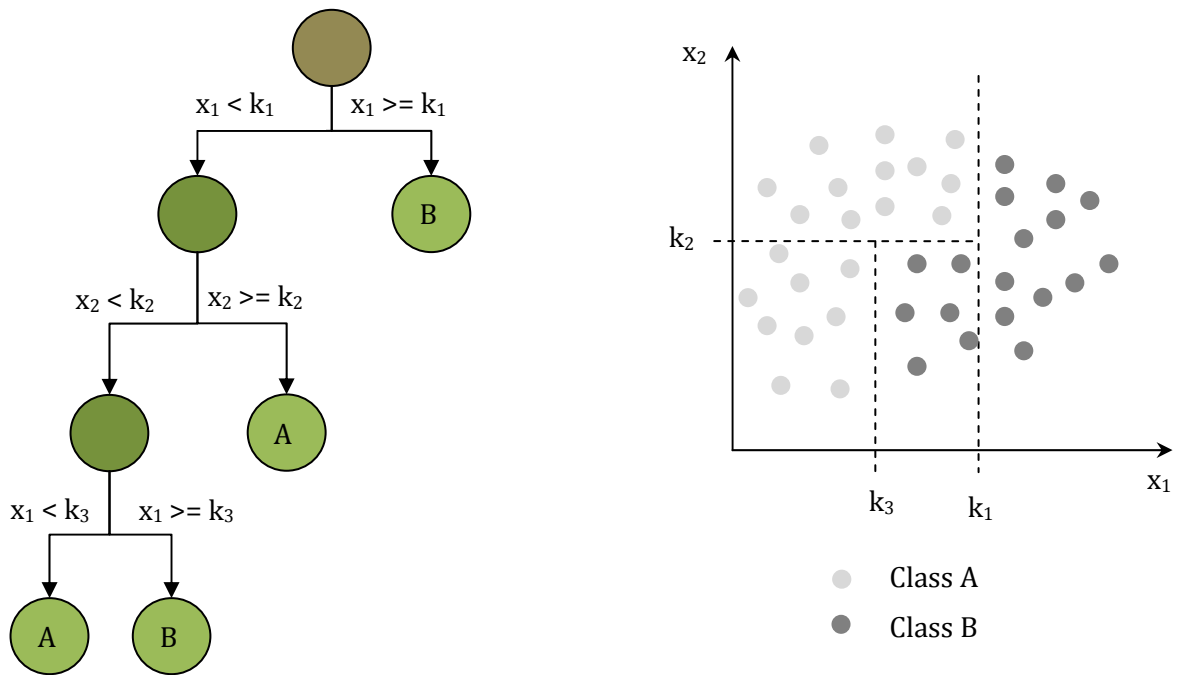
Figure 3.6: Example of a single decision tree.

A single tree is unstable because of the strong dependency of the tree structure on the given dataset. If a dataset changes slightly, split variables (order of x_1 and x_2) and split positions (values of k_1, k_2 and k_3) often change as well.

3.1.2 Random forests

It has been statistically proven that ensemble techniques perform better than a single member of the ensemble. The instability of a single tree becomes a positive attribute when an ensemble of trees forms a voting committee as this instability ensures a diverse committee of members that produce a more generalised result. (Breiman 2001)
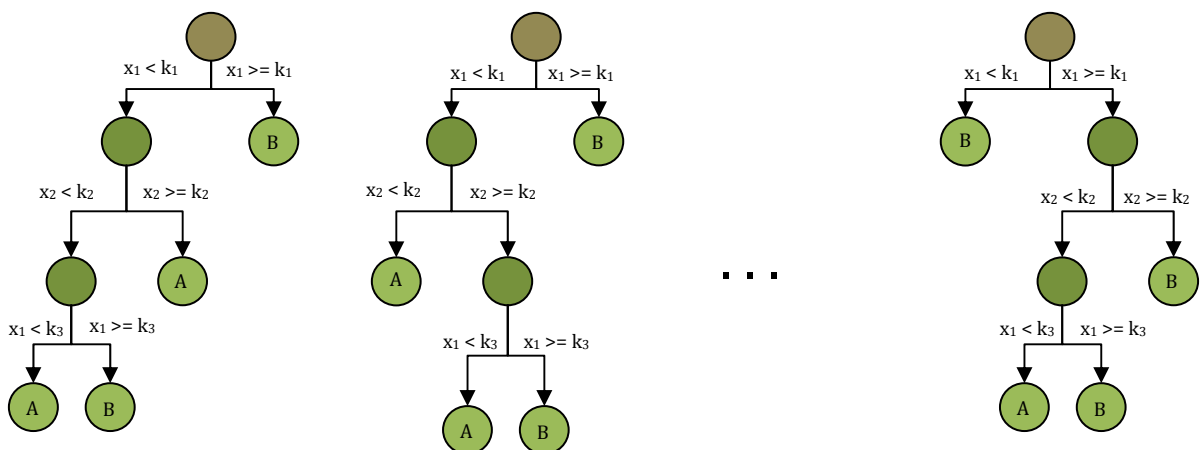

Figure 3.7: An ensemble of diverse classification trees.

The formal definition of a random forest in Breiman (2001) is as follows:

A random forest is a classifier consisting of tree structured classifiers $\{h(x, \emptyset_k), k = 1, ...\}$, where the $\{\emptyset_k\}$ are independent identically distributed random vectors and each tree casts a unit vote for the most popular class at input x.

Diversity among trees is introduced by growing each tree on a different subset of the data (bagging). Diversity is improved further by considering only a random selection of variables at each split in the tree (random split selection). (Breiman 2001)
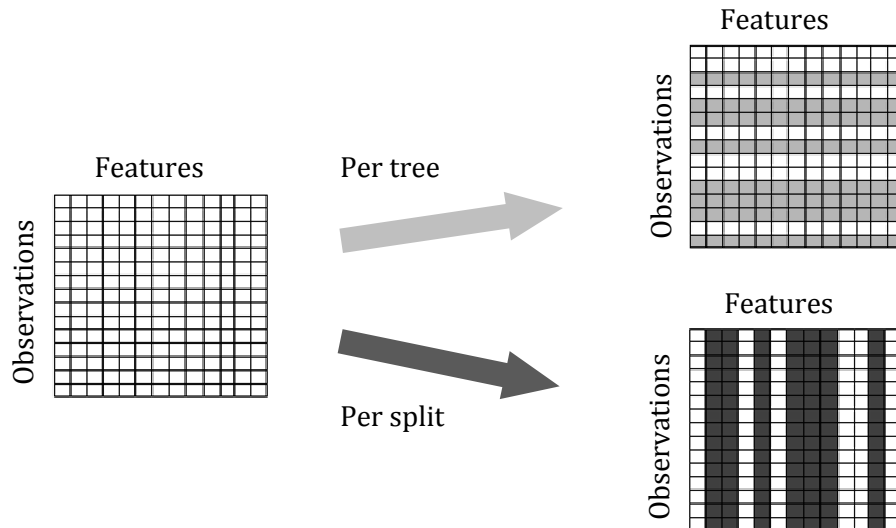

Figure 3.8: Random forest bagging and random split selection techniques for increased diversity among trees.

Specifications regarding the behaviour of each tree include splitting rules and pruning specifications. Splitting rules refer to the IF-THEN rules applied to split a node into smaller parts. Each node has a set of attributes (split variable choice and value) on which it might be split. The improvement in impurity from the parent node to the child nodes upon the application of a splitting rule is calculated for all attributes. Typical measures of the impurity of a node are entropy and the Gini index. The splitting rule with the best improvement is used in the tree structure. Pruning refers to tree depth or splitting layers. For fully grown trees, the splitting procedure is repeated until no more splits can be made. For a single tree this would overfit the data, however according to the Strong Law of Large Numbers, an ensemble of fully grown trees will always converge and therefore eliminates the possibility of the model over-fitting the data. The splitting can be stopped before it is fully grown, or cut back (pruned) afterwards. The minimum amount of observations allowable in a terminal node can be specified by the user. (Breiman 2001; Ripley 2009)

The performance of the forest is measured by the Out Of Bag (OOB) error estimate which gives an indication of how well the model classifies unseen (out of bag) data. The use of this OOB error estimate removes the need to set a test set aside. (Breiman 2001; Genuer et al. 2008)

3.1.3 Application specifications

The `randomForest` package in R was built from the seminal work of Breiman (2001). This package was used to generate random forests for the given datasets. The primary parameters were the number of trees that form the random forest (*ntree*), the number of variables available for selection at each split (*mtry*) and the minimum amount of observations allowed in a leaf node (*nodesize*).

The number of trees in the random forest needed to be established in order to produce a more generalised result. Each tree in the forest was grown one after the other, therefore results are updated as each tree was added. As the amount of trees increased, the forest stabilised and the results converged. When the results were not changing much with the addition of more trees, the forest was stopped to save on computational time and effort. Figure 3.9 is an example of random forest training results, showing the stabilization of the random forest as trees are added.
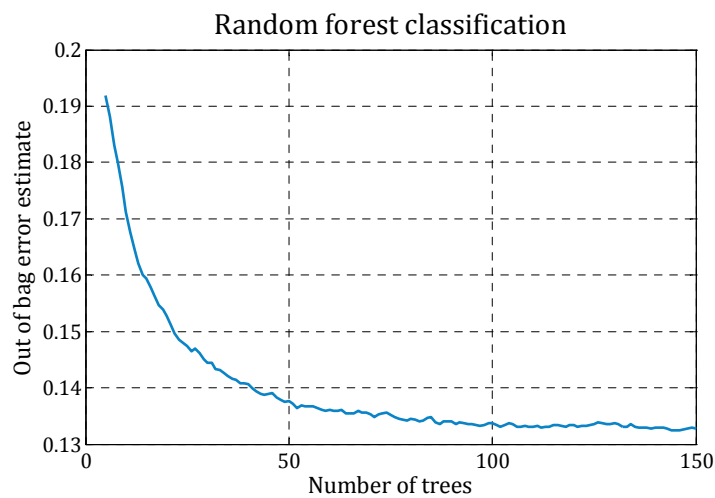

Figure 3.9: Graph of the random forest results to illustrate the converging error with increasing number of trees.

Genuer et al. 2008 gives insight in selecting the number of variables considered at each split. They have found that the default value of *mtry* in the R package, which is the square root of the total amount of variables, produce good classification results. Nevertheless, in this study a range of *mtry* values were evaluated. The default *nodesize* value in the R package for classification is 1 which was also used in this analysis. (Genuer et al. 2008)

3.2 Artificial neural network regression

3.2.1 Artificial neural networks

Artificial Neural Networks (ANNs) is a non-linear function mapping technique that can be applied to classification and for regression problems. ANNs were initially developed to imitate the brain from both a structural and computational perspective. Its parallel architecture is primarily responsible for its computational power which makes it such an attractive technique.

The multi-layer perceptron (MLP) network architecture is probably the most popular followed by the radial basis function (RBF) network. The MLP network architecture was used in this

study. The MLP network usually consists of three layers of nodes as illustrated in Figure 3.10. Each node links to another node with a weighted connection, *w(i,j)*.
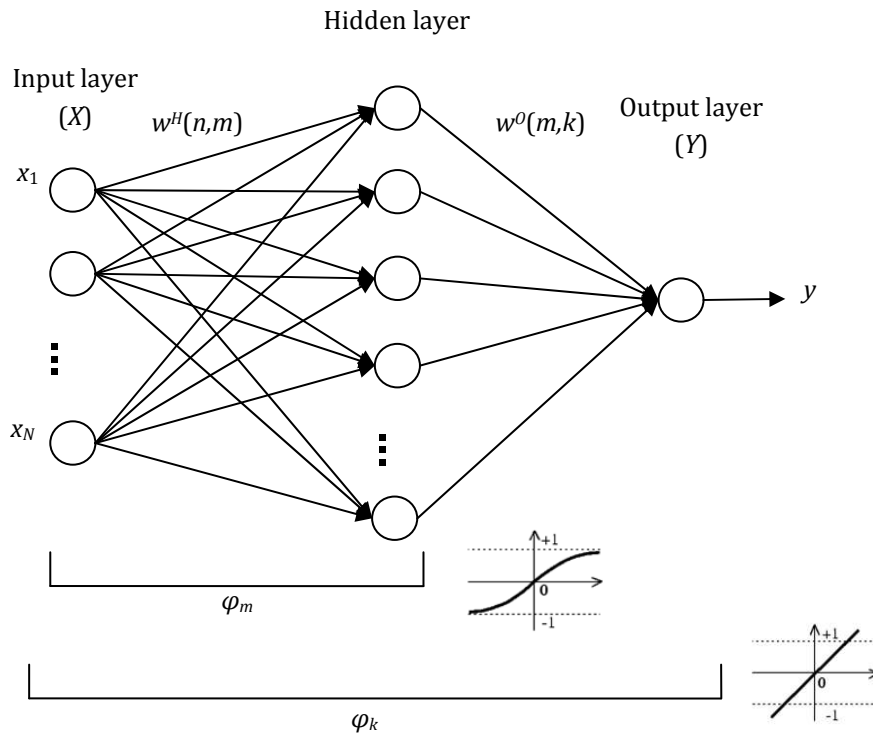

Figure 3.10: Multi-layer perceptron neural network.

X is a set of *n*-dimensional input vectors:

$$\boldsymbol{X} = \{\boldsymbol{x}_p\}, p = 1,2,3, \dots P$$

$$\boldsymbol{x} = [x_1, x_2, x_3, \dots, x_n]$$

(13)

Y is a set of *k*-dimensional output vectors:

$$\boldsymbol{Y} = \{\boldsymbol{y}_p\}, p = 1,2,3, \dots P$$

$$\boldsymbol{y} = [y_1, y_2, y_3, \dots, y_k]$$

(14)

$\boldsymbol{\varphi}$ is a set of *m* activation functions.

$\boldsymbol{W^H}$ is the network weight matrix of size [*m* x *j*] referring to the weights between the input and hidden nodes. $\boldsymbol{W^O}$ is the network matrix of size [*m* x *k*] referring to the weights between the hidden and output nodes. The network function for the *k*th output can therefore be formally expressed as follows:

$$\boldsymbol{y}_k = \varphi_k \left(\sum_{m=0}^{M} \boldsymbol{W}_{m,k}^{O} \varphi_m \left(\sum_{n=0}^{N} \boldsymbol{W}_{n,m}^{H} \boldsymbol{X}_n \right) \right)$$

(15)

The performance of an ANN is measured by the root-mean-square error (*RMSE*) which is also the function to be minimised. Since this is a minimisation problem general algorithms for unconstrained optimisation can be used (Ripley 2009).

$$RMSE = \sqrt{\frac{\sum_{n=1}^{N} SSE_n}{NK}} \qquad (16)$$

N refers to the training vector number (i.e. observation) and SSE_i is the sum-square error of the ith training vector for all *K* output nodes:

$$SSE_n = \sum_{k=1}^{K} \left(y_{true,k}^{n} - y_{pred,k}^{n}\right)^2 \qquad (17)$$

The weight matrices (W^H and W^O) are initially randomised. A subset of the input dataset is applied to the network input nodes and the outputs of the hidden and output nodes are calculated. The *SSE* is calculated as in equation (17) upon which the weight matrices are updated using the optimisation framework. The procedure is repeated for the remaining input dataset to calculate the *RMSE* which completes a single iteration. A number of these iterations are necessary to minimise the *RMSE*. (Kalyani et al. 2008)

3.2.2   Application specifications

Statistica's Automated Neural Networks tool was used to do an automated neural network search. The search evaluated 20 possible ANN architectures from which the user specified how many of the top performing networks were saved for further analysis. The specifications of the best performing network were then applied in Matlab environment, using the Matlab Neural Networks toolbox (version 6.0.1). A 10-fold cross validation was done to ensure that results were consistent and reliable. A validation set was kept aside for the final validation of the network.

CHAPTER 4
RESULTS AND DISCUSSION

1. LABORATORY STUDY

The laboratory study results comprise of the established grinding profile, the assay results received from the analysis laboratory as well as subsequent experimental design responses to determine variable effects on flotation performance. Results from the analysis of the images will then be discussed followed by those obtained from the data analysis.

1.1 Grinding profile

The mill grinding profile was established by evaluating the particle size distribution after 20, 30, 40, 50, 94 and 112 minutes of grinding an ore mass of 2kg. From the particle size analysis using laser diffraction the cumulative finer volume percentage was obtained as a function of particle diameter. The profiles were plotted on one axis in Figure 4.1.
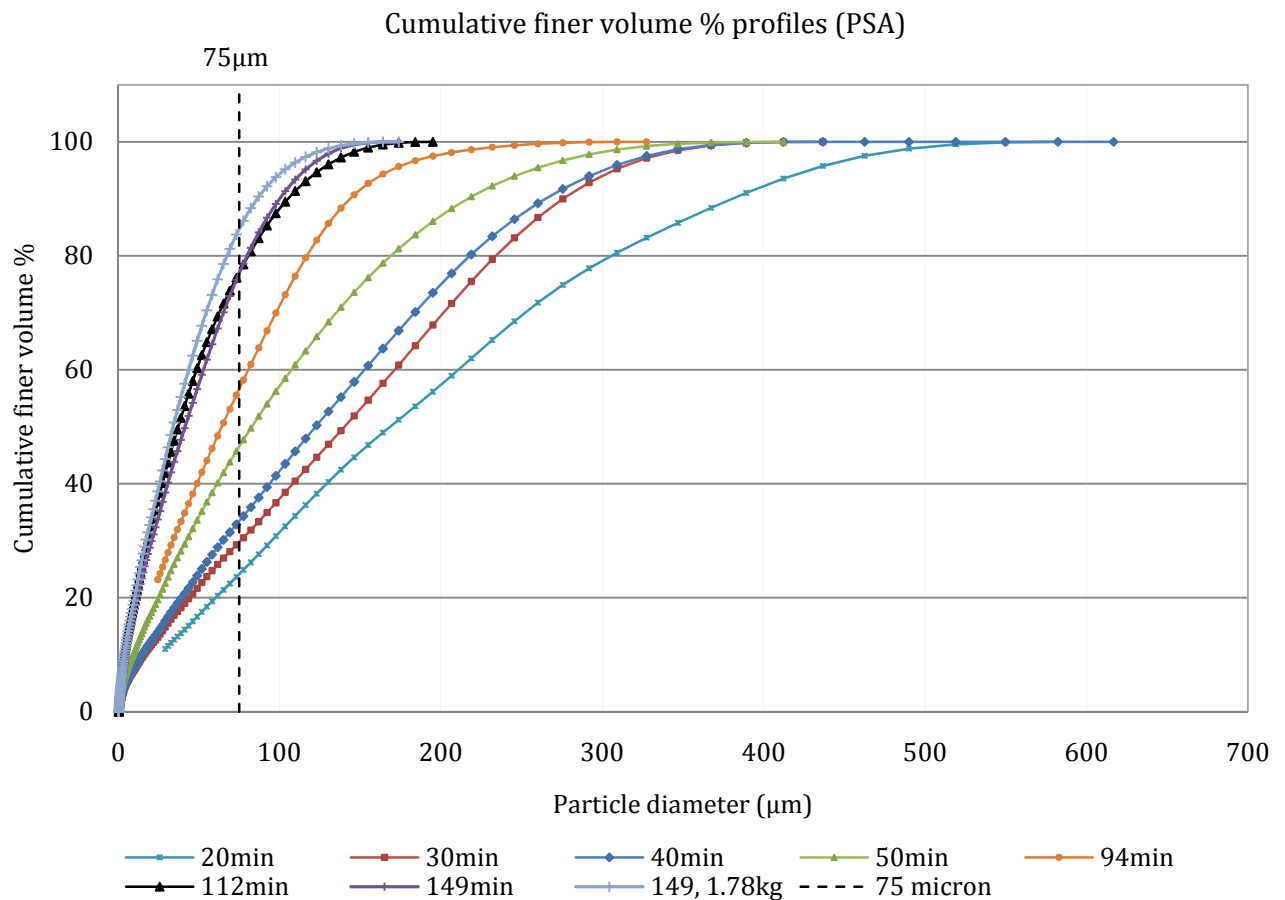

Figure 4.1: Cumulative finer volume percentage profiles from laser diffraction.

The black dashed line in Figure 4.1 indicates the 75μm threshold which is the required grinding size specific to the ore type for batch laboratory test work. The points where the threshold line and the cumulative graphs coincide are plotted to produce the final grinding profile for the specific mill used (Figure 4.2).
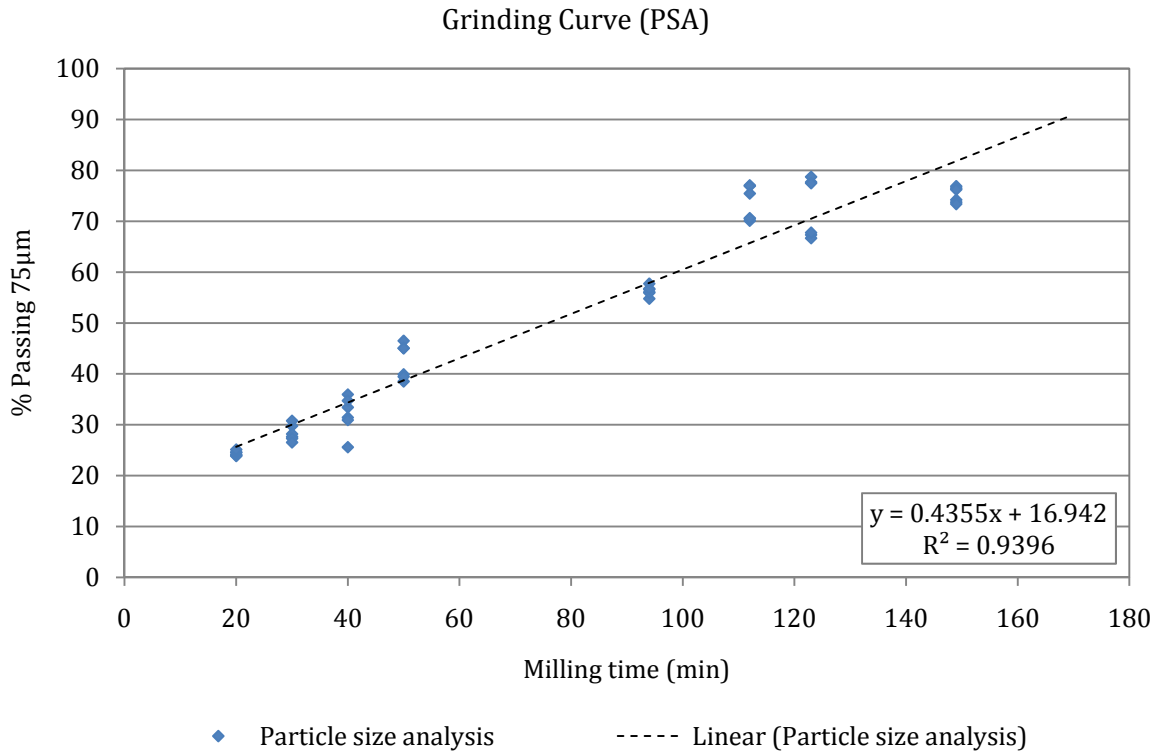
Grinding Curve (PSA)

Figure 4.2: Final grinding profile for the batch rod mill.

The mass of ore milled was varied to have a consisted initial pulp density inside the flotation cell for all the experiments. The required mass ranged between 1.8 kg and 1.9 kg and is not much of different in mass to the 2 kg used for the grinding curve; however additional milling test work was done to ensure the correct particle size distributions. The results for milling times for the given ore mass and particle size requirements were 99 minutes for 60% passing 75μm, and 145 minutes for 80% passing 75μm.

1.2   Assay results

The samples were analysed for platinum, palladium, copper and nickel by fire assay. From the assay results, the grade profiles (Figure 4.3) and grade-recovery profiles (Figure 4.4) were obtained. All the values were standardised to reflect values between 0 and 1.
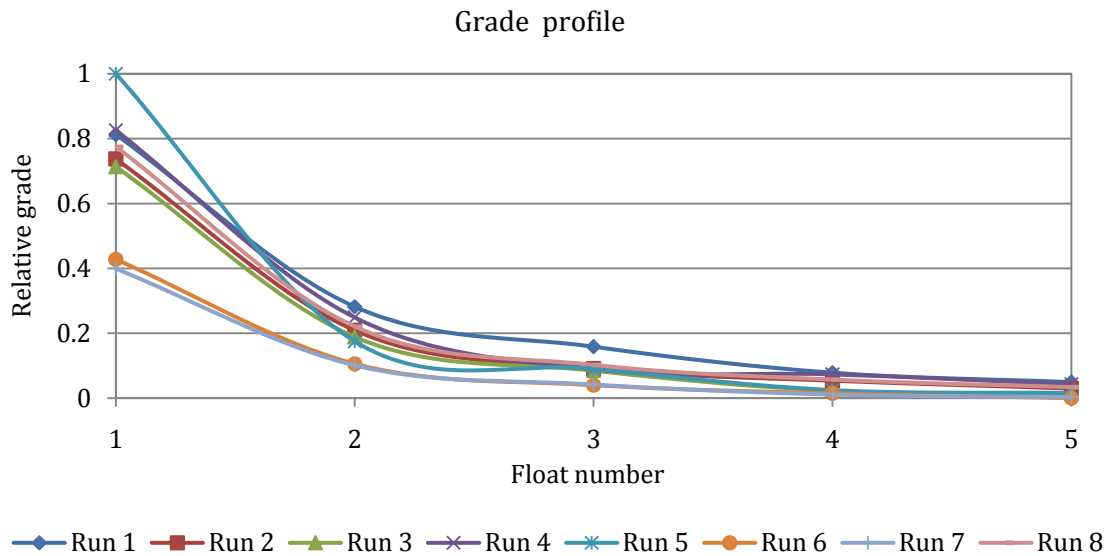
Figure 4.3: Grade profiles of the laboratory study.

As expected a very clear difference in float grade is obtained as the experiment proceeds. This relates very well to an industrial flotation bank, in this case specifically the primary rougher bank as the ore was sampled before the mill.

The grade-recovery profile is generally used as an indicator of bank performance in the industry. Both the grade and the recovery are reflected as cumulative amounts.
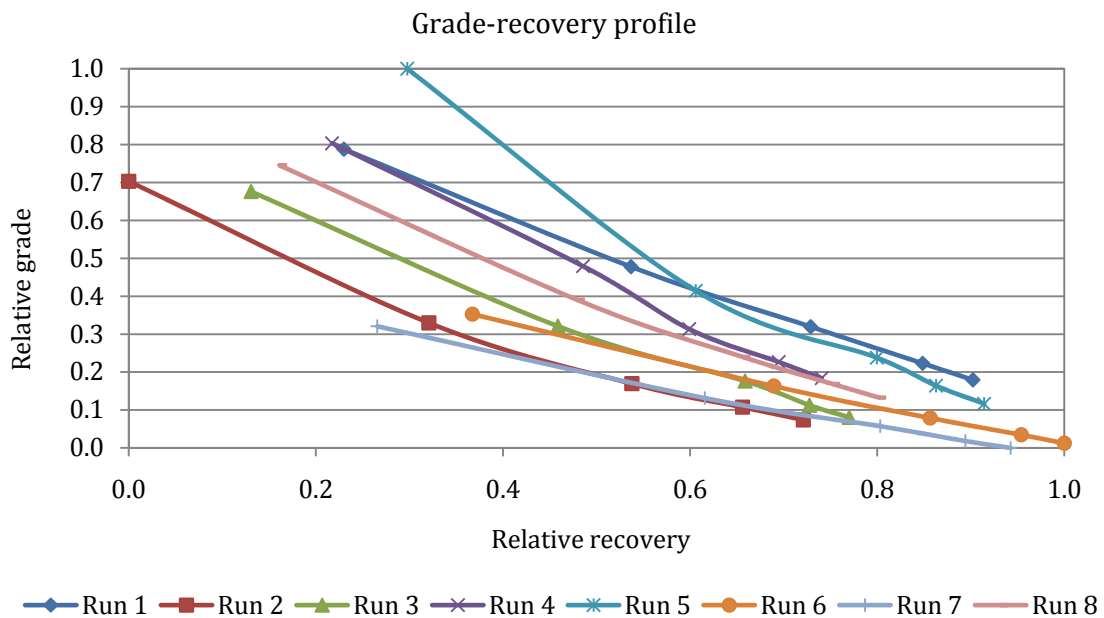

Figure 4.4: Grade recovery profiles of the laboratory study

1.3 Experimental design analysis

The purpose of an experimental design of experiments is for the identification of the main effects of the variables as well as their interaction effects of a target output. The certainty of this estimation of effects was determined from analysis of variance (ANOVA). The target outputs of interest were the platinum grade and recovery. The effects of the variables on the platinum grade of each float were also analysed. The effects are displayed in the format of a pareto graph (Figure 4.5). The vertical dashed line indicates the alpha value (p) that is the probability that the effect is not significant. A low alpha value therefore indicates a high confidence in the effect estimation. Very few conclusions could be drawn with certainty from this analysis. The only significant effects that could be identified were that of the pulp height and collector addition on the cumulative platinum grade with a certainty of 90%. The reason for the lack of reliable information regarding effect estimates could be due to the little variation in the assay results because of the mass pull restrictions on the experimental design's high and low levels.
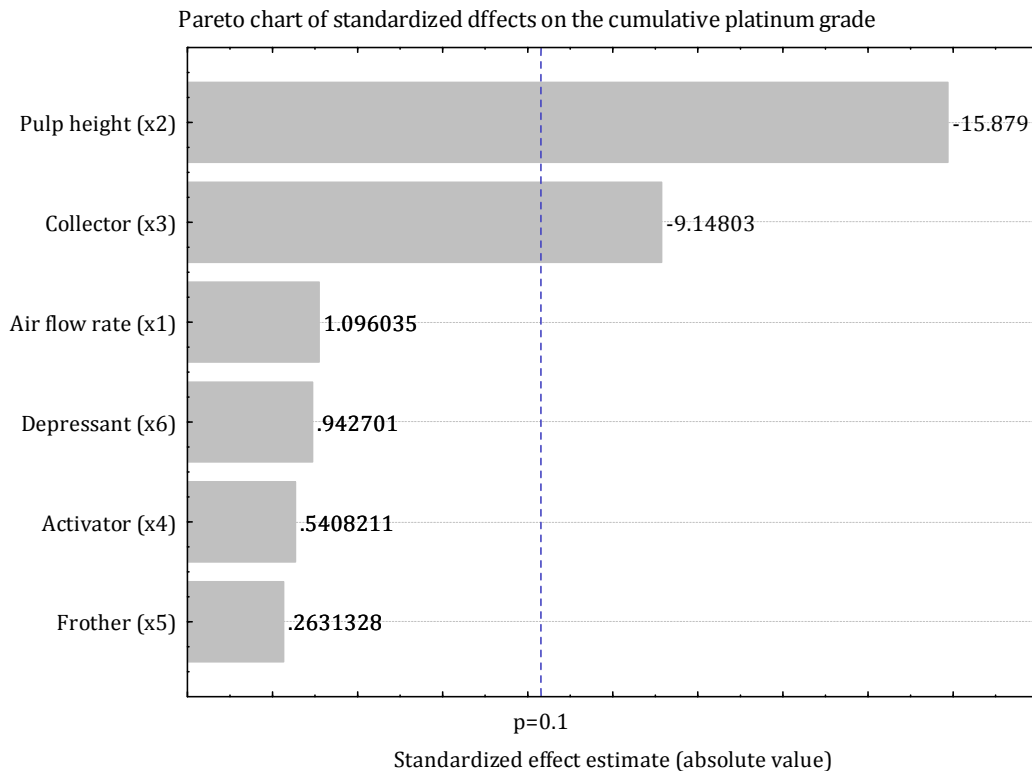

Pareto chart of standardized dffects on the cumulative platinum grade

Pulp height (x2)	-15.879
Collector (x3)	-9.14803
Air flow rate (x1)	1.096035
Depressant (x6)	.942701
Activator (x4)	.5408211
Frother (x5)	.2631328

p=0.1

Standardized effect estimate (absolute value)

Figure 4.5: Pareto chart showing the main effects of the variables on the cumulative platinum grade.

The results show that a decreasing pulp height will have a positive linear effect on the platinum grade. The results are confirmed when looking again at the grade recovery profile (Figure 4.4) where the bottom four lines (run 2, 3, 6 and 7) were executed at high pulp heights and the other four at a low pulp height. Within the lower group (high pulp level), runs 2 and 7 are below runs 6 and 3, the distinctive factor being collector, which has the 2nd most effect on the flotation performance according to the analysis of variance. A lower pulp height would allow a higher froth to develop, therefore allowing more drainage that will result in the drop back of more entrained particles. A decrease in collector addition is projected to have a positive linear effect

on the cumulative platinum grade as well. The reason could be due to a low selectivity of the collector and an ineffective depressing effect by the depressant. Nevertheless, the cumulative grade could be predicted using regression achieving R^2 and adjusted R^2 values of 0.997 and 0.979 respectively.

1.4   Image analysis

Texture features were extracted for each frame of each video by using in-house software. Representative froth images had to be extracted from the recordings as it includes the disturbance of sample taking as well as froth build up time. Only a few seconds before the sample is scraped off is considered representative. A difference matrix was created, subtracting data at i+1 from data at i from which big differences in consecutive points would be picked up, exposing the disturbance in the video. From this point, we collected the data from 6 seconds to 1 second prior to the disturbance i.e. i-6 to i-1. The resulting samples are shown in Figure 4.6, where the coloured strips represent the samples and the different colours represents the different floats. Representative images with their associated relative grades are collected in Figure 4.8
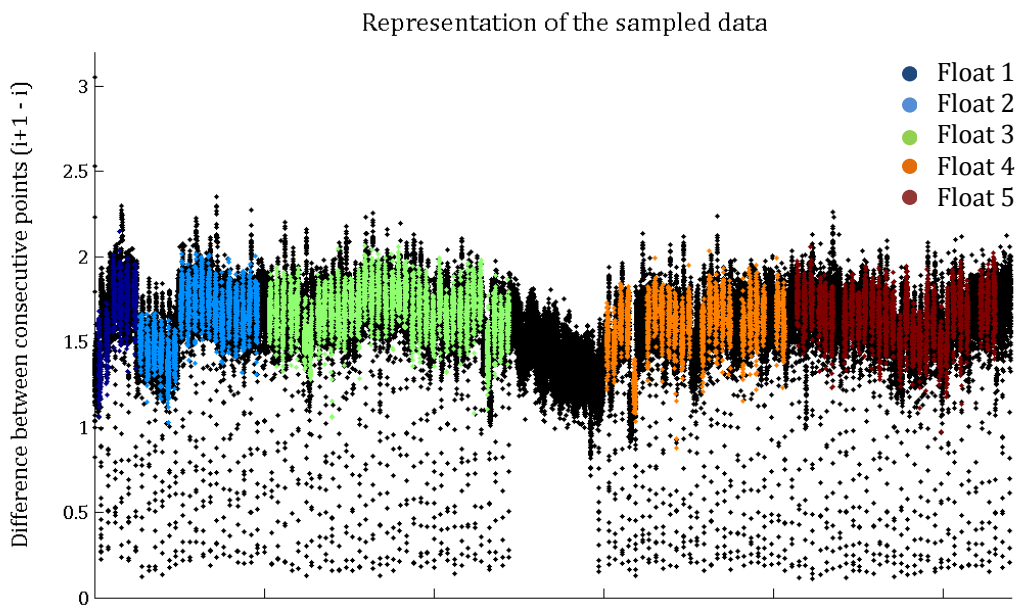

Figure 4.6: Illustration showing the sampling of the representative images from the laboratory study videos.

All the extracted points were combined with the target variables and process information for a complete dataset with approximately 17400 observations per run as illustrated by Figure 4.7. Although only one grade measurement was made for each float, that grade represents the combined samples for the specific duration and is therefore also associated with each image during that sampling time.
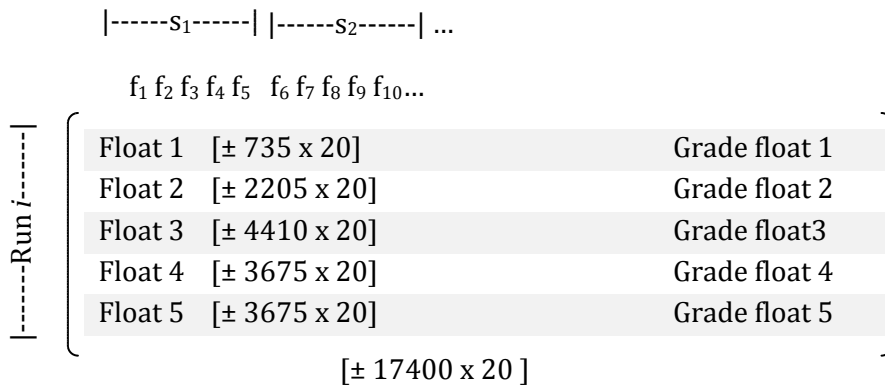
```
|------s₁------| |------s₂------| ...

    f₁ f₂ f₃ f₄ f₅   f₆ f₇ f₈ f₉ f₁₀...
```

$$|\text{------s}_1\text{------}|\ |\text{------s}_2\text{------}|\ ...$$

$$f_1\ f_2\ f_3\ f_4\ f_5\quad f_6\ f_7\ f_8\ f_9\ f_{10}...$$

Float 1 [± 735 x 20]	Grade float 1
Float 2 [± 2205 x 20]	Grade float 2
Float 3 [± 4410 x 20]	Grade float3
Float 4 [± 3675 x 20]	Grade float 4
Float 5 [± 3675 x 20]	Grade float 5

(Run i)

$$[\pm\ 17400\ x\ 20\ ]$$

Figure 4.7: The dataset structure for an experimental run.

	Float 1	Float 2	Float 3	Float 4	Float 5
Run 1	0.812	0.282	0.159	0.079	0.050
Run 2	0.737	0.209	0.092	0.054	0.030
Run 3	0.714	0.189	0.085	0.023	0.014
Run 4	0.826	0.249	0.089	0.073	0.043
Run 5	1.000	0.175	0.091	0.025	0.016
Run 6	0.428	0.106	0.040	0.015	0.000
Run 7	0.399	0.101	0.042	0.011	0.003
Run 8	0.775	0.221	0.102	0.057	0.034
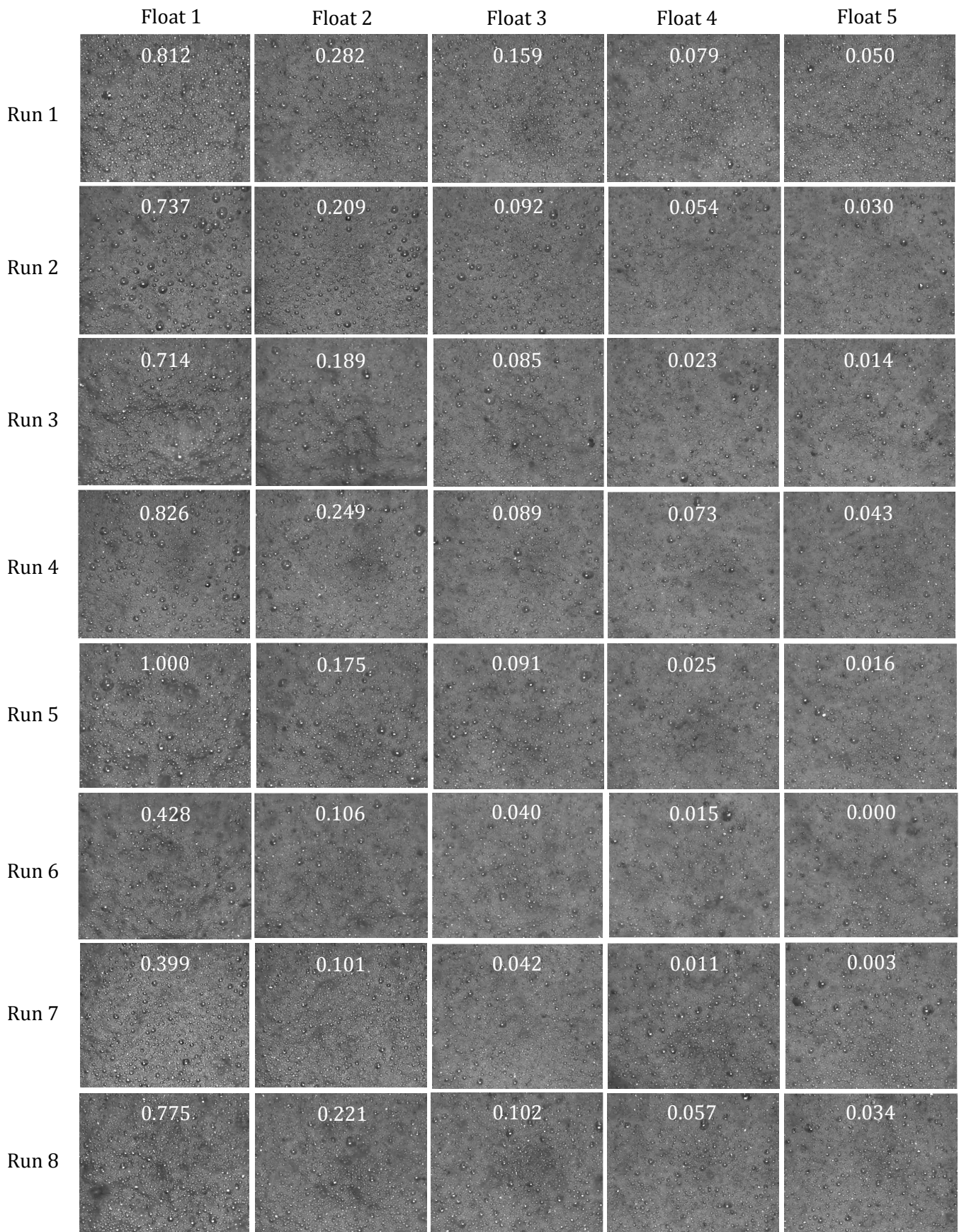
Figure 4.8: A collection of representative images for each experiment at each float.

1.5 Data pre-processing

Data pre-processing was necessary to understand the data from which the proper analysis techniques could be identified. Pre-processing involved the investigation of descriptive statistics and principal component analysis (PCA).

1.5.1 Descriptive statistics

Correlation indicates the strength of the relationships between variables. The correlation matrix is useful for getting familiar with the dataset and gives insight into the variables' relationship with the target variable, in this case the concentrate grade, shown in the last column and row.
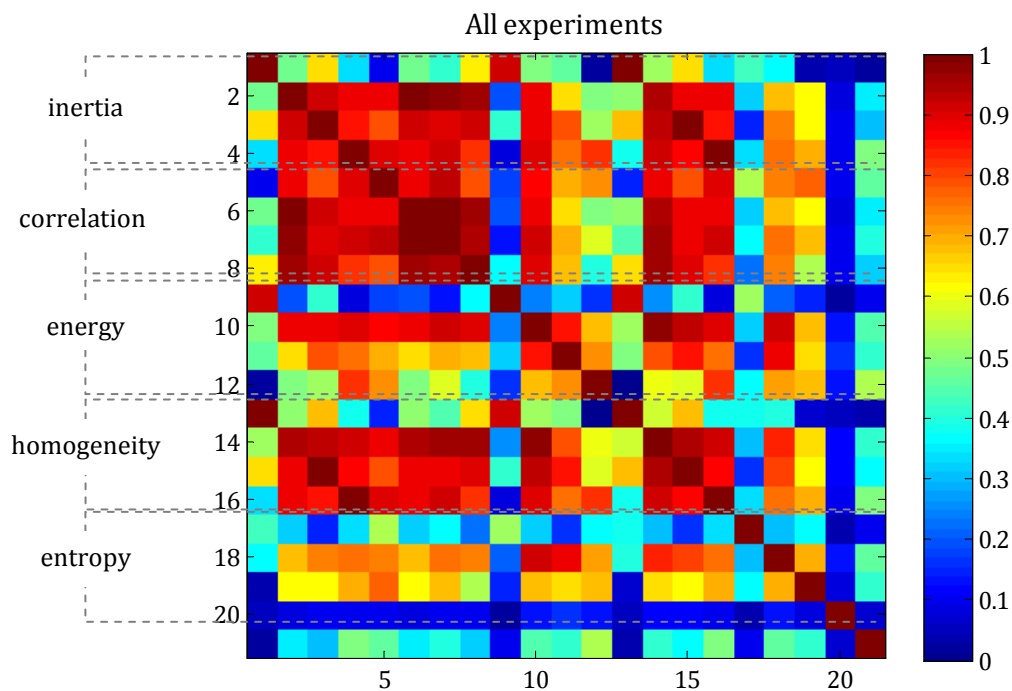

Figure 4.9: Correlation matrix of statistical features and concentrate grade.

From Figure 4.9 the correlation matrix showed that the inertia, correlation and homogeneity measures correlate well with one another. The relationship between each of the texture features and the concentrate grade was relatively low (<0.6) and there appeared to be no single dominant variable, however the inertia correlation and homogeneity measures could perhaps as a group be dominant features from the entire set of texture features.

1.5.2 Principal component analysis

Principal component analysis is most often used to reduce the dimensionality of a dataset by identifying a set of orthogonal axes that displays the maximum variance of a multidimensional dataset. Eigenvalues indicate the contribution to the total variance explained by a variable. The amount of principal components that will describe the complete dataset sufficiently is used for further analysis.
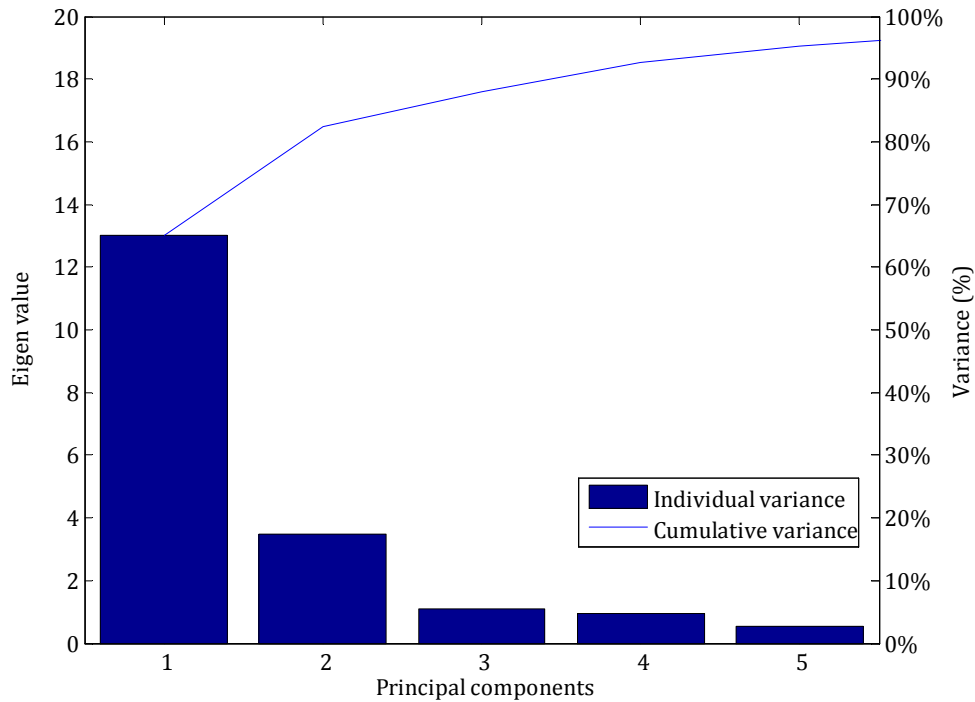
Figure 4.10: Principal component analysis results for all experiments showing the principal component variance contributions

The set of 20 variables could be reduced to a set of 5 principal components that captured 95% of the variance in the data as illustrated with a pareto graph in Figure 4.10. The bars indicate each individual principal component's contribution and the line indicates the cumulative contributions. The first three principal components failed to group the data into clusters based on the relative grade (scale 1 to 100) as shown in Figure 4.11. This indicated that a linear solution might not be possible. Individual PCA of each experiment could not achieve better separation that the combined dataset.
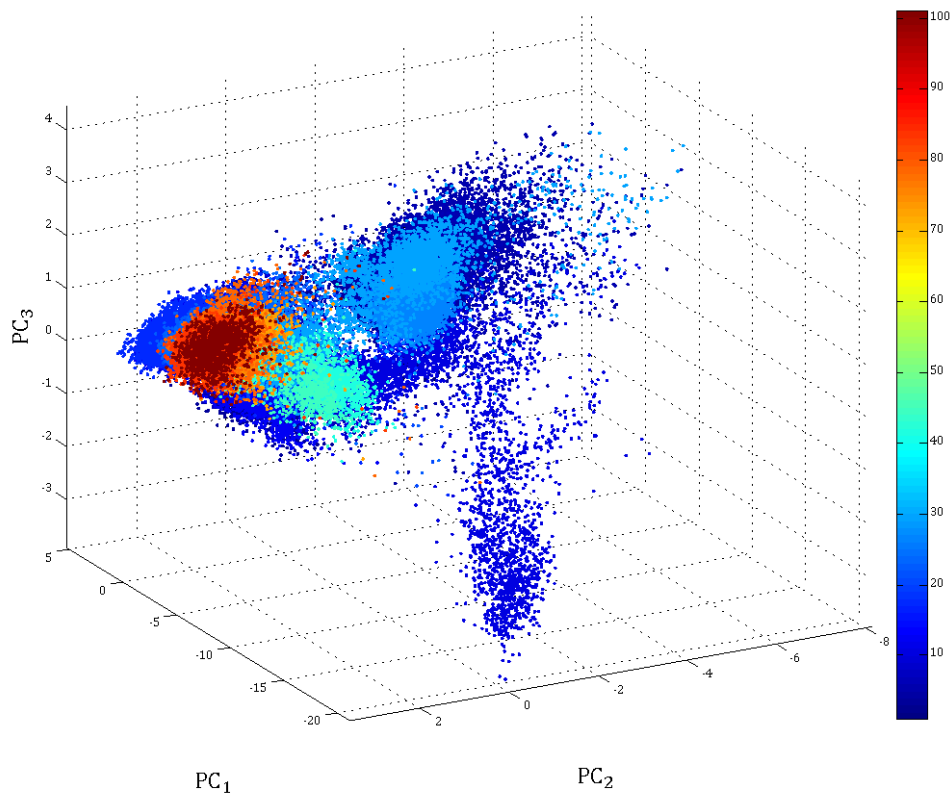
Figure 4.11: Principal component analysis results for all experiments showing the data on new set of axis, colour transition from blue to red indicates increase in concentrate grade.

1.6 Data analysis

1.6.1 Multiple linear regression

As expected from the poor correlation of the texture features to the concentrate grade (Figure 4.9), and confirmed by the poor separation based on the concentrate grade with PCA (Figure 4.11), a multiple linear regression (MLR) model achieved low R^2 and adjusted R^2 values - 0.394 and 0.393 respectively.

1.6.2 Random forest classification

Classification with random forests was successful in distinguishing from the 3 different classes by using only the texture features. The classes have been chosen as in Table 4.1 based on the distribution of the data points.

Table 4.1: Classification criteria for random forest classification.

Class	Performance criteria
Class 1	relative grade <= 0.12
Class 2	0.12 < relative grade <= 0.40
Class 3	relative grade > 0.40

The parameters that could be optimised were the number of trees in the forest (*ntree*) and the number of variables available for split rule selection (*mtry*). A range of each parameter was tested for each experiment. The resulting hyper plane of the combined experimental average results (Figure 4.12) was used to decide on an optimal combination. A number of 150 trees and 8 parameters performed well and was used for further analysis.
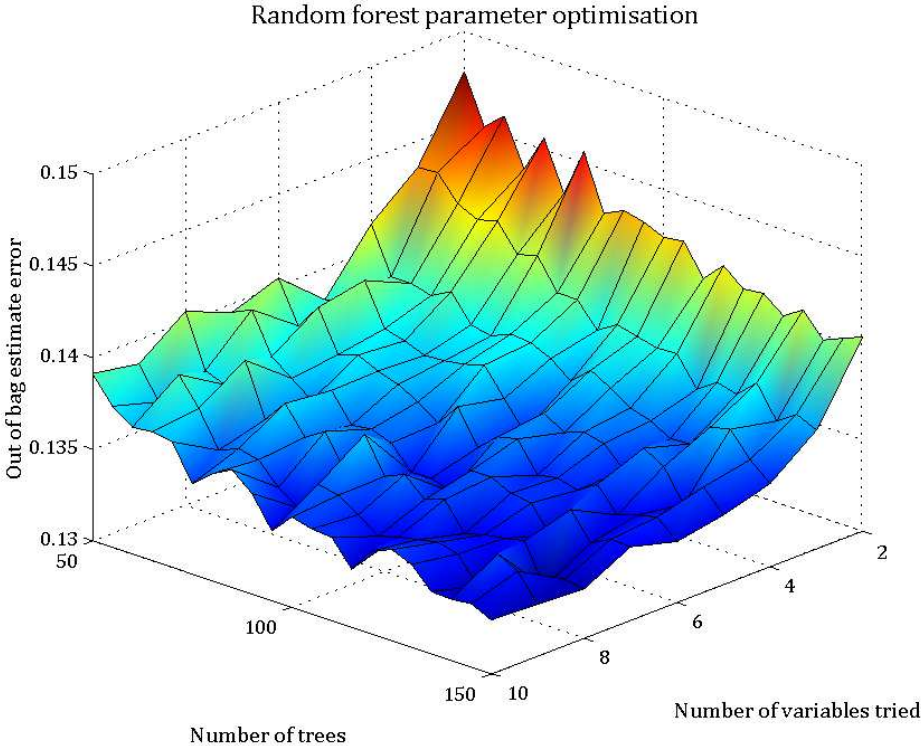

Figure 4.12: Random forest parameter optimisation for laboratory study.

The validation results are shown in the column plot (Figure 4.13) indicating an average overall performance of 86.8% classification accuracy, showing that image features alone are reliable measures for model building.
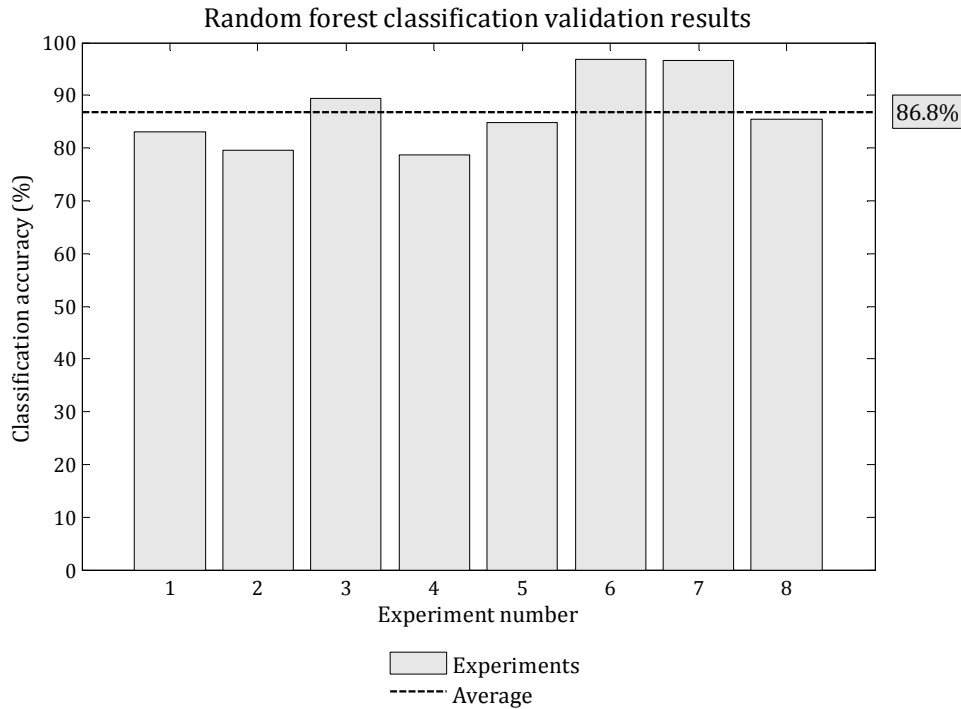
Figure 4.13: Random forest classification results for laboratory study.

The combination of all the information from all the experiments as one dataset was also evaluated. The texture features classified the float grades fairly well with an average classification accuracy of 75.5%. Process conditions were not used for analysis as process conditions remain the same for an entire run while the grade changes gradually. Process conditions may not always be reliably measurable on a minerals processing plant and their contributions should be evaluated to establish whether they will be suitable for inclusion into a grade predictive model.

1.6.3   Artificial neural network regression

For the experimental study each neural network input layer had 19 dimensions (N=19), consisting of the 19 texture features (the binary entropy had to be omitted from the dataset due to a standard deviation of 0). A number of possible network architectures were tested for each experiment to determine the appropriate amount of hidden nodes (M) and the activation functions. The error function (*RMSE*) was minimised using the error-back-propagation algorithm using a gradient-descent technique. The best performing networks are summarised in Table 4.2.

Table 4.2: Neural network results summary for laboratory study.

	N - M - K	R^2 Testing	Hidden layer activation function (φ_m)	Output layer activation function (φ_k)
Run 1	19-16-1	0.952	Logistic	Logistic
Run 2	19-12-1	0.917	Logistic	Logistic
Run 3	19-8-1	0.877	Tanh	Logistic
Run 4	19-17-1	0.831	Tanh	Logistic
Run 5	19-12-1	0.995	Tanh	Tanh

	N - M - K	R² Testing	Hidden layer activation function (φ_m)	Output layer activation function (φ_k)
Run 6	19-15-1	0.990	Tanh	Identity
Run 7	19-17-1	0.989	Logistic	Logistic
Run 8	19-15-1	0.991	Tanh	Tanh
Average		**0.943**		

The neural network built on the textural features performed well with an average R^2 value of 0.943 from which it was evident that the grade can be predicted reliably from image information alone.

The combination of all the experiments' information into a single dataset as input to a neural network was evaluated. The neural network had 19 input nodes (N=19) consisting of 19 texture features (binary entropy omitted), 8 hidden nodes (M=8) and one output node (K=1). With a logistic hidden layer activation function and logistic output layer activation function an R^2 value of 0.828 was achieved.

2. CASE STUDY

The air flowrate in meters per second (m/s) to the flotation cell was changed in steps as shown as time progressed, each point indicating the average air flowrate during the sampling period (Figure 4.14). The sample number is shown above each point.
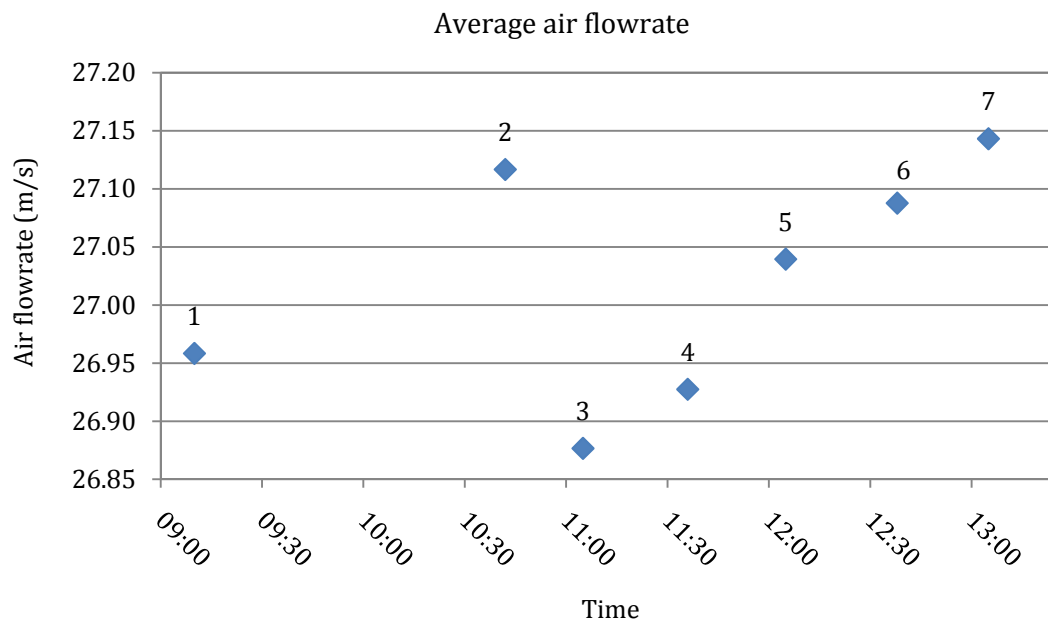

Figure 4.14: Average air flowrate profile of the industrial case study.

2.1 Assay results

The samples were analysed for platinum, palladium, copper and nickel by fire assay from which the grade profile for the test work was obtained (Figure 4.15).
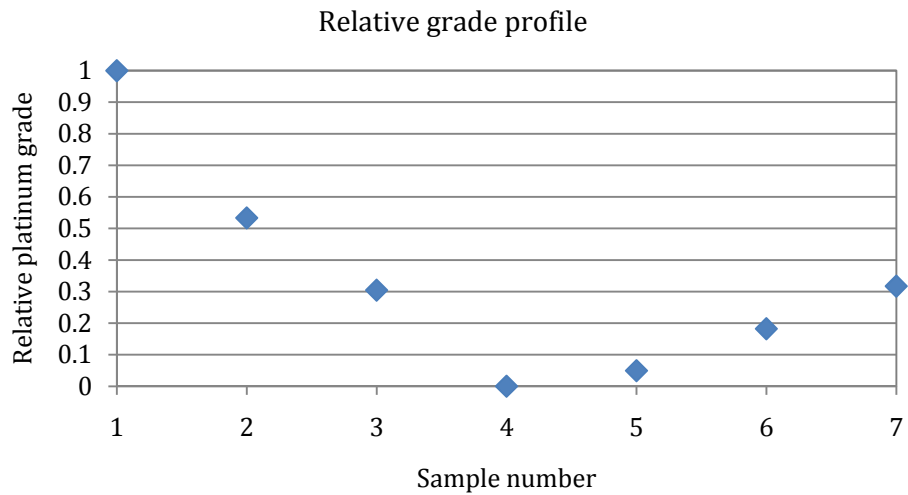
Figure 4.15: Grade results from the case study.

2.2 Image acquisition

Images representative of the samples are shown in Figure 4.16.
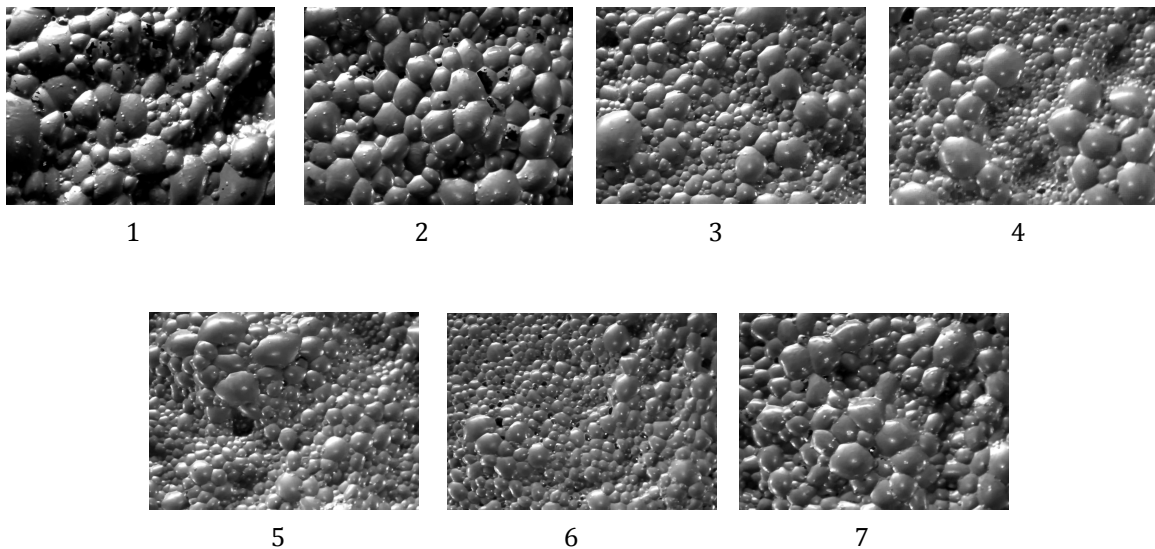

Figure 4.16: Representative sample images for industrial case study.

2.3 Image analysis

The collection of features were made up of 20 features describing the physical froth structure, 9 describing the dynamic froth properties and 20 textural features as illustrated in Figure 4.17.
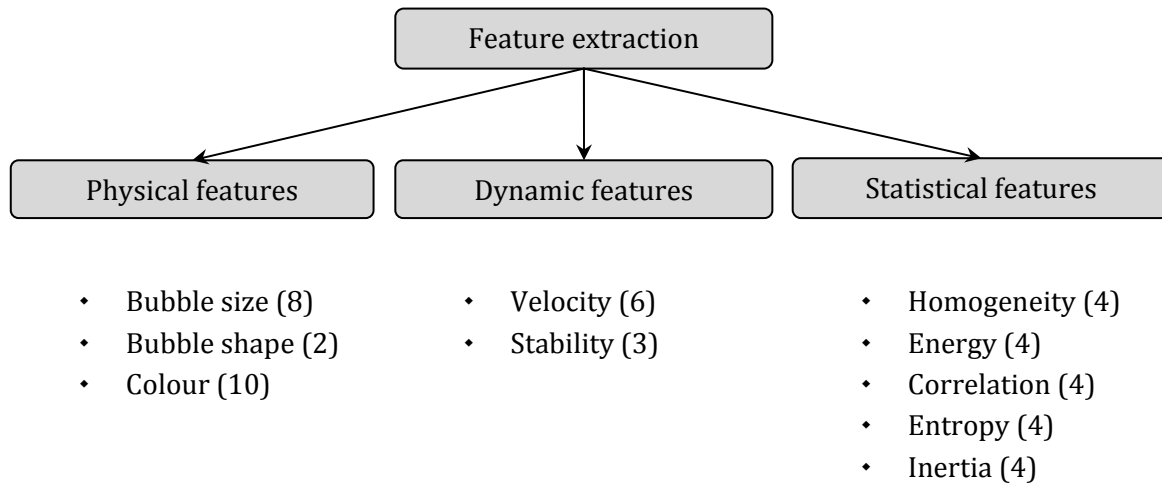
```
              Feature extraction


  Physical features     Dynamic features      Statistical features
```

- Bubble size (8)   - Velocity (6)   - Homogeneity (4)
- Bubble shape (2)   - Stability (3)   - Energy (4)
- Colour (10)   - Correlation (4)
                                                   - Entropy (4)
                                                   - Inertia (4)

Figure 4.17: Summary of extracted features.

Physical and dynamic features were calculated at half the frame rate of the video, i.e. 15 fps, due to software restrictions. The statistical features were therefore processed to match up with a 15 fps frame rate by using a moving average over two consecutive data points. The resulting dataset were as follows:
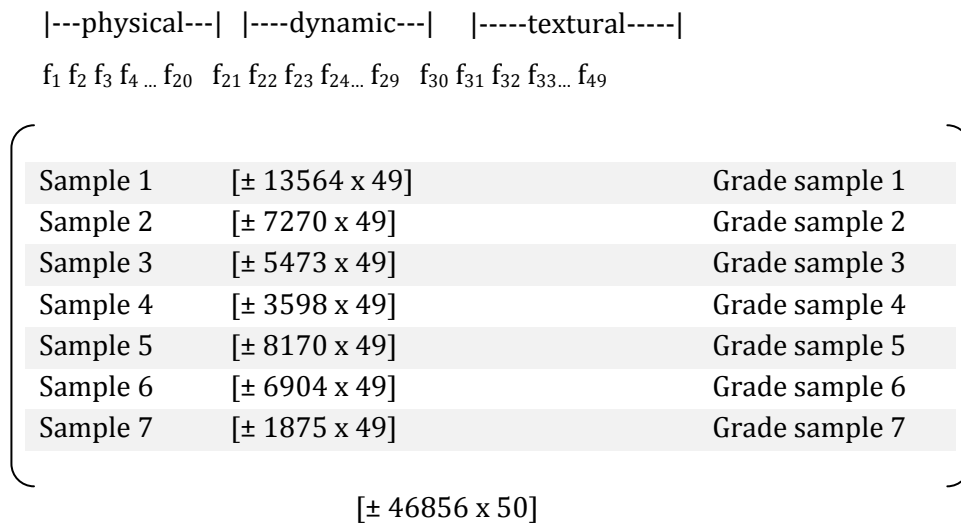
|---physical---| |----dynamic---| |-----textural-----|

$f_1\ f_2\ f_3\ f_4\ ...\ f_{20}$ $f_{21}\ f_{22}\ f_{23}\ f_{24}...\ f_{29}$ $f_{30}\ f_{31}\ f_{32}\ f_{33}...\ f_{49}$

Sample 1	[± 13564 x 49]	Grade sample 1
Sample 2	[± 7270 x 49]	Grade sample 2
Sample 3	[± 5473 x 49]	Grade sample 3
Sample 4	[± 3598 x 49]	Grade sample 4
Sample 5	[± 8170 x 49]	Grade sample 5
Sample 6	[± 6904 x 49]	Grade sample 6
Sample 7	[± 1875 x 49]	Grade sample 7

[± 46856 x 50]

Figure 4.18: The dataset structure for the industrial case study.

2.4 Data pre-processing

Similar to the laboratory dataset, pre-processing is necessary for the investigation of the datasets prior to the application of analysis techniques. Descriptive statistics were used to evaluate the various feature sets according to Figure 4.17. Other pre-processing steps include principal component analysis.

2.4.1 Descriptive statistics

Correlation matrixes have been generated for each group of features: physical, dynamic and statistical features. The information types as per Figure 4.17 are indicated. Grade was added as the last variable to show which features are expected to be important for concentrate grade prediction.
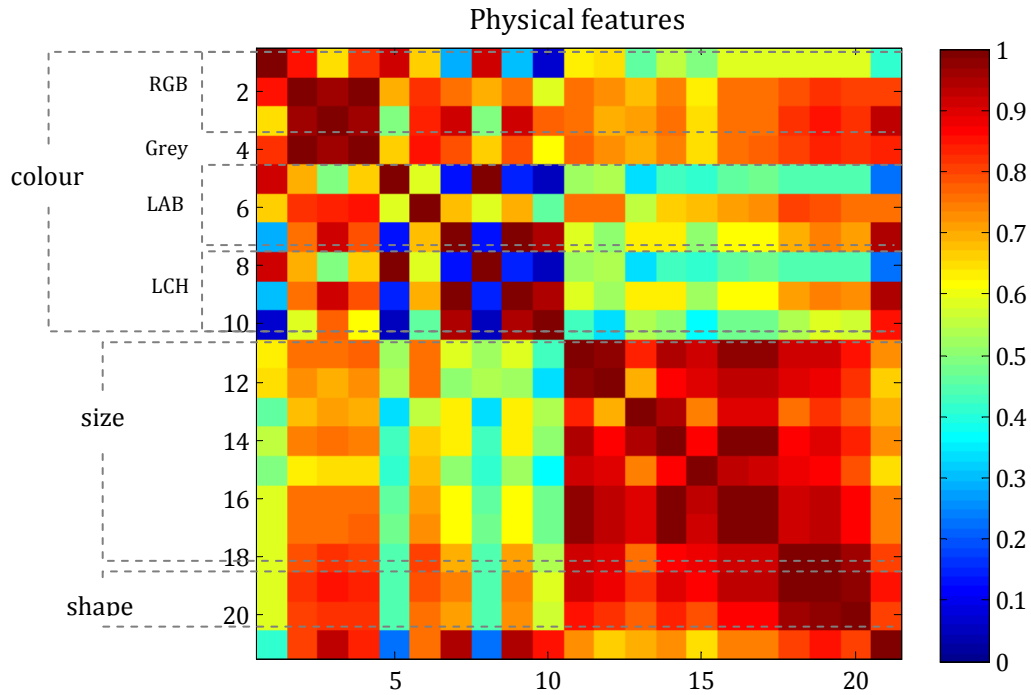

Figure 4.19: Correlation matrix of physical features and concentrate grade.

From the correlation matrix (Figure 4.19), the colour information was correlated strongly with the bubble size and shape information. Some colour measures also showed high correlation with the concentrate grade, indicating that it could be and important contributor to the grade prediction. The average grey level was well correlated with all of the physical features. The bubble size and shape data was highly correlated with itself; therefore this group of variables may be reduced to fewer measures. They also correlated well to the concentrate grade suggesting a strong contribution from this group for a predictive model.
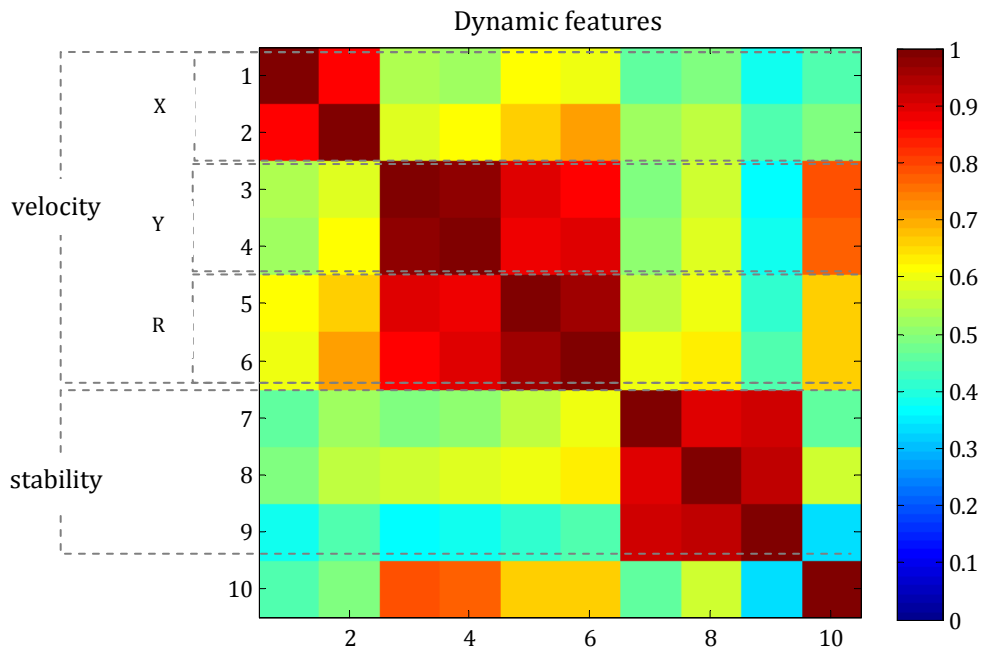
Figure 4.20: Correlation matrix of dynamic features and concentrate grade.

The dynamic features (Figure 4.20) did not show much promise in predicting grade sufficiently, except for the y-direction velocity. In this case the direction of flow was indeed the y-direction as determined by the camera position.
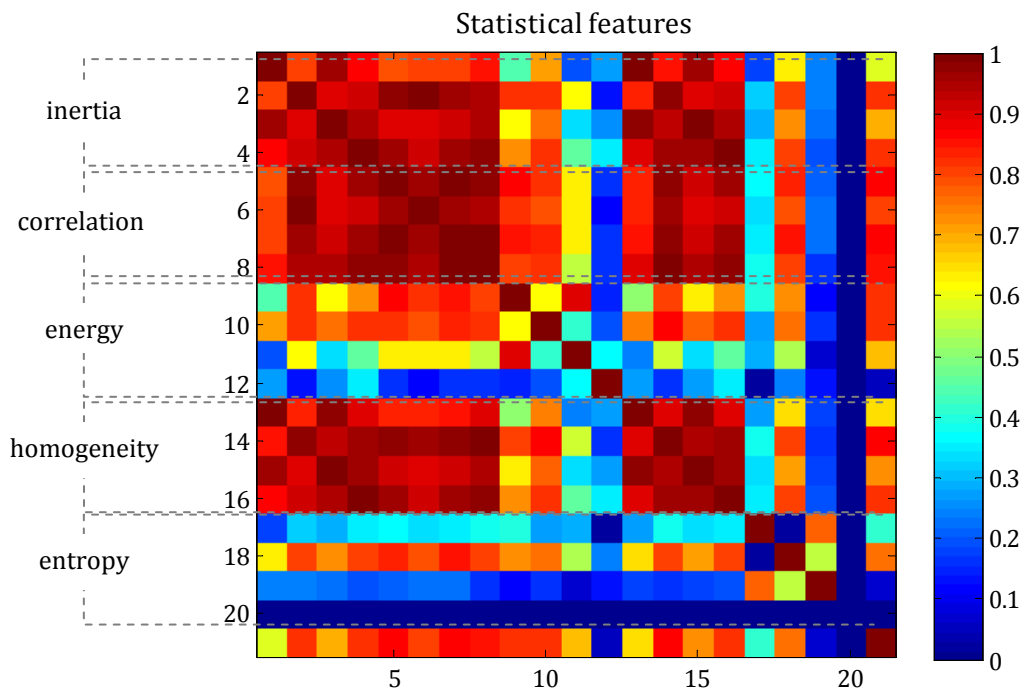

Figure 4.21: Correlation matrix of statistical features and concentrate grade.

The statistical features (Figure 4.21) showed that many of the texture features were highly correlated. Inertia, correlation and homogeneity were highly correlated with one another and with the concentrate grade.
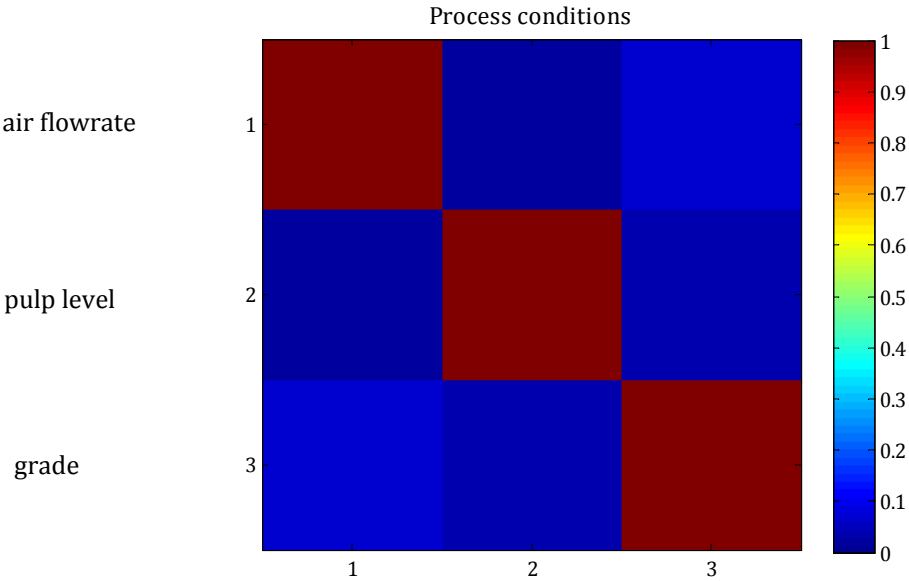

Figure 4.22: Correlation matrix of the process conditions and concentrate grade.

The process conditions did not correlate well with one another or with the concentrate grade suggesting that process conditions may not have a linear relationship with concentrate grade. It is well known that these two parameters are used primarily for mass pull control and not specifically the froth grade.

2.4.2   *Principal component analysis*

Principal component analysis was performed on the data from the case study, similar to the analysis done on the laboratory data. The different feature sets were investigated individually a with the correlation analysis followed by the principal component analysis on the entire dataset.
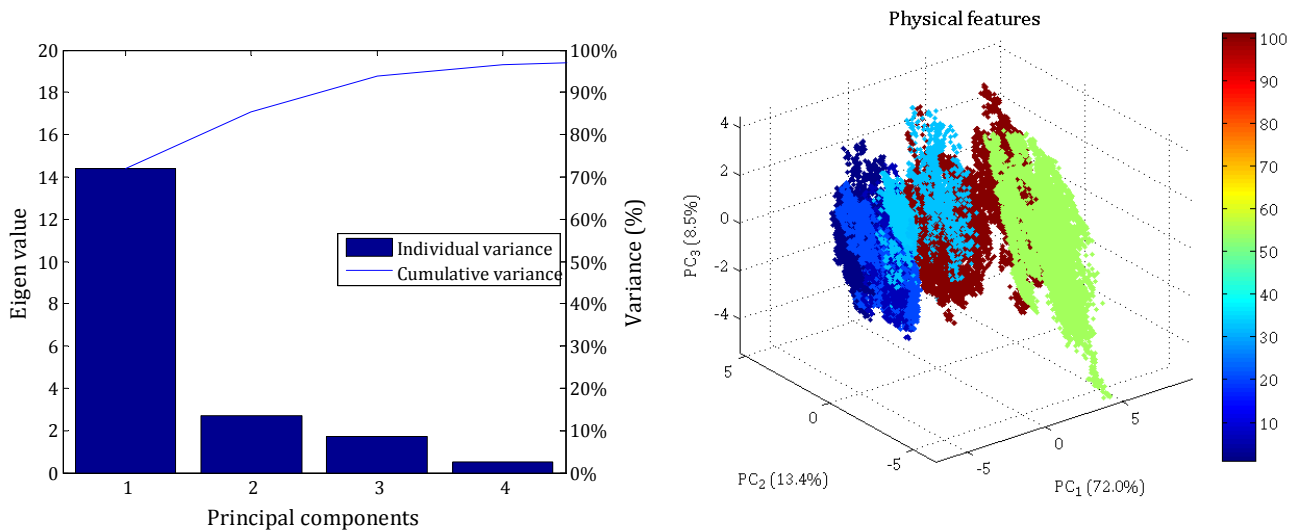
Figure 4.23: Principal component analysis results for physical features: a) principal component variance contributions and b) data on new axis, colour transition from blue to red indicating increase in grade.

Following Figure 4.23, 97% variance of the physical features could be captured in 4 principal components. The resulting illustration of the data on the new set of axis (b) did not separate the data well based on the grade, however data of similar grades were grouped together and not scattered. Concentrate grades were scaled from 1 to 100.

Figure 4.24: Principal component analysis results for dynamic features: a) principal component variance contributions and b) data on new axis, colour transition from blue to red indicating increase in grade.

Information from the dynamic features could be captured sufficiently with 4 principal components as shown in Figure 4.24. The new set of axis did not display good separation of different concentrate grade groups.
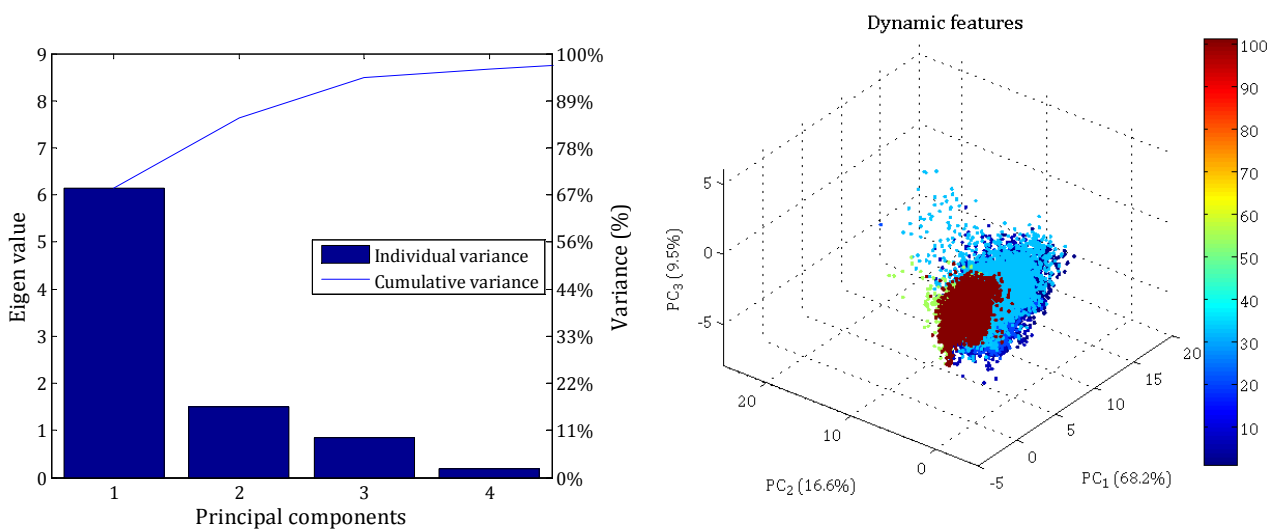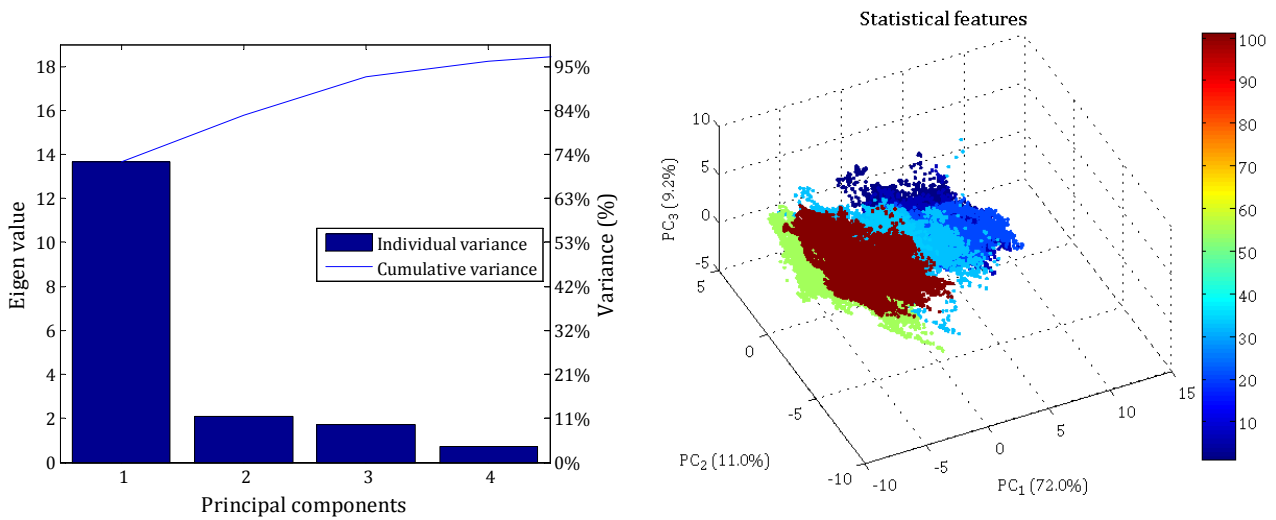
Figure 4.25: Principal component analysis results for statistical features: a) principal component variance contributions and b) data on new axis, colour transition from blue to red indicating increase in grade.

The 4 principal components of the statistical features captured approximately 97% of the variance in the original data (Figure 4.25). The data formed groups based on the concentrate grade however these groups were close to one another and without grade information the distinction between them would not have been possible.

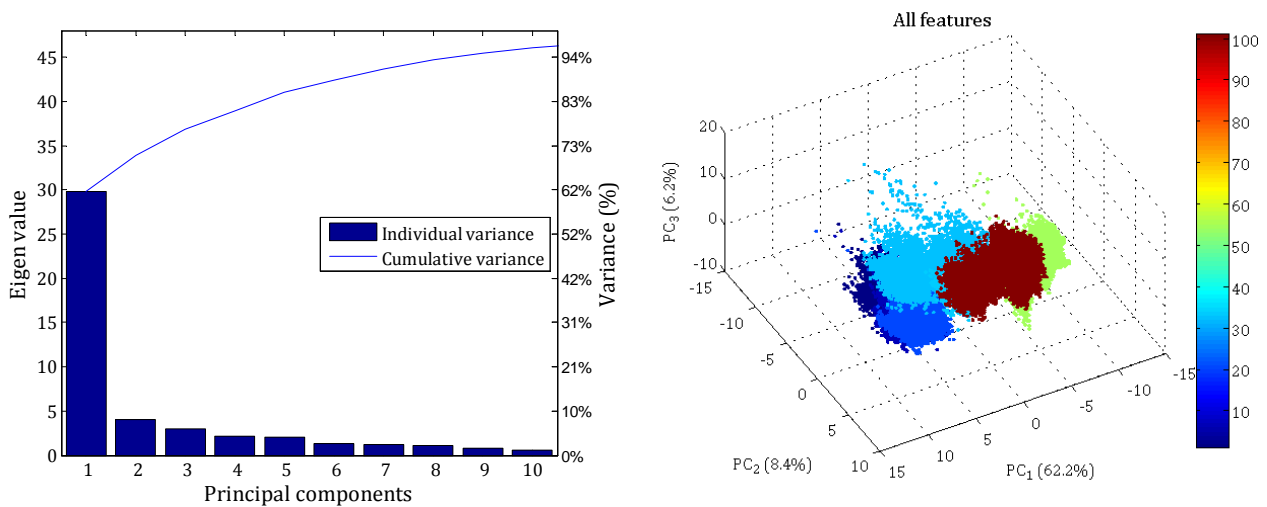*Figure 4.26: Principal component analysis results for all features: a) principal component variance contributions and b) data on new axis, colour transition from blue to red indicating increase in grade.*

From the original dataset, 10 principal components described 97% of the variance. From Figure 4.26 (b) different groups were identifiable on the new set of axis even though they are grouped closely together.
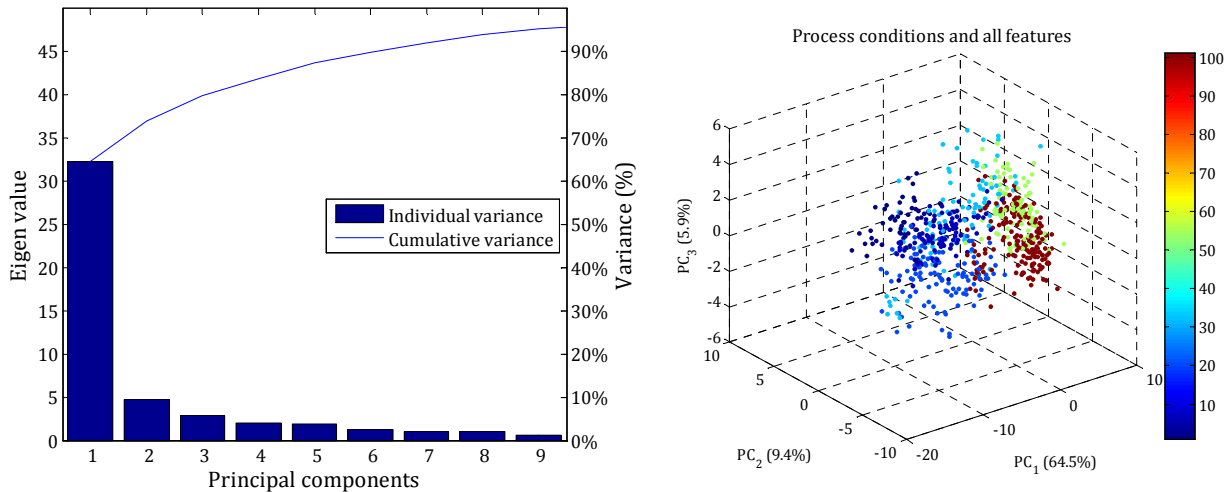
Figure 4.27: Principal component analysis results for process conditions and all features: a) principal component variance contributions and b) data on new axis, colour transition from blue to red indicating increase in grade.

Process conditions were sampled once every 5 seconds; therefore fewer data points were available for analysis (Figure 4.27). 9 principal components captured 95% of the variance in the data. The data were grouped together according to the concentrate grade; however, as with the other analyses they were overlapping at times and grouped close together.

2.5 Data analysis

2.5.1 Multiple linear regression

Multiple linear regression was applied to the different feature sets as well as the combined dataset. The results are shown in Table 4.3.

Table 4.3: Multiple linear regression results for industrial case study.

Adjusted R^2	MLR
Physical features	0.953
Dynamic features	0.743
Statistical features	0.887
All features	0.964
Process conditions	0.003

These results confirm what was expected from inspecting the correlation matrices. The physical features were highly correlated with the concentrate grade, thus the high adjusted R^2 value. Due to the success of the linear model it was not necessary to apply non-linear techniques on the data; however the some preliminary neural network results were obtained for comparison with the MLR models.

2.5.2 Artificial neural network regression

A comparison between the available feature sets was made for the case study using neural networks. The results are summarised in Table 4.4 and are only slightly better than the MLR model predictions.

Table 4.4: Neural network results for industrial case study.

	N - M - K	R^2 Testing	Hidden layer activation function (φ_m)	Output layer activation function (φ_k)
Physical features	20-15-1	0.994	Tanh	Logistic
Dynamic features	9-7-1	0.912	Logistic	Tanh
Statistical features	19-9-1	0.986	Tanh	Logistic
All features	48-14-1	0.997	Logistic	Logistic

The differences between the performances of the different feature sets were very little. The choice of feature set for online application will be dependent on other indicators such as the processing time and interpretability. Physical and dynamical features are for example easier to interpret than statistical features, especially for use by operators.

The case study results are slightly better than that of the laboratory study; however one needs to keep in mind that the range of process conditions was very limited. A data collection campaign over a longer duration of time could provide further validation of these preliminary results. It would also be valuable to investigate how image features relate to other performance indicators such as recovery and mass pull.

CHAPTER 5
FINAL DISCUSSION, CONCLUSIONS AND RECOMMENDATIONS

1. FINAL DISCUSSION

The findings from this study indicate that the information captured in froth images can be related reliably to platinum flotation performance criteria even for the limited experimental work conducted in this study; however the implementation of machine vision systems onto a plant poses various challenges. This includes challenges regarding both hardware and software requirements, specification and maintenance as well as aspects revolving around flotation monitoring and control.

Typical hardware involved are cameras, lighting units and data storage modules. In this study a high definition camera was used, however high definition is not necessarily the minimum requirement. The effect of image resolution on the predictive model accuracy and validity should therefore be evaluated in order to establish the minimum camera requirements. The effect of light variation also needs addressing. Additional lighting could be provided to mitigate the influence of light changes, perhaps paired with the use of the CIE Lab colour spectrum. Alternatively, other types of spectra such as infra-red can be considered, which might be more cost effective with less maintenance. Most importantly, the camera and lighting unit should be able to withstand harsh plant conditions to ensure consistent availability of reliable data. The other matter to consider is frequency of image sampling as this will affect the storage capacity required per machine vision unit. All these hardware challenges are related to some unit cost which will determine the amount of equipment made available for a machine vision system. The availability of machine vision units influences the strategic placement of these units and consequently the effectiveness of the machine vision system as a whole for flotation monitoring and control.

Software requirements include model initialisation, monitoring, maintenance and change strategies. In order to build a predictive model for a given flotation cell, sufficient data needs to be captured to ensure that enough operating conditions are accounted for. The manipulation of plant conditions to capture this required range is seldom, if ever, possible as it will affect plant production adversely. Data will therefore need to be obtained over longer durations. Once a model has been developed and tested, it will need to be monitored to test its validity to predict the flotation cell performance. Disturbances such as change in ore type will typically cause the model to become inadequate, in which case a strategy will need to be in place to update the existing model or build a new model.

Machine vision can either be employed as a process monitoring tool or directly applied for online control. Deep learning techniques such as reinforcement learning may be a valuable tool for modelling and control of a flotation cell. This technique will continuously evaluate the effect

of change of certain variables and penalise or promote a change based on its effect on the performance criteria.

Froth grade was chosen as predicted key performance indicator in this study, however in practice, plants often target mass pull for performance. Research regarding the relationship of image features with mass pull could prove to be more applicable for industrial application than the relationship of image features with froth grade.

2. CONCLUSIONS

Based on the results and discussions, it can be concluded that grades of platinum flotation processes can be predicted reliably from froth image information given the narrow system tested. Although a wider range of operating conditions needs to be investigated, in principle it would be possible to identify the state of the flotation cell from froth image data only, which could be used in advanced model-based control systems. More specifically it was found that

- Pulp height and collector dosage had the most significant effect on the grades yielded by batch flotation, but did not correlate well with grades measured on an industrial plant. The use of these measures as potential manipulated variables in model-based control systems requires the investigation of these effects under plant conditions.
- The laboratory results suggested that a non-linear relationship exists between the platinum froth grade and the textural image features extracted.
- Non-linear models, such as random forest classification and neural network regression performed significantly better than linear models (MLR) in predicting flotation froth grade, with a classification accuracy of 85% and an R^2 value of 0.943 respectively.
- The case study results showed that multiple linear regression can be used successfully to predict froth grade from image features when applied to a limited range of operating conditions.
- Physical, dynamic and statistical features predicted the grade sufficiently with R^2 values of 0.953, 0.743 and 0.887 respectively. The combination of these features performed slightly better with an R^2 value of 0.964. The role of all these features needs to be confirmed with an extensive data campaign to cover a wider range of process conditions.
- Non-linear modelling using neural networks outperformed the MLR model with R^2 values of up to 0.997.
- The plant operational variables of pulp level and air flowrate could not explain the variance in concentrate grades.

3. RECOMMENDATIONS

Based on the findings of this study the following recommendations are made for further investigation:

- An extension of the experimental design, to include the effects of impeller speed and particle size distribution on flotation performance could be useful for identifying interaction effects among variables.

- For the industrial case study it is suggested that data is collected over a longer duration to provide further validation of the preliminary findings and for the development of a comprehensive solution.
- The relationship between image features and other performance indicators such as recovery and mass pull should be investigated.
- Investigations regarding hardware requirements and specifications in terms of minimum resolution, lighting requirements, sampling frequency and data storage will provide useful information regarding the implementation challenges involved with machine vision systems.
- Software requirements, specifications and maintenance challenges will also need to be addressed for implementation purposes once a comprehensive solution has been found.
- Further work should include a strategy for the use of data driven models in flotation control.
- An investigation into deeper learning techniques such as reinforcement learning may be valuable.
- Investigations regarding a protocol for addressing the variability in ore type needs to be conducted and would be an essential component of a machine vision strategy.

REFERENCES

Aldrich, C., Moolman, D.W., Eksteen, J.J. & Van Deventer, J.S.J. Characterization of flotation processes with self-organizing neural nets. *Chemical Engineering Communications*, 1995. Vol. 139, pp. 25-39.

Aldrich, C., Moolman, D.W., Bunkell, S.J., Harris, M.C. & Theron, D.A. Relationship between surface froth features and process conditions in the batch flotation of a sulphide ore. *Minerals Engineering*, 1997a. Vol. 10(11), pp. 1207-1218.

Aldrich, C., Moolman, D.W., Gouws, F.S. & Schmitz, G.P.J. Machine learning strategies for control of flotation plants. *Control Engineering Practice*, 1997b. Vol. 5(2), pp. 263-269.

Aldrich, C., Marais, C., Shean, B. & Cilliers, J. Online monitoring and control of froth flotation systems with machine vision: A review. *International Journal of Mineral Processing*, 2010. Vol. 96(1-4), pp. 1-13.

Banford, A.W., Aktas, Z. & Woodburn, E.T. Interpretation of the effect of froth structure on the performance of froth flotation using image analysis. *Powder Technology*, 1998. Vol. 98(1), pp. 61-73.

Barbian, N., Ventura-Medina, E. & Cilliers, J.J. Dynamic froth stability in froth flotation. *Minerals Engineering*, 2003. Vol. 16(11), pp. 1111-1116.

Barbian, N., Hadler, K., Ventura-Medina, E. & Cilliers, J.J. The froth stability column: Linking froth stability and flotation performance. *Minerals Engineering*, 2005. Vol. 18(3), pp. 317-324.

Barbian, N., Hadler, K. & Cilliers, J. The froth stability column: Measuring froth stability at an industrial scale. *Minerals Engineering*, 2006. Vol. 19(6-8), pp. 713-718.

Barbian, N., Cilliers, J.J., Morar, S.H. & Bradshaw, D.J. Froth imaging, air recovery and bubble loading to describe flotation bank performance. *International Journal of Mineral Processing*, 2007. Vol. 84(1-4), pp. 81-88.

Bartolacci, G., Pelletier Jr., P., Tessier Jr., J., Duchesne, C., Bossé, P.A. & Fournier, J. Application of numerical image analysis to process diagnosis and physical parameter measurement in mineral processes - Part I: Flotation control based on froth textural characteristics. *Minerals Engineering*, 2006. Vol. 19(6-8), pp. 734-747.

Bezuidenhout, M., Van Deventer, J.S.J. & Moolman, D.W. The identification of perturbations in a base metal flotation plant using computer vision of the froth surface. *Minerals Engineering*, 1997. Vol. 10(10), pp. 1057-1073.

Bharati, M., Liu, J.J. & MacGregor, J.F. Image texture analysis: methods and comparisons. *Chemometrics and Intelligent Laboratory Systems*, 2004. Vol. 72(1), pp. 57-71.

Bonifazi, G., Serranti, S., Volpe, F. & Zuco, R. A combined morphological and color based approach to characterize flotation froth bubbles. *Proceedings of the 2nd International Conference on Intelligent Processing and Manufacturing of Materials*, 1999. Vol. 1, pp. 465-470.

Bonifazi, G., Massacci, P. & Meloni, A. Prediction of complex sulfide flotation performances by a combined 3D fractal and colour analysis of the froths. *Minerals Engineering*, 2000. Vol. 13(7), pp. 737-746.

Bonifazi, G., Giancontieri, V., Serranti, S. & Volpe, F. A full color digital imaging based approach to characterize flotation froth: An experience in Pyhasalmi (SF) and Garpenberg (S) plants. *2005 Beijing International Conference on Imaging: Technology and Applications for the 21st Century*, 2005a. pp. 172-173

Bonifazi, G., Serranti, S., Volpe, F. & Zuco, R. Characteristisation of flotation froth colour and structure by machine vision. *Computers and Geosciences*, 2005b. Vol. 27(9), pp. 1111-1117.

Botha, C.P. An on-line machine vision flotation froth analysis platform. *PhD Thesis*. Stellenbosch University, 1999.

Botha, C.P., Weber, D.M., van Olst, M. & Moolman, D.W. Practical system for realtime on-plant flotation froth visual parameter extraction. *IEEE AFRICON Conference*, 1999. Vol. 1, pp. 103-106.

Bradshaw, D.J., Buswell, A.M., Harris, P.J. & Ekmekçi, Z. Interactive effects of the type of milling media and copper sulphate addition on the flotation performance of sulphide minerals from Merensky ore Part I: Pulp chemistry. *International Journal of Mineral Processing*, 2006. Vol. 78(3), pp. 153-163.

Breiman, L. Random Forest. *Machine Learning*, 2001. Vol. 54(1), pp. 5-32.

Brown, N., Bourke, P., Ronkainen, S. & van Olst, M. Improving flotation plant performance at Cadia by controlling and optimizing the rate of froth recovery using Outokumpu FrothMaster. *33rd Annual Meeting of Canadian Mineral Processors*. Ottawa, Canada, 2001. pp. 25-36

Cany, J. A computational approach to edge detection. *IEEE Transactions on Pattern Analysis and Machine Intelligence*, 1986. Vol. 8, pp. 679-698.

Carter, R. Process Control: What's New, What's Next. *Engineering and Mining Journal*, 2010.

Cilliers, J., Asplin, R. & Woodburn, E. Kinetic flotation modelling using froth imaging data. *Frothing in Flotation II*. The Netherlands, Gordon and Breach Science Publishers, 1998. pp. 309-336

Cilliers, J. Physics-based froth modelling: new developments and applications. *International Journal of Computational Fluid Dynamics*, 2009. Vol. 23(2), pp. 147-153.

Cipriano, A., Sepúlveda, C. & Guarini, M. Expert system for supervision of mineral flotation cells using artificial vision. *IEEE International Symposium on Industrial Electronics*, 1997. pp. 149-153

Cipriano, A., Guarini, M., Vidal, R., Soto, A., Sepúlveda, C., Mery, D. & Briseño, H. A real time visual sensor for supervision of flotation cells. *Minerals Engineering*, 1998. Vol. 11(6), pp. 489-499.

Citir, C., Aktas, Z. & Berber, R. Off-line image analysis for froth flotation of coal. *Computers and Chemical Engineering*, 2004. Vol. 28(5), pp. 625-632.

Cruz, E. & Adel, G. Development of video-based sensors for off- and on-stream analysis. *Proceedings of the Annual ISA Analysis Division Symposium*, 1998. pp. 259-268

Cutting, G.W., Barber, S.P. & Newton, S. Effects of froth structure and mobility on the performance and simulation of continuously operated flotation cells. *International Journal of Mineral Processing*, 1986. Vol. 16(1-2), pp. 43-61.

Dai, Z., Fornasiero, D. & Ralston, J. Particle–bubble attachment in mineral flotation. *Journal of Colloid and Interface Science*, 1999. Vol. 217(1), pp. 70-76.

Deglon, D. The effect of agitation on the flotation of platinum ores. *Minerals Engineering*, 2005. Vol. 18(8), pp. 839-844.

Du Plessis, F. & Keet, K. The importance of a high sample frequency measurement of grade to avoid aliasing. *13th IFAC Symposium on Automation in Mining, Mineral and Metal Processing, Industry Papers*. Cape Town, South Africa, 2010.

Ekmekçi, Z. Effects of frother type and froth height on the flotation behaviour of chromite in UG2 ore. *Minerals Engineering*, 2003. Vol. 16(10), pp. 941-949.

Estrada-Ruiz, R.H. & Pérez-Garibay, R. Evaluation of models for air recovery in a laboratory flotation column. *Minerals Engineering*, 2009. Vol. 22(14), pp. 1193-1199.

Finch, J., Nesset, J. & Acuna, C. Role of frother on bubble production and behaviour in flotation. *Minerals Engineering*, 2008. Vol. 21(12-14), pp. 949-957.

Forbes, G. & De Jager, G. Bubble size distribution for froth classification. *Sixteenth Annual Symposium of the Pattern Recognition Association of South Africa*. Langebaan, South Africa, 2004a. pp. 99-104

Forbes, G. & De Jager, G. Texture measures for improved watershed segmentation of froth images. *Fifteenth Annual Symposium of the Pattern Recognition Association of South Africa*. Grabouw, South Africa, 2004b.

Forbes, G., De Jager, G. & Bradshaw, D. Effective use of bubble size distribution measurements. *XXIII International Mineral Processing Congress*. Istanbul, Turkey, 2006. pp. 554-559

Forbes, G. Texture and bubble size measurements for modelling concentrate grade in flotation froth systems. *PhD Thesis*. University of Cape Town, 2007a.

Forbes, G. & De Jager, G. Unsupervised classification of dynamic froths. *Transactions of the South African Institute of Electrical Engineers*, 2007b. Vol. 98(2), pp. 38-44.

Francis, J.J. Machine vision for froth flotation. *PhD Thesis*. University of Cape Town, 2001.

Fu, K. & Mui, J. A survey on image segmentation. *Pattern Recognition*, 1981. Vol. 13(1), pp. 3-16.

Gebhardt, J., Tolley, W.K. & Ahn, J. Color measurements of minerals and mineralized froths. *Minerals and Metallurgical Processing*, 1993. Vol. 10(2), pp. 96-99.

Genuer, R., Poggi, J. & Tuleau, C. *Random Forests: some methodological insights*. Sacley, French national institute for research in computer science and control, 2008.

Glembotskii, V.A. *Flotation*. New York, 1972.

Gupta, A. & Yan, D. Flotation. *Mineral Processing Design and Operation*, 2006. pp. 555-603

Hadler, K. & Cilliers, J.J. The relationship between the peak in air recovery and flotation bank performance. *Minerals Engineering*, 2009. Vol. 22(5), pp. 451-455.

Haralick, R.M., Shanmugam, K. & Dinstein, I. Textural features for image classification. *IEEE Transactions on Systems, Man and Cybernetics*, 1973. Vol. 3, pp. 610-621.

Hargrave, J.M., Miles, N.J. & Hall, S.T. The use of grey level measurement in predicting coal flotation performance. *Minerals Engineering*, 1996. Vol. 9(6), pp. 667-674.

Hargrave, J.M. & Hall, S.T. Diagnosis of concentrate grade and mass flowrate in tin flotation from colour and surface texture analysis. *Minerals Engineering*, 1997. Vol. 10(6), pp. 613-621.

Hargrave, J.M., Brown, G.J. & Hall, S. A fractal characterisation of the structure of coal froths. *Coal Preparation*, 1998. Vol. 19(1), pp. 69-82.

Holtham, P.N. & Nguyen, K.K. On-line analysis of froth surface in coal and mineral flotation using JKFrothCam. *International Journal of Mineral Processing*, 2002. Vol. 64(2-3), pp. 163-180.

Hyötyniemi, H. & Ylinen, R. Modeling of visual flotation froth data. *Control Engineering Practice*, 2000. Vol. 8(3), pp. 313-318.

Jeanmeure, L.F.C. & Zimmerman, W.B.J. CNN video based control system for a coal froth flotation. *Proceedings of the IEEE International Workshop on Cellular Neural Networks and their Applications*, 1998. pp. 192-197

Jemwa, G.T. & Aldrich, C. Kernel-based fault diagnosis on mineral processing plants. *Minerals Engineering*, 2006. Vol. 19(11), pp. 1149-1162.

Kaartinen, J., Haavisto, O. & Hyötyniemi, H. On-line colour measurement of flotation froth. *Proceedings of the IASTED International Conference on Intelligent Systems and Control*, 2006a. pp. 164-169

Kaartinen, J., Hätönen, J., Hyötyniemi, H. & Miettunen, J. Machine-vision-based control of zinc flotation - A case study. *Control Engineering Practice*, 2006b. Vol. 14(12), pp. 1455-1466.

Kalyani, V.K., Pallavika, Chaudhuri, S., Charan, T.G., Haldar, D.D., Kamal, K.P., Badhe, Y.P., Tambe, S.S. & Kulkarni, B.D. Study of a laboratory-scale froth flotation process using artificial neural networks. *Mineral Processing and Extractive Metallurgy Review*, 2008. Vol. 29(2), pp. 130-142.

Kottke, D. & Ying, S. Motion estimation via cluster matching. *IEEE Transactions on Pattern Analysis and Machine Intelligence*, 1994. Vol. 16(11), pp. 1128-1132.

Laplante, A., Toguri, J. & Smith, H. The effect of air flow rate on the kinetics of flotation. Part 1: The transfer of material from the slurry to the froth. *International Journal of Mineral Processing*, 1983a. Vol. 11(3), pp. 203-219.

Laplante, A., Toguri, J. & Smith, H. The effect of air flow rate on the kinetics of flotation. Part 2: The transfer of material from the froth over the cell lip. *International Journal of Mineral Processing*, 1983b. Vol. 11(3), pp. 221-234.

Laplante, A. The effect of air flow rate on the kinetics of flotation. Part 3: Selectivity. *International Journal of Mineral Processing*, 1984. Vol. 13(4), pp. 285-295.

Lin, X., Gu, Y. & Zhao, G. Calculation of the specific surface area of the froth in flotation. *Meitan Xuebao/Journal of the China Coal Society:*, 2007a. Vol. 32(8), pp. 874-878.

Lin, X., Zhao, G. & Gu, Y. A classification of flotation froth based on geometry. *Proceedings of the 2007 IEEE International Conference on Mechatronics and Automation*, 2007b. pp. 2716-2720

Liu, J.J., MacGregor, J.F., Duchesne, C. & Bartolacci, G. Flotation froth monitoring using multiresolutional multivariate image analysis. *Minerals Engineering*, 2005. Vol. 18(1), pp. 65-76.

Liu, J. & Macgregor, J. On the extraction of spectral and spatial information from images. *Chemometrics and Intelligent Laboratory Systems*, 2007. Vol. 85(1), pp. 119-130.

Liu, J.J. & MacGregor, J.F. Froth-based modeling and control of flotation processes. *Minerals Engineering*, 2008. Vol. 21(9), pp. 642-651.

Mathe, Z.T., Harris, M.C., O'Connor, C.T. & Franzidis, J.P. Review of froth modelling in steady state flotation systems. *Minerals Engineering*, 1998. Vol. 11(5), pp. 397-421.

Mathe, Z.T., Harris, M.C. & O'Connor, C.T. Review of methods to model the froth phase in non-steady state flotation systems. *Minerals Engineering*, 2000. Vol. 13(2), pp. 127-140.

McKee, D.J. Automatic flotation control - a review of 20 years of effort. *Minerals Engineering*, 1991. Vol. 4(7-11), pp. 653-666.

Moolman, D.W., Aldrich, C., Van Deventer, J.S.J. & Stange, W.W. Digital image processing as a tool for on-line monitoring of froth in flotation plants. *Minerals Engineering*, 1994. Vol. 7(9), pp. 1149-1164.

Moolman, D.W. The on-line control of an industrial flotation plant using videographic images and signal processing. *PhD*. South Africa, University of Stellenbosch, 1995a.

Moolman, D.W., Aldrich, C., van Deventer, J.S.J. & Bradshaw, D.J. Interpretation of flotation froth surfaces by using digital image analysis and neural networks. *Chemical Engineering Science*, 1995b. Vol. 50(22), pp. 3501-3513.

Moolman, D.W., Aldrich, C. & Van Deventer, J.S.J. The analysis of videographic data with neural nets. *Chimica Acta Slovenica*, 1995c. Vol. 42(1), pp. 137-142.

Moolman, D.W., Aldrich, C., Van Deventer, J.S.J. & Stange, W.W. The classification of froth structures in a copper flotation plant by means of a neural net. *International Journal of Mineral Processing*, 1995d. Vol. 43(3-4), pp. 193-208.

Moolman, D.W., Aldrich, C., Schmitz, G.P.J. & Van Deventer, J.S.J. The interrelationship between surface froth characteristics and industrial flotation performance. *Minerals Engineering*, 1996a. Vol. 9(8), pp. 837-854.

Moolman, D.W., Eksteen, J.J., Aldrich, C. & Van Deventer, J.S.J. The significance of flotation froth appearance for machine vision control. *International Journal of Mineral Processing*, 1996b. Vol. 48(3-4), pp. 135-158.

Morar, S.H., Forbes, G., Heinrich, G.S., Bradshaw, D.J., King, D., Adair, B.J.I. & Esdaile, L. The use of colour parameter in a machine vision system, SmartFroth, to evaluate copper flotation performance at Rio Tinto's Kennecott copper concentrator. *Cententenary of Flotation Symposium*. Brasbane, QLD, 2005.

Muller, D., De Villiers, P. & Humphries, G. A holistic approach to flotation mass pull and grade control. *13th IFAC Symposium on Automation in Mining, Mineral and Metal Processing - Preprints*. Cape Town, South Africa, 2010. pp. 127-130

Murphy, D., Woodburn, E. & Cilliers, J. Modelling of froth dynamics with implications for feed-back control. *Frothing in flotation II*. Goron and Breach Science Publishers, 1998. pp. 205-244

Neethling, S.J. & Cilliers, J.J. The effect of weir angle on bubble motion in a flotation froth: Visual modelling and verification. *Minerals Engineering*, 1998. Vol. 11(11), pp. 1035-1046.

Neethling, S.J., Cilliers, J.J. & Woodburn, E.T. Prediction of the water distribution in a flowing foam. *Chemical Engineering Science*, 2000. Vol. 55(19), pp. 4021-4028.

Neethling, S.J. & Cilliers, J.J. The entrainment of gangue into a flotation froth. *International Journal of Mineral Processing*, 2002a. Vol. 64(2-3), pp. 123-134.

Neethling, S.J. & Cilliers, J.J. Solids motion in flowing froths. *Chemical Engineering Science*, 2002b. Vol. 57(4), pp. 607-615.

Neethling, S.J., Lee, H.T. & Cilliers, J.J. Simple relationships for predicting the recovery of liquid from flowing foams and froths. *Minerals Engineering*, 2003a. Vol. 16(11), pp. 1123-1130.

Neethling, S.J. & Cilliers, J.J. Modelling flotation froths. *International Journal of Mineral Processing*, 2003b. Vol. 72(1-4), pp. 267-287.

Neethling, S.J. & Cilliers, J.J. Predicting air recovery in flotation cells. *Minerals Engineering*, 2008. Vol. 21(12-14), pp. 937-943.

Neethling, S.J. & Cilliers, J.J. The entrainment factor in froth flotation: Model for particle size and other operating parameter effects. *International Journal of Mineral Processing*, 2009. Vol. 93(2), pp. 141-148.

Nguyen, K.K. & Thornton, A.J. The application of texture based image analysis techniques in froth flotation. *Conference Proceedings on Digital Image & Vision Computing*, 1995. pp. 613-618.

Nguyen, K.K. & Holtham, P. The application of pixel tracing techniques in the flotation process. *Proceedings of the first joint Australian and New Zealand biennial conference on Digital Imaging and Vision Computing and Applications*, 1997. pp. 207-212

Nguyen, A.V., Phan, C.M. & Evans, G.M. Effect of the bubble size on the dynamic adsorption of frothers and collectors in flotation. *International Journal of Mineral Processing*, 2006. Vol. 79(1), pp. 18-26.

Nguyen, P. & Nguyen, A. Validation of the generalised Sutherland equation for bubble–particle encounter efficiency in flotation: Effect of particle density. *Minerals Engineering*, 2009. Vol. 22(2), pp. 176-181.

Niemi, A.J., Ylinen, R. & Hyötyniemi, H. On characterization of pulp and froth in cells of flotation plant. *International Journal of Mineral Processing*, 1997. Vol. 51(1-4), pp. 51-65.

Núñez, F. & Cipriano, A. Hybrid modeling of froth flotation superficial appearance applying dynamic texture analysis. *Proceedings of the 27th Chinese Control Conference*. Kumming, China, 2008. pp. 117-121

Núñez, F. & Cipriano, A. Visual information model based predictor for froth speed control in flotation process. *Minerals Engineering*, 2009. Vol. 22(4), pp. 366-371.

O'Connor, C. The effect of temperature on the pulp and froth phases in the flotation of pyrite. *Minerals Engineering*, 1990. Vol. 3(6), pp. 615-624.

Oestreich, J.M., Tolley, W.K. & Rice, D.A. The development of a color sensor system to measure mineral compositions. *Minerals Engineering*, 1995. Vol. 8(1-2), pp. 31-39.

Pal, N.R. & Bhandari, D. Object background classification: some new techniques. *Signal Processing*, 1993. Vol. 33

Pérez-Garibay, R., Estrada-Ruiz, R.H. & Gallegos-Acevedo, P.M. Relationship between the bubble surface flux that overflows and the mass flow rate of solids in the concentrate of flotation processes. *Minerals Engineering*, 2010. Vol. 23(7), pp. 541-548.

Reddick, J.F., Hesketh, A.H., Morar, S.H. & Bradshaw, D.J. An evaluation of factors affecting the robustness of colour measurement and its potential to predict the grade of flotation concentrate. *Minerals Engineering*, 2009. Vol. 22(1), pp. 64-69.

Ripley, B. Tree Structured Classifiers. *Pattern Recognition and Neural Networks*. New York, Cambridge University Press, 2009. pp. 213-241

Runge, K., McMaster, J., Wortley, M., Rosa, D. & Guyot, O. *Correlation between VisioFroth measurements and the performance of a flotation cell*. 2007. pp. 79-86.

Sadr-Kazemi, N. & Cilliers, J.J. An image processing algorithm for measurement of flotation froth bubble size and shape distributions. *Minerals Engineering*, 1997. Vol. 10(10), pp. 1075-1083.

Shahbazi, B., Rezai, B. & Javadkoleini, S. The effect of hydrodynamic parameters on probability of bubble–particle collision and attachment. *Minerals Engineering*, 2009. Vol. 22(1), pp. 57-63.

Supomo, A., Yap, E., Zheng, X., Banini, G., Mosher, J. & Partanen, A. PT Freeport Indonesia's mass-pull control strategy for rougher flotation. *Minerals Engineering*, 2008. Vol. 21(12-14), pp. 808-816.

Symonds, P. & De Jager, G. A technique for automatically segmenting images of the surface froth structures that are prevalent in flotation cells. *Proceedings of the 1992 South African Symposium on Communications and signal Processing*. University of Cape Town, Rondebosch, South Africa, 1992. pp. 111-115

Trahar, W. A rational interpretation of the role of particle size in flotation. *International Journal of Mineral Processing*, 1981. Vol. 8(4), pp. 289-327.

Van Deventer, J. Visualisation of plant disturbances using self-organising maps. *Computers & Chemical Engineering*, 1996. Vol. 20, pp. s1095-s1100.

Van Olst, M., Brown, N., Bourke, P. & Ronkainen, S. Improving flotation plant performance at Cadia by controlling and optimising the rate of froth recovery using Outokumpu FrothMaster. *Australasian Institute of Mining and Metallurgy Publication Series*, 2000. pp. 127-135

Van Schalkwyk, T. Multivariable control of a rougher flotation cell. *PhD Thesis*. University of Cape Town, South Africa, 2002.

Vathavooran, A., Batchelor, A., Miles, N.J. & Kingman, S.W. Applying Froth Imaging Techniques to Assess Fine Coal Dewatering Behavior. *Coal Preparation*, 2006. Vol. 26(2), pp. 103-121.

Ventura-Medina, E. & Cilliers, J.J. Calculation of the specific surface area in flotation. *Minerals Engineering*, 2000. Vol. 13(3), pp. 265-275.

Ventura-Medina, E. & Cilliers, J.J. A model to describe flotation performance based on physics of foams and froth image analysis. *International Journal of Mineral Processing*, 2002. Vol. 67(1-4), pp. 79-99.

Vera, M.A., Mathe, Z.T., Franzidis, J.P., Harris, M.C., Manlapig, E.V. & O'Connor, C.T. The modelling of froth zone recovery in batch and continuously operated laboratory flotation cells. *International Journal of Mineral Processing*, 2002. Vol. 64(2-3), pp. 135-151.

Wang, W. & Stephansson, O. A robust bubble delineation algorithm for froth images. *Proceedings of the 2nd International Conference on Intelligent Processing and Manufacturing of Materials*, 1999. pp. 471-476

Wang, W., Bergholm, F. & Yang, B. Froth delineation based on image classification. *Minerals Engineering*, 2003. Vol. 16(11), pp. 1183-1192.

Wang, Z., Lu, M. & Liu, W. Predicting the performance of coal flotation by using the features of froth image. *Computer Applications in the Minerals Industries*, 2001. pp. 487-490.

Wills, B. Froth Flotation. *Mineral Processing Technology*. Butterworth Heinemann, 1997. pp. 258-341

Woodburn, E., Austin, L. & Stockton, J. Froth based flotation kinetic model. *Chemical Engineering Research and Design*, 1994. Vol. 72(A2), pp. 211-226.

Wright, B.A. The development of a vision-based flotation froth analysis system. *MSc Thesis*. University of Cape Town, South Africa, 1999.

Yang, C.-., Yang, J., Mou, X., Zhou, K. & Gui, W. Segmentation method based on clustering pre-segmentation and high-low scale distance reconstruction for colour froth image. *Journal of Electronics and Information Technology*, 2008. Vol. 30(6), pp. 1286-1290.

Yianatos, J., Moys, M., Contreras, F. & Villanueva, A. Froth recovery of industrial flotation cells. *Minerals Engineering*, 2008. Vol. 21(12-14), pp. 817-825.

Zanin, M., Wightman, E., Grano, S. & Franzidis, J. Quantifying contributions to froth stability in porphyry copper plants. *International Journal of Mineral Processing*, 2009. Vol. 91(1-2), pp. 19-27.

Zheng, X. & Knopjes, L. Modelling of froth transportation in industrial flotation cells Part II - Modelling of froth transportation in an Outokumpu tank flotation cell at the Anglo Platinum Bafokeng-Rasimone Platinum Mine (BRPM) concentrator. *Minerals Engineering*, 2004. Vol. 17(9-10), pp. 989-1000.

Zheng, X., Franzidis, J. & Johnson, N. An evaluation of different models of water recovery in flotation. *Minerals Engineering*, 2006. Vol. 19(9), pp. 871-882.

Zhu, J. & Yu, K. Application of image recognition system in flotation process. *Proceedings of the World Congress on Intelligent Control and Automation*, 2008. pp. 6555-6659

Zimmerman, W.B.J., Jeanmeure, L.F.C. & Laurent, F. Simple model of equilibrium froth height for foams: an application for CNN image analysis. *Proceedings of the IEEE International Workshop on Cellular Neural Networks and their Applications*, 1996. pp. 237-241

Zu, J. & Yu, K. Application of image recognition system in flotation process. *Proceedings of the World Congress on Intelligent Control and Automation*, 2008. pp. 655-659

APPENDIX A
PUBLICATIONS

1. PEER REVIEWED JOURNAL PAPERS

Aldrich, C., Marais, C., Shean, B. & Cilliers, J.J. On-line monitoring and control of froth flotation systems with machine vision: A review. *International Journal of Minerals Processing*, 2010, Volume 96, Issue 1-4, pp. 1-13

2. SUBMITTED PEER REVIEWED JOURNAL PAPERS

Marais, C. & Aldrich, C. Prediction of platinum flotation grade from froth image data. *Minerals Engineering* (Conditionally accepted October 2010)

3. PEER REVIEWED CONFERENCE PAPERS

Marais, C. & Aldrich, C. The relationship between froth image features and platinum flotation grade. In *Proceedings of the IFAC MMM Symposium*, pp 131 - 135, Cape Town, 2010.

Marais, C. & Aldrich, C. The estimation of platinum flotation grade from froth image features by using artificial neural networks. In *Proceedings of the 4th International Platinum Conference, Platinum in transition 'Boom or Bust'* , The Southern African institute of Mining and Metallurgy, Sun City, South Africa, 2010.

4. NON-PEER REVIEWED CONFERENCE PRESENTATIONS

Marais, C. & Aldrich, C. The relationship between froth image features and platinum flotation grade. *Minerals Processing Conference*, Cape Town, 2010.